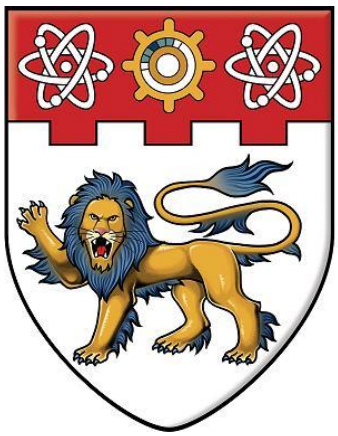

NANYANG TECHNOLOGICAL UNIVERSITY

Electrokinetic Transport and Manipulation of Particles in Confined Microfluidic Domains

LIANG QIAN

School of Mechanical and Aerospace Engineering

2012

Electrokinetic Transport and Manipulation of Particles in Confined Microfluidic Domains

By

LIANG QIAN

A Thesis Submitted to Nanyang Technological University

in Partial Fulfillment of the Requirements for the Degree of

Doctor of Philosophy

School of Mechanical and Aerospace Engineering

2012

Abstract

Electrokinetic phenomena have their fundamental significance and have found their wide applications for manipulating fluid flows, particles and cells in microfluidics. However the electrokinetic phenomena in confined microfluidic domains have been received less attention. The phenomenon of particle transport in confined microfluidic domains is a complex process which may simultaneously involve electrophoresis, electroosmosis and dielectrophoresis. Therefore, classic theories describing particles electrokinetic transport in unbounded domains are no longer valid because of the hydrodynamic and electric interactions among the particle-fluid-solid walls. This thesis research aims at advancing our understanding of the coupled electric and hydrodynamic processes in the electrokinetic transport of particles in confined microfluidic domains, and explores novel approaches for particle transport and manipulation in confined microfluidic structures.

In this thesis the studies of electrokinetic transport and manipulation of particles in confined microfluidic domains can be divided into two parts. The first part investigates the electrokinetic transport phenomena in open-ended microfluidic domains by employing both experimental and numerical approaches with the focus placed on the hydrodynamic and electric interactions among particles, fluid and the bounded domain boundaries. Fundamental study of wall effects on electrokinetic transport of microspheres in a rectangular microchannel is carried out. An experimental technique to study the near-wall enhancement of electrophoretic mobility of microspheres with respect to the flexible controlled particle-wall

separations is proposed for the first time. Specifically, the particle-wall separations are modulated in the vertical plane by adjusting the equilibrium height of the particle motion above the bottom wall within the microchannel based upon the force balance between the gravitational force against the wall-induced DEP force. A three dimensional numerical simulation is carried out to explain the experimental results and a reasonably good agreement is found. In addition, a method is proposed for continuous concentration of particles in a confined microfluidic chamber. Both experimental and numerical studies are carried out. Experimental results and numerical simulations showed that under a very low applied voltage, particles enrichment is achieved in the confined chamber with a short time.

In the second parts of this study, the focuses are placed on exploring novel approaches for particle manipulations in closed microfluidic domains. A method for on-chip particle assembly in non-uniform electric field is demonstrated by using the combined effects of dielectrophoresis and dipole attractive force. Moreover, two novel electronic paper display technologies are developed and experimentally demonstrated by using polystyrene particles dispersed in DI water. Two prototypes of the proposed electronic paper displays are fabricated. The first type of electronic paper display relies on the phenomenon of our proposed in-plane dielectrophoresis. While, the second type is based on the combined effects of dielectrophoresis and dipole interaction forces. The proposed novel technologies can realize electronic paper displays with fast switching response, high resolution, superior optical transmittance while likely keeping low manufacturing costs.

Acknowledgements

This work would not have been possible to be achieved without the help of many people. Firstly, I would like to express my deepest gratitude to my supervisors, Associate Professor Yang Chun, Charles and Associate Professor Miao Jianmin for their excellent and tirelessly guidance for the work done in this thesis. It has been a great honor and pleasure to work with them during the past four years. As my Ph.D. supervisor, Prof. Yang opened the door for me to the world of an exciting research area - microfluidics and nanofluidics. Prof. Yang always gives me confidence in my abilities by showing his own example in his student life and encourages me promptly once a progress is made in my project. His dedication and enthusiasm for research impress me very much and set an example for me during my four-year study. As my Ph.D. co-supervisor, Prof. Miao also helps me a lot. The discussion with him, especially in microchip fabrication methods, is critical to the completion of this thesis research.

In addition, I would like to thank all my colleagues in Thermal and Fluids Research Laboratory for their assistance which facilitates the completion of this work. I would thank our group members: Dr. Lewpiriyawong Nuttawut, Dr. Ge Zhengwei, Dr. Wang Wei, Mr. Milad Radiom, Mr. He Jinhua, Mr. Hon Kar Cherng Louis, Mr. Zhao Yugang, Ms. Zhou Yi and Ms. Jiao Yanmei for the helpful discussions with them. Specifically, I would like to thank Dr. Zhao Cunlu for his kind help on mathematic model development and Dr. Suhanya Duraiswamy for her critical proof-reading of the thesis.

I would like to thank Mr. Yuan Kee Hock, the technician in charge of Thermal and Fluids Research Laboratory for purchase matters. Also technical guidance and assistance in microfabrication from the research staff, technical staff and research students at Micro-Machines Centre (MMC) are much appreciated.

Furthermore, I would extend my gratitude to Nanyang Technological University for offering me the Ph.D. scholarship and providing me with the opportunity to come to Singapore and pursue my interests in research.

Finally, I would like to express my gratitude to my parents and parents-in-law. A special appreciation is given to my son Liang Xuanming and my wife Ms. Wen Yadan, a Ph.D. candidate in Yong Loo Lin School of Medicine, National University of Singapore, for their continuous love, encouragement and support in the past four years. Without them, I definitely cannot have reached where I am now.

Contents

List of figures

List of tables

Nomenclature

a,	Radius of a microsphere [m]
b, d, h	Geometrical parameters
c	Correction factor
D	Diffusion coefficient [m^2/s]
E	Electric field [V/m]
F	Force [N]
n	Number density of ions [$/m^3$]
p	Pressure [Pa]
q	Surface charge density [C/m^2]
U	Velocity vector [m/s]
u, v	velocity components [m/s]
x, y	Cartesian coordinates

Greek symbols

ε	Dielectric constant
ε_0	Permittivity of vacuum, 8.854×10^{-12} F/m
ζ	Zeta potential [V]
μ	Electrophoretic mobility [C s/kg]
ψ	Electric potential [V]
κ	Debye-Hückel parameter [m^{-1}]
λ_D	Debye length [m]
η	Dynamic viscosity [$Pa \cdot s$]

Subscripts

d	Parameters related to the dielectrics
f	Parameters related to the fluid
p	Parameters related to the particle
i	Induced quantities
r	Reference quantities
s	Smoluchowski velocity

Chapter 1: Introduction

1.1 Background

Microfluidics is referred to as emerging science and technology dealing with systems that process or manipulate nano-liter and even pico-liter amounts of fluids, using channels with dimensions of tens to hundreds of micrometers (Whitesides 2006). The fast development of microfluidics is due to its promising applications in chemical analyses and biomedical diagnoses such as DNA separation, enzyme assays, immunoassays, PCR amplification etc. (Bousse et al. 2000). Microfluidic devices offer a number of capabilities, including consuming very small quantities of samples and reagents, separation and detection with high resolution and sensitivity, low costs, and fast analysis and detection.

In microfluidics interfacial phenomena play an extremely important role because of the great surface-to-volume ratio of microchannel. As a result, the transport mechanisms in microscale fluid flow, heat and mass transfer processes as well as particle and droplet motion are different from those in a macroscale system due to the significant surface forces (Ren 2004). In microfluidics the surface forces typically dominate over body and inertia forces, leading to the overwhelming utilization of surface-phenomena-based electrokinetic transport approaches instead of the traditional pressure driven methods in manipulations of cells and micro/nano-sized objectives and fluid pumping. This is because surface forces scale with the characteristic length to the first or second power, while body and inertia forces scale

with the characteristic length to the third power (Maynes and Webb 2002). Therefore, surface forces become much stronger than body and inertia forces as the length scale decreases.

Electrokinetic phenomena provide one of the most popular non-mechanical transport means in microfluidics. The basic idea behind electrokinetic phenomena is as follows: a diffuse cloud of surface charge exists adjacently to solid surfaces when they are brought into contact with an aqueous medium. As a result, an externally applied electric field can exert a force on this charged diffuse layer due to the Coulombic interaction, giving rise to a fluid flow relative to the charged particle or surface. The bulk flow relative to charged stationary surfaces is known as electroosmosis, and the motion of charged suspended particles is known as electrophoresis. Electroosmosis and electrophoresis find their wide applications in analytical chemistry, genomics and proteomics. Normally, the electrokinetic motion of a cell/microparticle in charged microfluidic channels is a combination of electroosmosis and electrophoresis, and the translational velocity of the cell/microparticle in an electrolyte solution is given by the well-known Smoluchowski equation. In addition, for a microparticle suspended in liquid solution medium under non-uniform electric field, the electrostatic forces acting on the induced asymmetric dipoles of the particle are imbalanced, yielding net forces on the microparticle. This is known as dielectrophoresis.

Up to date, most investigations on the microparticle electrokinetic transport in microfluidic devices have put efforts on flow-through channels with applications in

flow pumping, continuous cells separation and sorting etc. The electrokinetic transport phenomena in confined microfluidic domains are also of significance. For example, it is found that the classic Smoluchowski equation describing the electrophoretic mobility of a particle electrokinetic transport in an unbounded microfluidic domain is no longer valid either when the particle size is comparable with the channel dimension or for the case that the particle motion is close to the boundary. This is because in the above situations both of the electric potential distribution and the flow field around the particle are obviously disturbed by the presence of the particle. Unlike the electrokinetic transport of particles in an infinite domain, the existence of solid boundaries plays an important role in particle's motion because of the complicated hydrodynamic and electric interactions among the particle-fluid-solid walls. The near wall electrophoretic mobility of microspheres in a microchannel is predicted to be retarded at a larger particle-wall separation due to the viscous stress but enhanced at a smaller particle-wall separation because of the strong electric stress within the narrow gap. However, the experimental verifications of boundary effect on electrokinetic transport of particles in a microchannel are still lagged theoretical studies. This is especially true for the experimental study of near wall electrophoretic mobility enhancement because the microscale particle-wall separations were unknown in the previous investigations.

Nowadays, electrokinetics is widely utilized in microfluidic systems for cells and bacteria concentration, manipulation, separation and sorting. Most electrokinetic particles manipulation methods in microfluidics involve complicated hydrodynamic

and electric interactions among the particle-fluid-solid walls as well. For example, in order to utilize dielectrophoresis for particles/cell separation and focusing, insulating structures are always employed to disturb the externally applied electric field and thus a local electric field gradient is created. However, electrokinetic methods for particles manipulation mostly have to work under a very strong externally applied electric field. The used of high voltage power supply or amplifier is always needed.

In addition, the particles transport and manipulation in closed microfluidic domains are of great significance to many applications such as the development of electrophoretic displays (Ota et al. 1973; Dalisa 1977; Hopper and Novotny 1979; Comiskey et al. 1998), electrophoretic deposition technology (Sarkar and Nicholson 1996; Besra and Liu 2007) and on-chip particles assembly (Lumsdon et al. 2004; Velev 2004; Velev and Bhatt 2006; Simon and Orlin 2008). Electronic papers, also called e-papers for abbreviation, are based on new display technologies designed to mimic the appearance of ordinary inks on a normal paper. Electronic paper display exhibits some of the qualities of a good grade of white papers, including the reflection of light off the surface of papers. At the moment, distinct electronic paper products have been commercialized using several different working principles, among which the most widely used one is the electrophoretic display (EPD). EPD is a reflective display technology based upon the phenomenon of electrophoresis. However, due to its operation principle, the further development of EPD is limited in many aspects. For example, only one or two types of particles can be controlled simultaneously in a typical EPD cell and thus the full color display is a challenge for the current EPD

technology. In addition, although the switching response of the EPD (~300 ms) is sufficient for normal reading, it is still too slow to display video frames.

This study serves as an attempt to fulfill the void in previous investigations by carrying out a series of fundamental and systematic experimental and numerical researches to explore the electrokinetic transport phenomena in confined microfluidic domains and their applications in microfluidic systems.

1.2 Research objective and scope

The main objective of this thesis is to investigate the fundamental electrokinetic transport phenomena in confined microfluidic domains and to explore their new applications in microfluidic systems. To accomplish this objective, the scope of this thesis is as follows:

(1) Carrying out experimental and numerical studies of the near wall electrophoretic mobility of microsphere transport in a microchannel.

(2) Exploration of the particle-wall-fluid interactions in confined microfluidic domain and development of a technique for continuous concentration of particles.

(3) Investigation of novel particle assembly methods in a closed microfluidic space and systematically analyze the physical mechanism underlying the proposed methods.

(4) Development of novel electronic paper display technologies with fast switching response, high resolution, superior transmittance with possible low manufacturing cost.

1.3 Outline of the thesis

In order to fulfill the research objective of this thesis, the studies are carried out in two parts. The first part, including two chapters, studies electrokinetic transport phenomena in confined microfluidic devices with the focus placed on the hydrodynamic and electric interactions among particle-fluid-wall. The second part, including three chapters, investigates the fundamental electrokinetic manipulations of microparticles in closed microfluidic domains and their new applications (Figure 1.1). The complete thesis comprises eight chapters as following:

Chapter 1 introduces the background and motivation of this work. The recent development of electrokinetic transport phenomena and particles transport and manipulation in confined microfluidic domains are briefly reviewed. The main objective and research scope of this thesis are clearly stated.

Chapter 2 provides a literature review of fundamental electrokinetic phenomena involved in this thesis. Previous studies of boundary effects on electrokinetic transport of particles in microfluidics are reviewed. A broad literature review of working principles and recent development of electronic paper display technologies is presented as well.

Chapter 3 reports experimental and numerical studies of the near wall electrophoretic mobility enhancement of microsphere transport in a rectangular microchannel. Flexible control and precise measurement of particle-wall separations are demonstrated for the first time. A three dimensional numerical simulation is carried out, and a reasonably good agreement between the experiment and numerical results is achieved.

Chapter 4 presents a technique for continuous concentration of particles in a confined microfluidic chamber. A novel copper imbedding method is used to create 3D side wall electrodes within the confined chamber. A numerical simulation describing the mass transport within the computational domain is performed.

Chapter 5 reports a novel electronic paper display technology using dielectrophoresis for manipulating neutral particles suspended in aqueous medium. The particle patterning within the electronic display panel is realized by using in-plane DEP force. Effects of operational parameters on the performance of the proposed electronic paper display are discussed. A numerical simulation is conducted to analyze the electric field and DEP force for particle manipulation.

Chapter 6 presents a fundamental experimental study of on-chip particle assembly under non-uniform electric field. The particles are manipulated by using the combined effects of DEP and dipole attractive force. A remarkable electric field gradient is created by applying AC electric field to co-planar electrodes with

microscale separations. A hypothesis is proposed to explain the underlying physical mechanisms of the experimental observation.

Chapter 7 demonstrates another novel electronic paper display technology based on the experimental observations from chapter 6. The proposed electronic paper display has fast switching response, high resolution and superior transmittance.

Finally, chapter 8 summarizes the major findings and results of this work. Some possible directions for the future studies are briefly outlined.

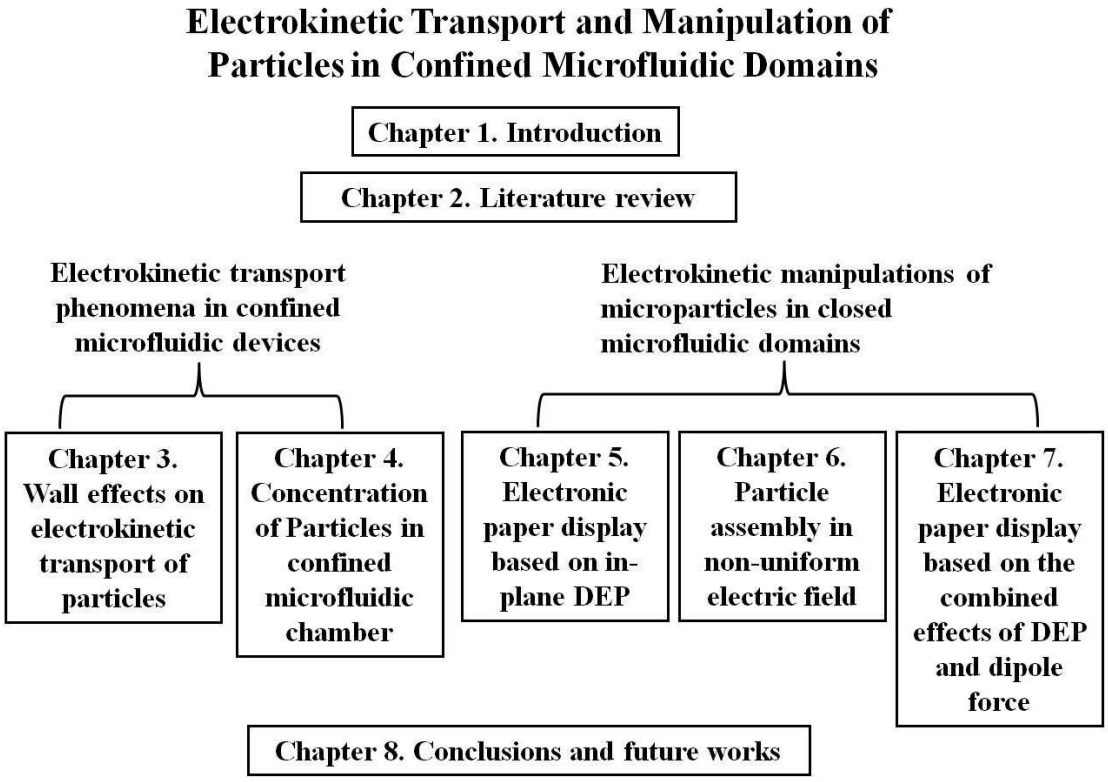

Figure 1.1 Structure of the thesis.

Chapter 2: Literature review

2.1 Fundamental electrokinetic phenomena

2.1.1 Electric double layer (EDL)

It is well-acknowledged that most solid surfaces tend to acquire surface charges when in contact with an aqueous solution. The surface charging can occur by a few of mechanisms, such as ionization, ion adsorption, and ion dissolution (Li 2004). When a solid objective is in contact with an electrolyte, the chemical state of the surface is generally altered, either by ionization of covalently bound surface groups or by ion adsorption (Zhao 2008). As a result, the surface inherits a charge while counterions are released into the liquid. At equilibrium, a balance between electrostatic interactions and thermal agitation yields a charge density profile. The liquid is electrically neutral, but for a charged layer adjacent to the boundary, which bears a charge locally equal in amplitude and opposite in sign to the bound charge on the surface. This charged layer is commonly known as the electric double layer (EDL). In spite of the traditional use of the word “double”, its structure can be very complex, not fully resolved in many instances, and it may contain three or more layers, extending over varying distances from the solid surface (Hunter 1981).

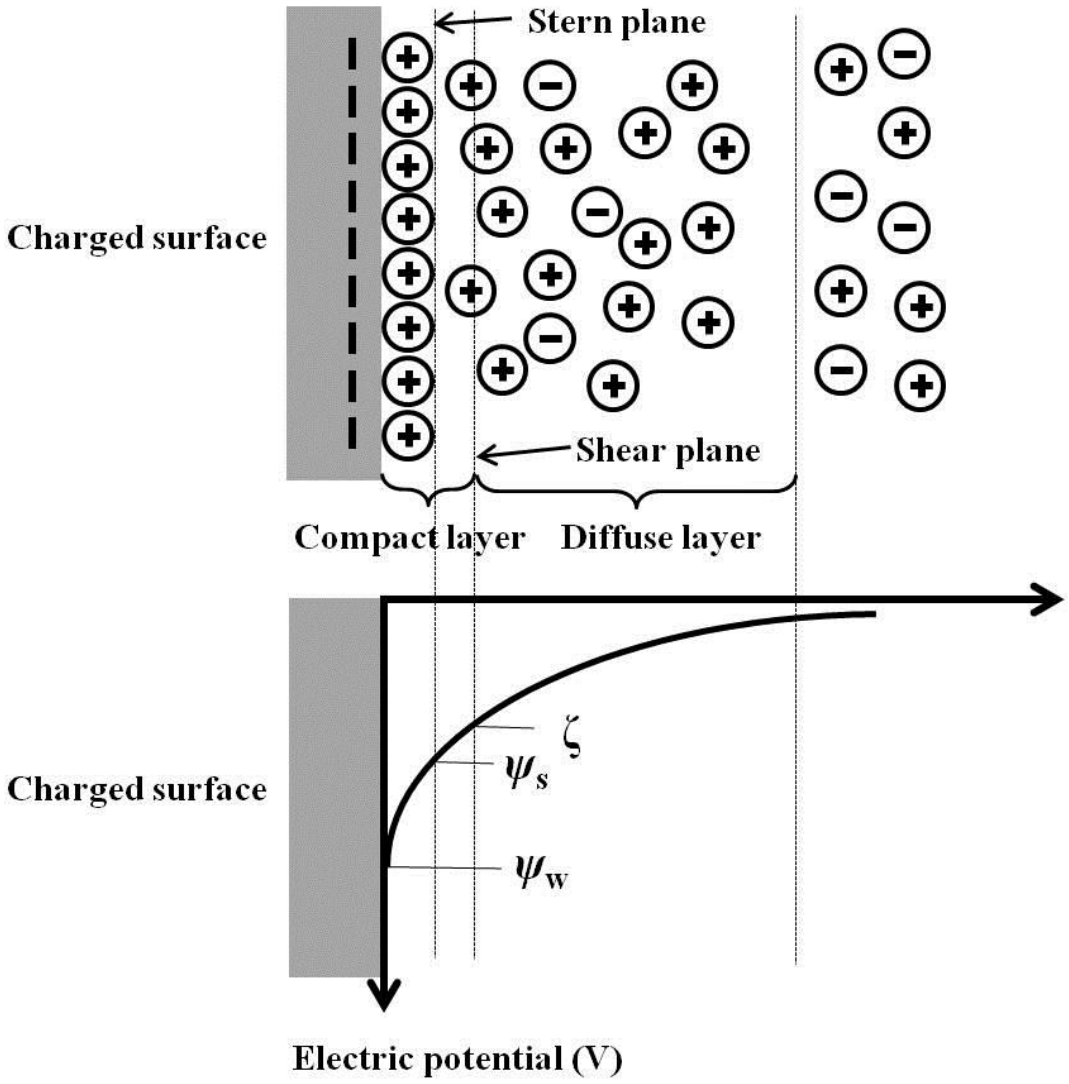

Figure 2.1 Schematic representation of the electric potential distribution at a negatively charged interface.

A schematic illustration depicting the charge and the potential distribution within an EDL is shown in Figure 2.1. Immediately next to the charged surface, a layer of immobilized counterions is present, which is known as the compact layer or the Stern layer with less than one nanometer in thickness (Schoch et al. 2008). The net charge

density gradually drops to zero from the compact layer to the electrically neutral bulk liquid. Because the Compact layer is extremely thin (of the order of the ion hydration radius, typically ~0.1 nm) compared with the typical microchannel dimensions, the shear effects are virtually confined within this thin layer. The layer of mobile ions outside the Compact layer is termed the Guoy-Chapman layer, or the diffused layer of the EDL. These two layers are separated by a shear plane at which the electric potential is known as the zeta potential (ζ). The thickness of the EDL is known as the Debye length (λ). The electric potential on the charged wall and Stern plane are defined as surface potential (ψ_w) and Stern potential (ψ_s), respectively.

In order to neutralize the surface charge on the solid boundary, the net charge density within the EDL is no longer zero because ions are repelled away from the compact layer and mobilized in the diffuse layer. According to the classic EDL theory, ion distribution within the diffuse layer can be described mathematically in a simple way and the equilibrium condition for ions in this layer can be written as

$$-ez_i \nabla \psi - k_b T \nabla \ln n_i = 0 \tag{2.1}$$

where e, z_i, ψ, K_b, T and n_i are respectively the fundamental electric charge, the valence of type i ion, electric potential, the Boltzmann constant, the absolute temperature and the ionic concentration for the i-th species. The first term corresponds to the electrostatic force on ions of type i and the second term is the

thermodynamic force. Integration of the equation under the condition $n_i = n_i^0(\infty)$ for $\psi = 0$ leads to the well-known Boltzmann distribution,

$$n_i(\mathbf{r}) = n_i^0(\infty)\exp\left[-ez_i\psi(\mathbf{r})/k_bT\right] \tag{2.2}$$

where $n_i^0(\infty)$ is the number concentration of ions of type *i* far from the charged surface. Finally, the Poisson equation will give the relationship between the potential and ionic concentrations,

$$\nabla^2\psi(\mathbf{r}) = -\frac{1}{\varepsilon_0\varepsilon}\rho(\mathbf{r}) = -\frac{1}{\varepsilon_0\varepsilon}\sum_{i=1}^{N} ez_i n_i^0(\infty)\exp\left[-\frac{ez_i\psi(\mathbf{r})}{k_bT}\right] \tag{2.3}$$

where ε_0 and ε being the dielectric permittivity of the vacuum ($\varepsilon_0 = 8.854\times10^{-12} C/V\cdot m$) and the local dielectric constant of the solution medium. The Poisson–Boltzmann equation is the starting point of the Gouy–Chapman description of the diffuse layer.

2.1.2 Electroosmosis (EO)

As a charged solid surface is surrounded by an EDL when contact with an electrolyte solution, the excess ions within the EDL can response to an externally applied electric field, which in turn drives adjacent fluid motion. This phenomenon is termed

electroosmosis (EO). The non-zero charge density yields a net body force on the fluid proportional to the local net charge density if the electric field is applied perpendicular to the decay of the EDL. As shown in Figure 2.2, the velocity of electroosmotic flow (EOF) increases from zero at the shear plane to its bulk phase velocity $\mathbf{U}_{EO}$ at the edge of the EDL, and thus a very high shear rate is generated at the region near the charged surface. The electroosmotic mobility μ_{EO}, which describes the flow velocity per unit field strength, is a function of both surface and solution phase properties. Unlike pressure-driven flows, a flat or "plug flow" velocity profile is exhibited outside the EDL region for a uniform electroosmotic flow (Erickson 2008).

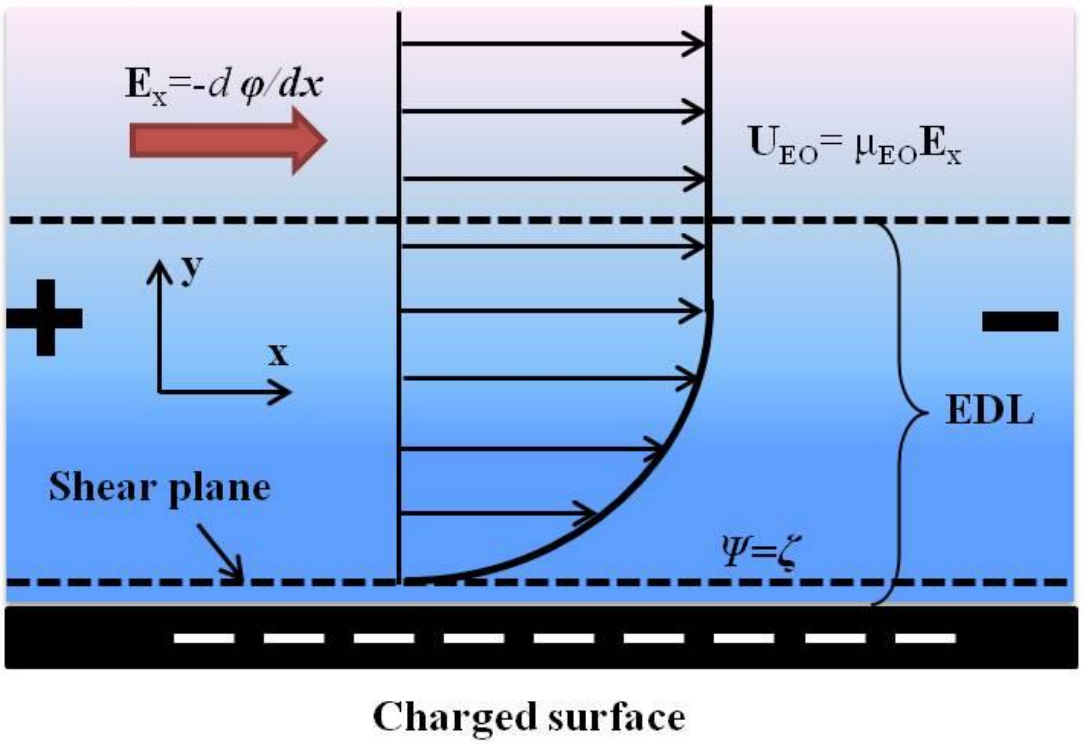

Figure 2.2 Schematic illustration of electroosmosis.

The incompressible flow field normally is governed by the Navier-Stokes equation and the Continuity equation (Deen 1998):

$$\rho(\frac{\partial \mathbf{v}}{\partial t} + \mathbf{v} \cdot \nabla \mathbf{v}) = -\nabla p + \eta \nabla^2 \mathbf{v} - \rho_e \nabla \phi \tag{2.4}$$

$$\nabla \cdot \mathbf{v} = 0 \tag{2.5}$$

where $\mathbf{v}$, t, p, η and ρ are velocity, time, pressure, viscosity and density of the fluid, respectively. The last term in the right hand side of Equation (2.4) represents the electroosmotic body force and is equivalent to the product of the net charge density ρ_e in the double layer, multiplied by the gradient of the total electric potential ϕ. The latter of these comprises of the summation of the electric potential ψ induced by EDL, and the applied electric potential φ, as indicated by

$$\phi = \varphi + \psi \tag{2.6}$$

The electrical potential generated by the presence of the EDL and the net charge density are related by the Poisson equation,

$$\nabla \cdot (\varepsilon \varepsilon_0 \nabla \psi) = -\rho_e \tag{2.7}$$

The most common simplification employed in electroosmotic flow analysis is the "Helmholtz–Smoluchowski" approximation with a few of assumptions during the

derivation as follows (Liu 2005). Firstly, the nonlinear and transient term in Equation (2.4) are dropped since the inertia terms are negligible compared with the pressure and viscous terms. In other words, the Reynold's number is much smaller than unity. Secondly, for a pure electroosmotic flow (no applied pressure) with uniform surface (zeta potential) and solution (viscosity and conductivity) properties, the applied pressure gradient is zero. Thirdly, the length of the channel is assumed much greater than its height. Therefore a one-directional approximation is created, and the applied electric field is imposed along the channel length. Finally, the thickness of the EDL is much thinner than the channel size, thus the Boltzmman distribution for the ion concentration can be used. Under these postulations, the flow velocity at the shear plane can be approximated as,

$$\mathbf{U}_{eo} = \mu_{eo} E_x = \frac{\varepsilon \varepsilon_0 \zeta}{\eta} E_x \tag{2.8}$$

which is commonly known to as the Helmholtz-Smoluchowski equation and is descriptive of a plug flow velocity profile (Masliyah and Subir 2006).

2.1.3 Electrophoresis (EP)

When a colloidal particle is freely suspended in an electrolyte solution, the surface charges are acquired due to the similar mechanism of electroosmosis. A negatively charged particle is surrounded by EDL which includes excessive number of positive

mobile ions as shown in Figure 2.3. The charged particle moves towards the anode under a uniform electric field applied. This movement is generated by the interaction between the net charge in the EDL of the particle and the applied electric field. The motion of the particle induced by the Coulombic force is known as electrophoresis (EP) (Dorfman 2008).

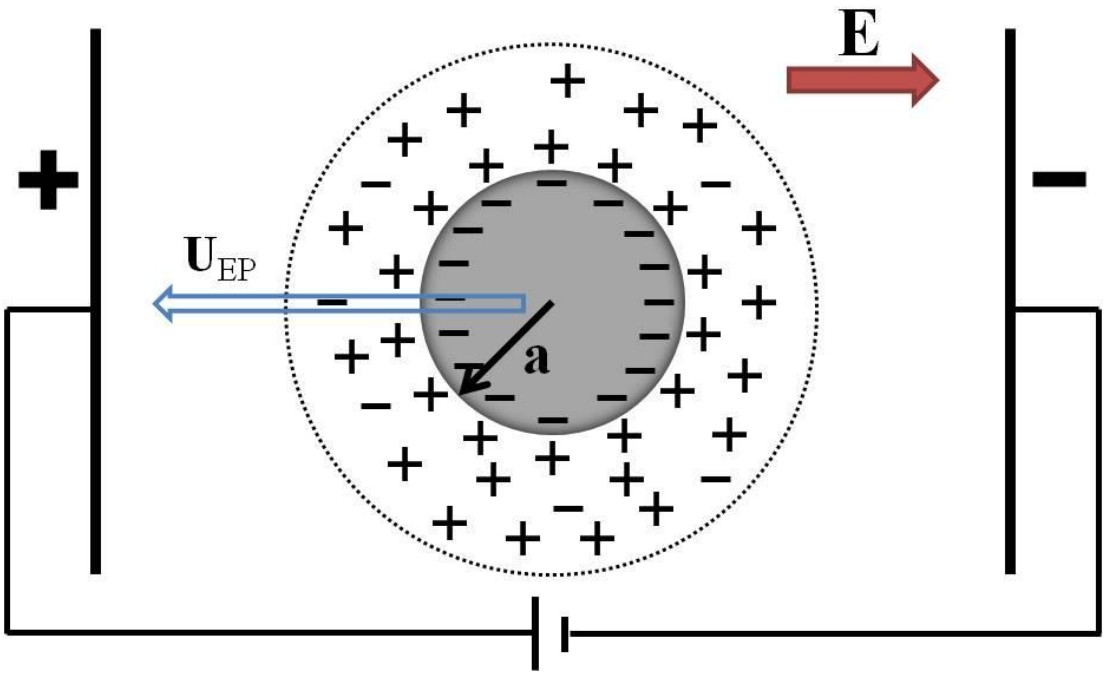

Figure 2.3 Schematic illustration of electrophoresis for a negatively charged spherical particle.

The electrophoretic force acting on a microparticle with a net charge *q* under electric field strength of **E** is given by (Kang and Li 2009),

$$\mathbf{F_{EP}} = q\mathbf{E} \tag{2.9}$$

The electrophoretic velocity with which the particle moves with regard to its carrier solution is proportional to the intensity of the applied electric field. The electrophoretic velocity per unit field strength is called electrophoretic mobility. The electrophoretic mobility μ_{EP} is also proportional to the magnitude of the net charge on the particle, and is inversely proportional to the size of the particle (Probstein et al. 1994).

$$\mu_{EP} = \frac{U_{EP}}{E} = \frac{q}{f} \tag{2.10}$$

where U_{EP} is the electrophoretic velocity and $f = 6\pi\eta a$ is the Stokes drag factor for a spherical particle in a Stokes flow. a is the radius of the spherical particle. Considering the EDL is thick, one can treat the particle as a point charge in an unperturbed electric field E, the electrophoretic velocity of the particle can be expressed by using the Huckel equation (Probstein et al. 1994).

$$\mathbf{U}_{EP} = -\frac{2}{3}\frac{\varepsilon\varepsilon_0\zeta_p}{\eta}\mathbf{E} \tag{2.11}$$

where ζ_p is the zeta potential of the particle. For the cases of high ionic strengths or large particles of micron size, the EDL is commonly thin compared with the particle. The electrophoretic velocity is given by the Helmholtz–Smoluchowski equation

$$\mathbf{U}_{EP} = -\frac{\varepsilon\varepsilon_0\zeta_p}{\eta}\mathbf{E} \tag{2.12}$$

For the electrokinetic motion of a charged particle within a microchannel, however, EP and EOF are typically effect simultaneously. By ignoring the polarization and the retardation effects under the thin EDL assumption, the electrophoretic force is given by

$$\mathbf{F}_{EP} = 6\pi\varepsilon\varepsilon_0\zeta_p a\mathbf{E} \tag{2.13}$$

The relative motion of the particle with regards to the EOF yields a hydrodynamic drag force on a charged particle and it is given by

$$\mathbf{F}_{stokes} = -6\pi\eta a(\mathbf{U}_{EP} - \mathbf{U}_{EOF}) \tag{2.14}$$

Consider the force balance between Equation (2.13) and (2.14) at a steady state, one can derive an expression for the apparent velocity of electrokinetic motion of a spherical particle with substituting Equation (2.12), given by

$$\mathbf{U}_p = -\frac{\varepsilon\varepsilon_0(\zeta_p - \zeta_w)}{\eta}\mathbf{E} \tag{2.15}$$

It should be pointed out that Equation (2.12) is obtained for a spherical particle in an infinitely large fluid domain, namely without considering any boundary effects on the particle's transport. Equation (2.15) is relying on the assumptions that the electric field and flow field are both symmetric in their distributions. In fact, for a large particle comparable to the channel's dimension, or when a particle moves very close to the solid boundary of a channel, Equation (2.12) and (2.15) are no longer applicable due to the asymmetric local electric field and flow field.

2.1.4 Dielectrophoresis (DEP)

Dielectrophoresis (DEP) refers to the interaction between a dielectric particle in a carrier liquid and a non-uniform electric field. Physically, polarization effects are induced by an applied electric field due to mismatch of dielectric and electric properties of the particle and its suspending medium (Jones 1995), as represented in Figure 2.4. Due to the polarization, electric charge separation appears within the dielectric particle as well as in the liquid side of the particle-liquid interface, giving rise to a dipole moment. Under a non-uniform electric field, electrostatic forces acting on the dipole are unbalanced, giving rise to a net force which is called DEP force. When a dielectric particle with polarizability greater than the suspending medium at

which the electric field lines bend towards the particle (Figure 2.4 (a)), it is usually termed positive DEP with the direction towards the region of high electric field. While, when the polarizability of the particle is less than its surrounding medium at which the electric field lines bend around the particle (Figure 2.4 (b)), the direction of the DEP force is away from the region of high electric field, which is usually called negative DEP.

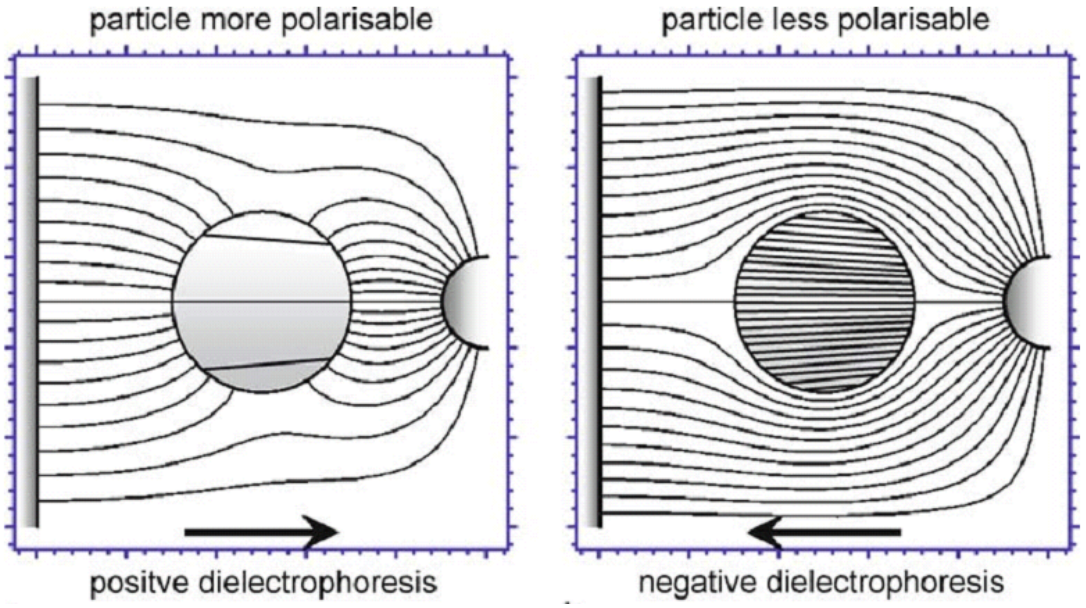

(a) (b)

Figure 2.4 Polarization of a dielectric particle in a nonuniform electric field. The arrows show the direction of dielectrophoresis (DEP) force and particle movement. (a) particle more polarisable than the suspending medium; (b) particle less polarisable than the suspending medium. (Morgen and Green 2008).

When the polarizability of the particle and electrolyte are the identically it is like the case that the particle does not exist and the field lines are continuous everywhere. The

induced dipole is a function of frequency of the applied electric field as well. Therefore, the direction of particle movement is not only depends on the properties of the particle and the carrier fluid, but also affected by the frequency of the applied field. This provides the possibility that using electrokinetics as an effective tool to manipulate and transport particles in microfluidics.

The effective dipole moment of a spherical particle is given by Jones (1995)

$$\mathbf{P_{eff}} = 4\pi\varepsilon\varepsilon_0 a^3 \cdot K_{CM} \cdot \mathbf{E} \tag{2.16}$$

where K_{CM} is the Clausius-Mossotti (CM) factor, and it is dependent on the dielectric and electric properties of the particle and the suspending medium, as well as the frequency of the external applied electric field. The CM factor is a measure of the effective polarizability of a particle in a liquid medium and is given by (Pethig 2010),

$$K_{CM} = \frac{\varepsilon_p^* - \varepsilon_m^*}{\varepsilon_p^* + 2\varepsilon_m^*} \tag{2.17}$$

where ε_p^* and ε_m^* are the complex permittivities of the particle and medium, respectively. For a homogeneous particle and medium, the complex dielectric constant $\varepsilon^* = \varepsilon - i(\sigma/\omega)$ is a function of the conductivity σ, the permittivity ε, and the angular frequency ω. $i = \sqrt{-1}$.

Unlike the electrophoretic force that is the pure Coulombic force acting on the charged particle, the DEP force is actually a net effect of the unbalanced Coulombic forces acting on the induced dipoles. In terms of the dipole moment, the DEP force acting on a spherical particle is given by Jones (1995)

$$\mathbf{F}_{\mathbf{DEP}} = \mathbf{P}_{\mathbf{eff}} \cdot \nabla \mathbf{E} = 2\pi\varepsilon\varepsilon_0 a^3 \cdot K_{CM} \cdot \nabla \left|\mathbf{E}\right|^2 \tag{2.18}$$

From above equation, it is acknowledged that the DEP force vector is direct along the gradient of the electrical field intensity $\nabla \left|\mathbf{E}\right|^2$, which, in general, is not parallel to the electric field $\mathbf{E}$. The DEP force also depends upon the magnitude and sign of the CM factor K_{CM}. Dielectrophoresis has many applications such as trapping particles/cells, manipulating and separating large numbers of biological objectives, creating ordered arrays of particles etc. However, all of these applications rely upon the existence of well-defined electric field gradients. This is generally performed by using microelectrodes fabricated onto insulating substrates (e.g. glass) as part of a microfluidic or Lab-on-a-Chip system. Modern techniques allow the fabrication of micro-electrodes with precise sizes and dimensions, enabling accurate control of the electric field geometry and therefore particle motion.

2.2 Studies of boundary effects on electrokinetic transport of particles in microfluidic devices

2.2.1 Theoretical studies of boundary effects on electrokinetic transport of particles

Electrokinetic force and hydrodynamic force are often employed to drive flows and control colloidal particles for electrokinetic transport and manipulation of microparticles in electrolyte solutions. For a charged colloidal particle in a microfluidic channel, the interface between solid / fluid phases is a transition of finite thickness. No matter the length scale of the interface is thicker or comparable to the particle (i.e., the thick EDL case), or even may be orders of magnitude smaller than the particle size (i.e., the thin EDL case), the details of transport processes occurring within this thin layer often control the fluid dynamics outside (Anderson 1989). The charge on the particle's surface is balanced by a diffuse cloud with opposite charged sign. The charge density within the cloud decays exponentially at distances of the order of the Debye screening length κ^{-1} from the surface. Taken together, the surface charge and the diffuse cloud (the EDL) are considered as a neutral body. A classic method to deal with such problem is to divide the computational domain as two parts: an inner region and an outer region.

As shown in Figure 2.5, the inner region is defined as the diffuse layer adjacent to the particle and the solid boundaries, where the important length scale is the Debye

length κ^{-1} (Keh and Anderson 1985). The rest part of the fluid is known as the outer region, where the particle dimension is the characteristic length scale. Under the assumption of thin EDL, the charged particle with the surrounding diffuse cloud is always taken as a neutral sphere. Due to the negligible volume of the EDL, the details of flow transport within the inner region are not necessary to be analyzed. The effect of the EDL on the flow field is reflected by approximating a slip boundary condition on the solid surface in instead of the classic non-slip condition. For the neutral sphere motion under an electric field is applied, the sphere is driven by the hydrodynamic force in the outer flow region. While for the case of thick EDL, the flow field in both inner and outer regions has to be calculated with the non-slip condition applied on these solid surfaces. In this situation, the charged particle experiences a Coulombic attraction under an applied electric field due to the surface charge and this force is balanced against the hydrodynamic force in the inner flow region when the particle motion at a steady state.

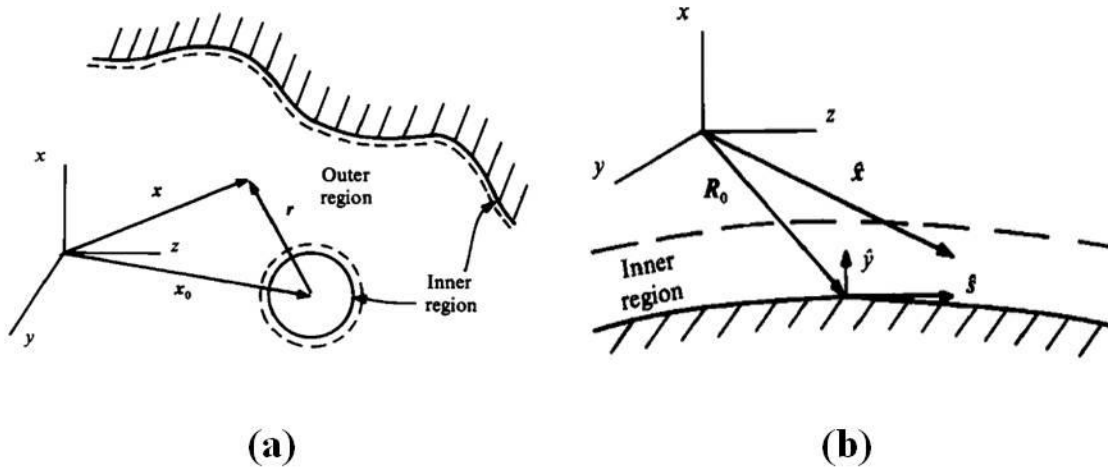

Figure 2.5 (a) Sketch of the inner region and outer region of the fluid phase; (b) Geometry of the inner region. (Keh and Anderson 1985)

Numerous theoretical studies have been reported on the electrokinetic transport of a single particle motion in bounded domains. Keh and Anderson (1985) analytically investigated boundary effects on electrophoretic motion of a colloid sphere moving parallel or perpendicular to a plane surface and through the axis of a circular orifice under the thin EDL assumption. The corrections for the classic Smoluchowski formula were derived by using the successive Reflections method to explore the influence of a nearby non-conducting wall on the particle's motion. However, the results are valid only for a relatively large particle-wall separation. Subsequently, an exact solution to this problem was proposed (Keh and Chen 1988) by using the bipolar coordinates to evaluate the electric field. It was demonstrated that for a large particle-wall separation, their results predict a reduction in particle electrophoretic mobility in agreement with their previous findings. At small particle-wall separation distances, however, the net wall effect was predicted to reinforce the particle electrophoretic mobility. This near wall enhancement was later confirmed by Yariv and Brenner (2003) and Unni et al. (2007). The former employed the Reciprocal theorem to obtain the asymptotic expressions for the force and torque acting on the particle, thereby avoiding the need for solving the pertinent Stokes equation. In the latter study, closed-form solutions for the particle velocity and disturbed electrical and fluid velocity field were obtained and the effects of the relative particle size and eccentricity on a particle's translational and rotational velocity were analyzed.

Moreover, Ye and Li (2002) analytically studied the electrophoresis of a sphere in a microchannel under the gravitational field, and the separation distance was calculated

based on the balance between colloidal surface forces against gravitational force. However, the electric and hydrodynamic interactions between the particle and channel boundaries are not included. In their subsequent work (Ye et al. 2005), the eccentric electrophoretic motion of a sphere in circular cylindrical microchannels with consideration of particle-fluid-wall interactions was numerically studied by a 3D finite element simulation. It was found that the near wall sphere motion is enhanced in smaller channels. Without restricting to the thin EDL assumption, the electrophoretic motion of a spherical particle has been theoretically analyzed either close to a plane wall (Ennis and Anderson 1997; Shugai and Carnie 1999; Hsu et al. 2008; Chang and Keh 2008) or along a capillary axis (Ennis et al. 1996; Shugai and Carnie 1999) or in a spherical cavity (Zydney 1995). It was found that the wall effects become more significant with increasing the EDL thickness.

Apart from the electrokinetic transport of spherical particles in microfluidics devices, the particle-wall interaction between the domain boundary and non-spherical particles have been investigated as well. The electrophoretic transport of a cylindrical particle with hemispherical ends in a circular cylindrical microchannel was numerically studied by Ye et al. (2002). The influence of the ratio of particle radius to channel radius, the ratio of particle's axial length to its radius and the zeta potential ratio of particle to channel wall were analyzed. The analytical studies on the similar problem were reported by Hsu and Kao (2002) and Liu et al. (2004 a). The dielectrophoresis of cylindrical and spherical particles submerged in shells and in semi-infinite media was analyzed by Liu and Bau (2004 b), in which the dielectrophoretic forces and the

resulting velocities of cylindrical and spherical particles suspended in perfectly dielectric viscous fluids were calculated analytically. In their subsequent work (Liu et al. 2004 c), the electrophoresis of concentrically and eccentrically positioned cylindrical particles in a long tube was studied. Their model accounts for the flow induced by the particle's motion (the particle acts as a leaky piston) and the electroosmotic flow in the tube. The electrophoretic velocity of the particle and the forces and torques acting on it are determined as functions of the particle's radius, length, and position, the particle's and tube's zeta potentials, the tube's length, and the externally imposed pressures. Liu et al. (2007) also theoretically studied the electric field induced translocation of cylindrical particles through nanopores with circular cross sections. The theoretical predictions are compared, and used to explain experimental data pertaining to the translocation of DNA molecules through nanopores. The similar research was reported by Chein and Dutta (2009) in which the cylindrical particle was replaced by a nanosphere. In addition, the effect of induced electroosmosis on a cylindrical particle next to a planar surface was studied by Zhao and Bau (2007). It was found that the induced hydrodynamic and electrostatic force may adversely affect the interaction between macromolecules in solution and wall-immobilized molecules.

2.2.2 Experimental study of boundary effects on electrokinetic transport of particles

Although theoretical analyses of the wall effects on particle electrokinetic transport in a microchannel have been intensively explored, very few experimental studies have been reported in the literature. Through measuring fluorescence intensities, the transport rates of fluorescent polystyrene particles through porous membranes that separate an aqueous medium with different electrolyte concentrations was detected by Ebel (1988). It was found that the resultant diffusiophoretic velocities of the particles decelerate as the pore size shrinks. Subsequently, Ennis (1996) observed the reduced electrophoretic velocity of proteins (e.g., bovine hemoglobin with diameters of 9.6 nm) in a membrane with different pore sizes by measuring the solute concentration with a UV–visible spectrophotometer. In recent years, the near-wall electrophoretic motion of a spherical polystyrene particle in a cylindrical glass capillary was studied by Xuan et al. (2005 a), from which they found that the velocity of two groups of particles increases with decreasing capillary diameter. The particle-wall separation distance, however, was unknown in their study. Xuan et al. (2006) also experimentally examined the electrophoretic motion of spherical polystyrene particles in a converging-straight-diverging PDMS microchannel. It was demonstrated that that larger particles are more viscously retarded by the sidewalls of the channel with a smaller width. Another work (Xuan et al. 2005 b) from the same group focused on accelerated particle electrophoretic motions in converging-diverging microchannels on PDMS chips. It was found that the ratio of the particle velocity in the throat to that

in the straight channel is increased for smaller particles moving through symmetric converging-diverging channels under lower electric fields.

2.2.3 Solid wall induced dielectrophoresis on a particle transport in a microchannel

Dieletrophoresis (DEP) refers to the phenomenon that a net force acts on a polarized particle under applied non-uniform electric field due to mismatch of dielectric and electric properties of the particle and its suspending fluid. A sufficient condition of such phenomenon is the existence of an electric field gradient. As a result, electrostatic forces acting on the induced dipole of the particle are not balanced, yielding a net force on the particle which is known as the DEP force. When a microsphere electrophoretically moves in a straight microchannel, although the electric field is indeed perturbed by the presence of the solid particle and an electric field gradient is therefore created, DEP is not considered because of the symmetrically electric potential distribution around the particle. However, this symmetry is broken either when the particle moves close to the channel boundary or a large particle eccentrically moves in a microchannel. Under these circumstances, due to the conservation of the electric current, the electric field within the narrow particle-wall gap is much stronger than that on the other wide gap side. A net DEP force is thus generated due to the asymmetric electric field around the particle. We term this force as the wall induced DEP force. The wall induced DEP decays sharply when the

particle is away from the channel wall, and vanishes when the particle moves towards the center of the channel.

Young and Li (2005) analytically studied solid wall induced DEP on a microsphere near a planar boundary. With integration of the Maxwell stress over the surface of the particle, the DEP force was calculated in the presence of an externally applied electric field. The particle's position above the wall, i.e. the particle-wall gap, is determined by balancing the van der Waals force, EDL interaction, and gravitational force with the DEP force. They found that the particle-wall gap can be increased with lower particle density, higher electric field strength, higher particle and wall zeta potentials, as well as lower Hamaker constant. Another numerical investigation (House and Luo 2011) focused on the DC DEP effect on the trajectory of a microsphere electrokinetic transport in an L-shape bent microchannel. In order to obtain an accurate numerical approach, a boundary-element method was employed to solve the coupled electric field, flow field as well as particle motion and the DEP is computed by integrating the Maxwell stress tensor. The results were compared with that calculated by utilizing the point-dipole method of which the volume of the particle is ignored. It was concluded that the wall-induced DEP can significantly affect the particle's transient motion as it moves close to the wall.

Recently, the wall induced DEP was demonstrated to focus particle streams in a straight microchannel under an externally applied electric field (Liang et al. 2010 a). As a particle motion in electrophoresis through a rectangular microchannel, the wall

induced DEP can repel particles from the solid boundaries toward the center of the channel. The efficiency of the particles focusing was reported to be enhanced with a longer axial traveling distance, a stronger electric field and a larger particle size. Because the channel height is comparable to its width, a three dimensional particles stream focusing is also achieved by using this method (Liang et al. 2010 b).

2.3 Electronic display technologies

The rapid development of computer related technologies extremely stimulate the information acquisition and transmission in the past decades. As most documents and materials can be directly accessed, read and edited through the computer, it is predicted that a "paperless era" is approaching (Kirk 2009). Unfortunately, these digital products actually did not reduce the consumption of paper. In contrast, the huge volumes of digital information ultimately promote the demand for printing, causing end users to desire comfortable and low-cost media for reading the information. With the growing requirements for information transmission and acquisition in daily life and work, paper consumption has reached a prodigious level.

One option to solve this problem is to develop and implement the novel display technologies. For instance, electronic paper, also called e-paper for abbreviation, is a kind of display technologies designed to mimic the appearance of ordinary ink on paper (Graham-Rowe 2007). Unlike a conventional flat panel display, which uses a

backlight to illuminate its pixels, electronic paper reflects light like ordinary paper. Therefore the energy consumption of electronic paper is much lower compared with other prevailing display technologies like Cathode Ray Tube (CRT), Plasma Display Panel (PDP) and Liquid Crystal Display (LCD). In addition, due to the stable image shown in the screen, which does not need to be refreshed frequently, and the fact of its reflecting ambient light rather than emitting its own light, electronic paper is more comfortable for reading than other conventional display technologies. Nowadays several electronic display technologies have been developed to realize and commercialize the electronic paper products, on the basis of different working principles, such as electrophoresis (Hopper and Novotny 1979; Comiskey et al. 1998; Kim et al. 2005; Baker et al. 2007), electrowetting (Hayes and Feenstra 2003; Paulson 2003; Feenstra et al. 2004), liquid powder (Hattori et al. 2006; Hattori et al. 2007; Takagi et al. 2007; Sakurai et al. 2008), electrofluidics (Drzaic 2009; Heikenfeld et al. 2009) and so on. Among them, Electrophoretic display (EPD) is considered prime examples of the electronic paper category, because of their paper-like appearance and low power consumptions

2.3.1 Electrophoretic display (EPD)

Electrophoretic display (EPD) is a passive device that operates under ambient lighting conditions based on the transport of charged pigment particles in a suspending medium (Dalisa 1977). The charged pigment particles are transported by means of an applied electrical field and this phenomenon is commonly known as electrophoresis. Nowadays, the EPD has been extensively used in digital products like E-readers,

electronic watches, monochrome display mobile phones and price labels. Currently, there are two electronic papers products using the EPD technique based on the pixel component as microcapsule (Comiskey et al. 1998) and microcup (Xie et al. 2005); (Zang et al. 2007), commercialized by E Ink Corporation and Sipix imaging Inc, respectively.

Today EPD with the technology developed by E Ink have achieved a remarkable maturity. The Microcapsule EPD system has synthesized an electrophoretic ink by microencapsulating oil droplets of an electrophoretic dispersion in individual microcapsules with diameters in the range of 30~300 μm. Figure 2.6 (a) illustrates the working principle of the E Ink EPD system of microencapsulated differently colored and charged particles. Particles can be transported towards the viewer with an externally electric impulse. Figure 2.6 (b) shows cross-sectional photographs of a single microcapsule addressed with positive and negative field. When a positive electric field is applied, the white particles (for example, if they are negatively charged) move toward the top of the microcapsule where they become visible to the user. This makes the surface appear white at that spot. At the same time, an opposite electric field repels the black particles to the bottom of the microcapsules where they are hidden. By reversing this process, the black particles appear at the top of the electronic display panel, which now makes the surface appear dark at that spot.

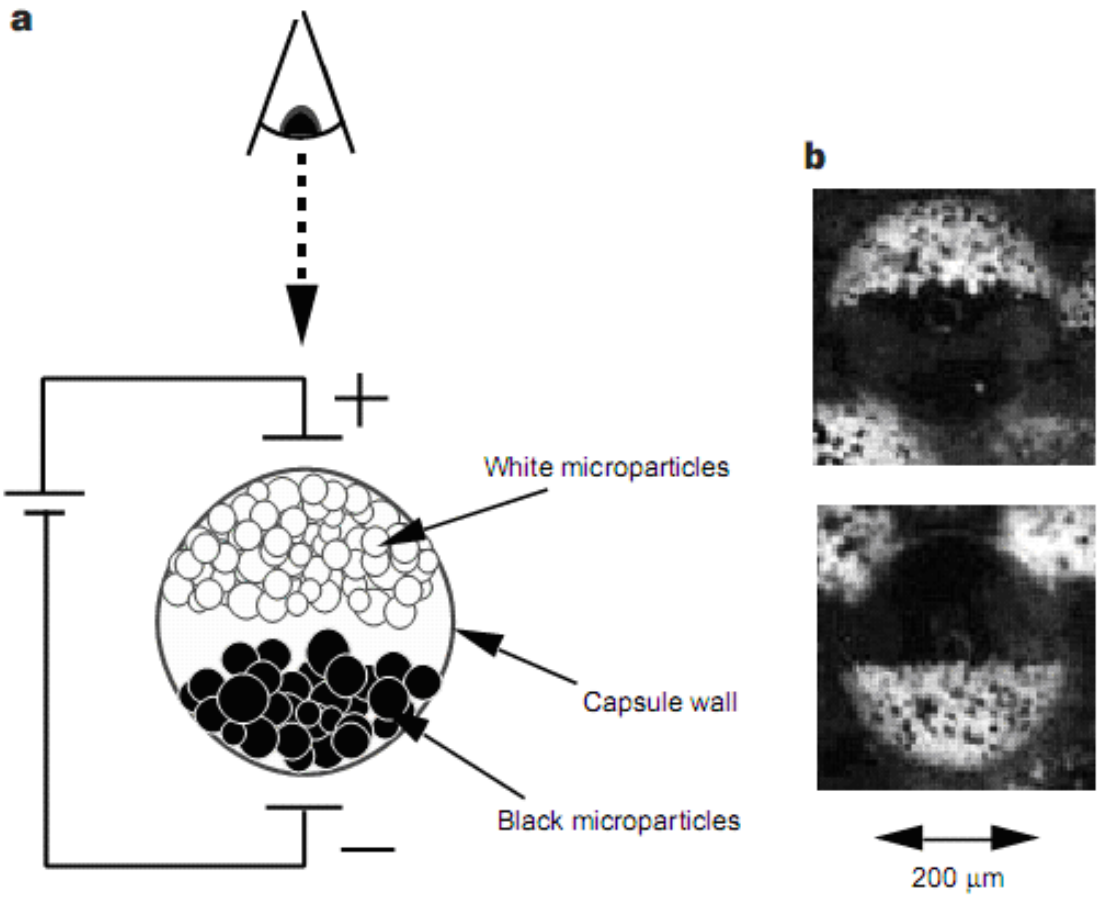

Figure 2.6 E-Ink Electrophoretic display microcapsule. (a) Schematic illustration of the E-Ink electrophoretic display. (b) Photographs of an individual microcapsule addressed with a positive and negative electric field. (Comiskey et al. 1998)

An alternative construction of EPD cells was realized by Sipix imaging Inc using an embossed polymer matrix to carry fluid and dyed particles. The cubic chambers, which are used to contain dielectric fluid and charged particles, are termed Microcup. Unlike to E Ink EPD, the Mcirocup EPD only has one type of charged particles packaged in the cells. Depending on applications, the dimension of the EPD cell may vary in a range of 60~200 μm (width) × 30~60 μm (height). Upon the electric voltage

is applied, the white particles (if the particles are negatively charged) will be driven to the anode electrode. As a result, a white color is displayed on the top surface. On the contrary, the particles will move to the bottom of the chamber and the surface shows a dark color by the black-dyed fluid.

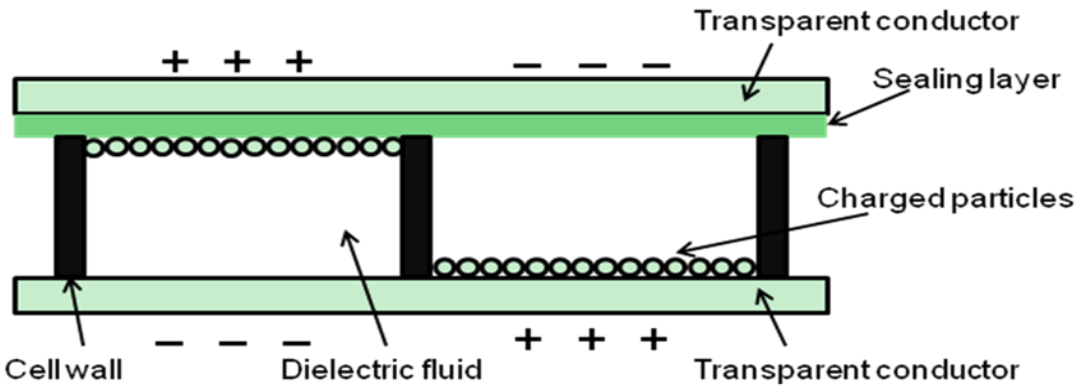

Figure 2.7 Schematic illustration of a typical Microcup Electrophoretic display cell.

Nowadays, Sipix imaging has developed a roll-to-roll manufacturing process (Liang et al. 2003) to fabricate Microcup EPD. On a continuous plastic substrate, the EPD material is created with coating, embossing, sealing and lamination processes. With the roll-to-roll manufacturing, it is possible to satisfy a high volume fabrication of display materials with a short time. On the other hand, because the microencapsulate process is excluded, the fabrication of Microcup EPD is much easier than E Ink EPD. However, due to the fact that only a single type of particles is enclosed in the cell, the reflectivity of the Microcup EPD is inferior to the E Ink EPD.

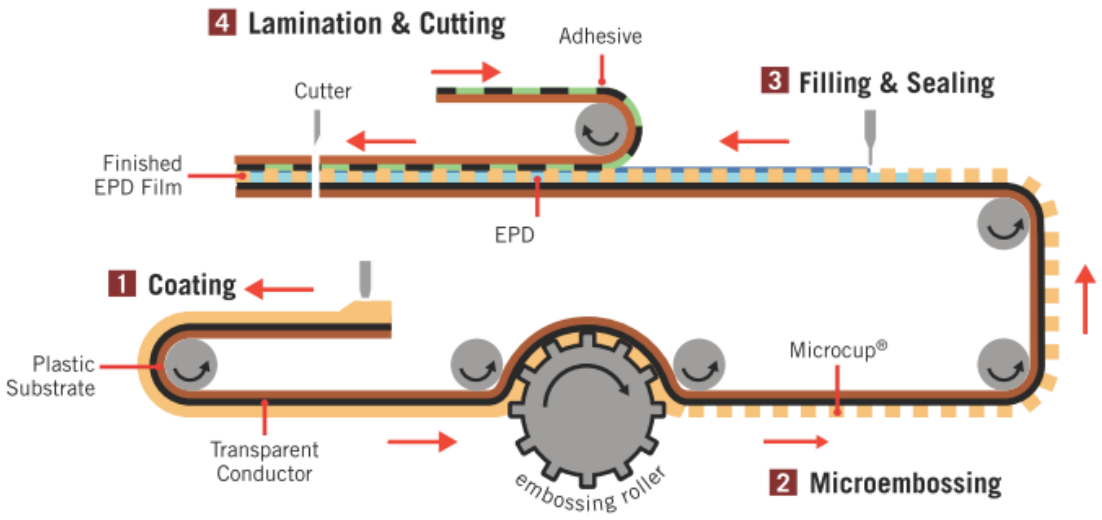

Figure 2.8 Sipix imaging roll-to-roll manufacturing process. (Liang et al. 2003)

2.3.2 In-plane Electrophoretic display (EPD)

Although the technology of Electrophoretic display has been intensively applied in many digital products, it is a long journey for engineers to develop and optimize EPDs. Due to the fact that only one or two types of dyed particles are under effectively controlled in EPD cells, the full color display is still a great challenge for the current EPD products (Koshimizu 2008). In despite of some approaches, such as the use of a color-filter array or subpixels with different dyed particles, have been attempted to create a colorful EPD, besides the costs, the loss of both brightness and resolution are also significant (Heikenfeld et al. 2011). Recently an in-plane Electrophoretic display (Lenssen et al. 2008; Lenssen et al. 2009); (Verschueren et al.) has been reported to be able to realize a full color electronic paper.

In-plane Electrophoretic display is a horizontal EPD display operates through the lateral movement of pigments across a display cell. The working mechanism of in-plane EPD is shown in Figure 2.9. There are two typical states in the operation of in-plane EPD. In the spread state, without electric voltage applied, the particles are distributed randomly throughout the cell and maximally absorb the incident light, screening a color observed by the viewer. While in the cleared state, with an electric field applied, the electric force attracts pigment particles toward the negative electrode, and light can pass through the device, showing a bright color on the display panel.

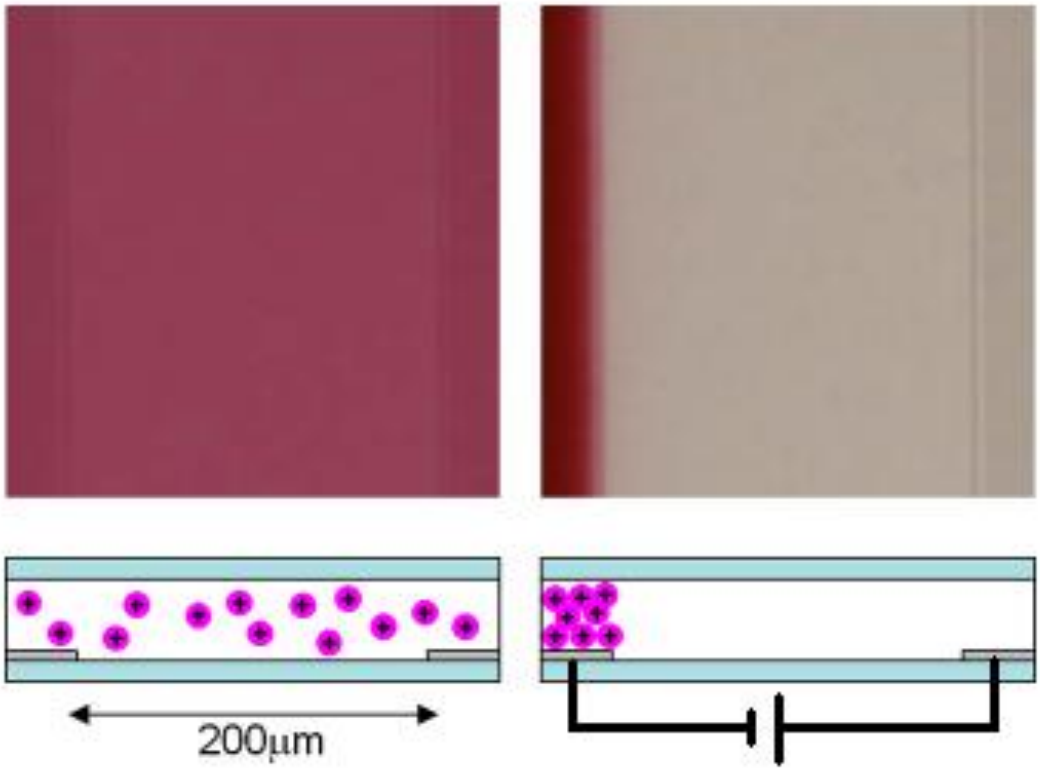

Figure 2.9 Schematic illustration of the operation of an in-plane EPD. (Verschueren et al. 2010)

By using the in-plane EPD technology, a full color display with a superior brightness is successfully realized. In-plane EPD employs a subtractive color scheme and stacks more than one layer with different dyed particles suspension above a piece of white substrate. As shown in Figure 2.10, since pigment particles in each layer can be switched separately, a multi-color display is therefore realized. In addition, because of the fact that two types of particles can be controlled independently in a single layer of suspension, this innovation truly enables a multi-color display with two layers stacked (consider four basic colors created by pigment particles plus a white reflector and the possible extra colors with the combination of any two kind basic colors). However, the switching response of in-plane EPD is experimentally demonstrated very long compared with conventional EPD products, and thus the applications of in-plane EPD are extremely limited.

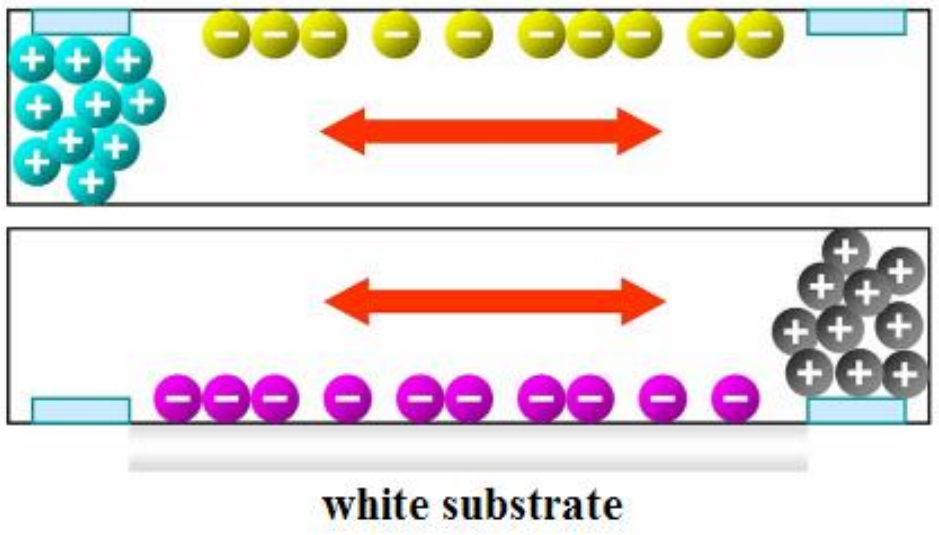

Figure 2.10 Schematic illustration of a full-color display concept by using an in-plane EPD. (Lenssen et al. 2009)

2.3.3 Electrorheological display (ERD)

Electrorheological display (ERD) (Wen et al. 2005) is a novel electronic display technology relying on the use of the electrorheological effect (Klingenberg et al. 1993; Gulley and Tao 1997; Dassanayake et al. 2000). By employing organic nanoparticles suspended in silicon oil, an electronic display is realized in both compact storage display mode and diffusive scattering mode. The operation mechanism of ERD is shown in Figure 2.11. Without applying electric field, as seen in the left part of the figure, no contrast is observed from the display panel as the nanoparticles are dispersed randomly in the oil. Once an electric voltage is imposed between the crossed top–bottom electrodes, as illustrated in the right part of the figure, the aligned columnar particle strips across the top and bottom electrodes block the light and the rest areas of the display panel are mostly transparent, allowing light transmission. As a result, contrast can be yielded between areas with and without electric field.

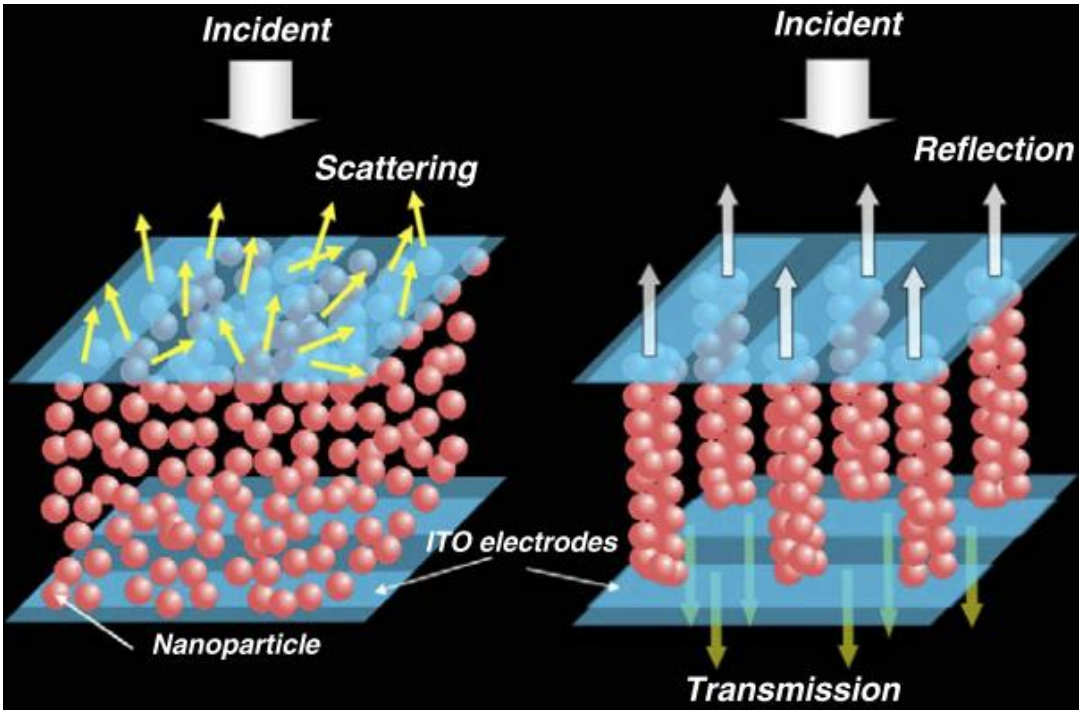

Figure 2.11 Schematic illustration of Electrorheological display. (Wen et al. 2005)

By applying an electric signal with a voltage of 50 V, a clear contrast is observed with an optical transmittance around ~30%. With an electric potential drop across two neighboring electrodes on the top plane, another way of displaying can be created with the columnar particle strips parallel to the top surface, in between the parallel electrodes.

2.3.4 Electronic display based on particles polarization

Recently, researchers from Taiwan developed a novel reflective electronic display technology using electric polarized particle chains in an AC electric field (Chiu et al.

2007; Chiu et al. 2008; Hsu et al. 2008; Chen et al. 2009). The electronic display consists of 5 μm polystyrene particles suspended in either deionized (DI) water or oil in a 200 μm thick chamber. The operation mechanism of such electronic display places on the fact that particles can be aligned as chains along direction of the electric field due to the induced dipole moment, in some aspect similar to the ERD.

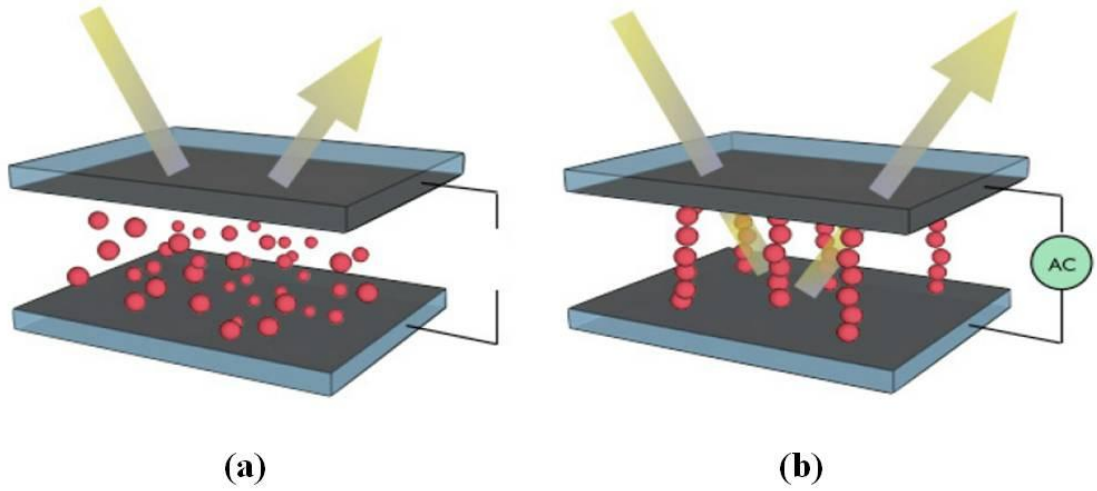

Figure 2.12 Schematic illustration of the electronic display based on particle polarization. (a) Dark state (without voltage) and (b) bright state (with voltage). (Chiu et al. 2007)

As shown in Figure 2.12, in the absence of an electric field, particles are randomly dispersed in the carrier solution (Figure 2.12 (a)). Incident light would be absorbed or scattered by the particles, and thus the color of particles is observed by viewers, which screen the dark state. While when an electric voltage is applied, the particles would be polarized by the electric field and particle chains are formed due to the attraction through the induced dipole. As a result, the scattering of incident light

would be reduced and most of the incident light can pass through the display panel (Figure 2.12 (b)). This is the bright state.

The electronic display based on particles polarization can be realized using either polystyrene particles suspended in DI water or toners in silicone oil. The device works under an AC electric field with amplitude of ~50 Vrms and frequencies from 200 KHz to 600 KHz.

Chapter 3: Wall effects on electrokinetic transport of particles in a rectangular microchannel

3.1 Introduction

Electrokinetic phenomena (i.e. electroosmotic flow, electrophoresis and dielectrophoresis) are very prevailing approaches to transport species and cells in many lab-on-a-chip devices as they provide significant advantages over the traditional pressure driven method. For the electrokinetic motion of a microparticle in an electrolyte solution, the velocity of such microparticle with arbitrary shape can be described by the well-known Smoluchowski formula, as described by equation (2.12). One of the important assumptions in the Smoluchowski formula is that the particle is transported in an infinite fluid domain and the effect of the particle volume on the local field is not taken into account. Although in most situations this assumption is reasonable, it becomes invalid when the particle size is comparable with the channel dimension because the electric potential distribution and the flow field around the particle are obviously disturbed by the presence of the particle. This is especially true for the case that the particle motion is close to the boundary at which the presence of device walls will significantly affect the particle transport. In this situation, the presence of the particle can significantly disturb the local flow field and electric

potential distribution. The disturbed electric and flow fields can in turn change the forces acting on the particle and thus affect the particle transport in the channel.

In the past decades, a number of studies have been reported to examine the solid wall effects on a microsphere transport in a microchannel. As summarized in the literature review, theoretical studies predicted that the solid wall effects on a particle have two competing aspects. When a large particle in a microchannel with a relatively greater separation, the electrophoretic mobility is less than which calculated by using the Smoluchowski formula due to the viscous retardation. However, once the particle moves close to the channel boundary with a very small particle-wall gap, electrophoretic mobility of the particle is enhanced due to a strong electric field generated within the narrow gap. The viscous retardation wall effect was qualitatively experimentally validated by transporting polystyrene particles in a microchannel with various channel heights (Xuan et al. 2006). However, the key parameter, i.e. the particle-wall separation, was unknown in those investigations. In fact, both the flexible control and precise measurement of the particle-wall gap in a dynamic particle transport system, especially at small particle-wall separation cases, are very difficult and also are critical to this problem.

In this chapter, an experimental technique is proposed to examine the solid channel wall effects on the electrokinetic transport of microspheres in microfluidic channels with respect to the flexible controlled particle-wall separations. Specifically, the particle-wall separations are modulated in the vertical plane by adjusting the

equilibrium height of the particle motion above the bottom wall within the microchannel. The equilibrium height of the particle motion depends on the force balance between the gravitational force against the wall-induced DEP force, and it could be flexible controlled with externally applied electric voltages. A simple experimental setup is employed with a side-mounted CCD camera to observe and capture the particle movement in the vertical plane. The dimensionless electrophoretic mobility are plotted to eliminate the effect of side channel walls. Furthermore, the numerical model is solved in a workstation with 128 GB RAM to describe the observed phenomenon and 3D numerical simulation is carried out to compare with the experimental results.

3.2 Theory

An illustration of electrophoretic transport of a microsphere in a rectangular microchannel is depicted in Figure 3.1. *a*, *b*, *d* and *h* denote the sphere radius, the distance from particle centre to the bottom wall, the channel height and the particle-wall separation, respectively. In most microfluidic experiments, particles (polystyrene microspheres, latex beads, biological cells, or macromolecules) are typically denser (~1020-1300 kg/m^3) than liquid fluid (water, ~1000 kg/m^3), and therefore particles tend to sink down to the bottom wall because of the gravity. When an electric field is turned on parallel to the solid wall, particle experiences a dielectrophoretic (DEP) force due to the presence of non-uniform electric field generated around the particle.

Such wall-induced DEP repels the particle from the solid wall and exactly balances the gravitational force at a certain particle-wall separation.

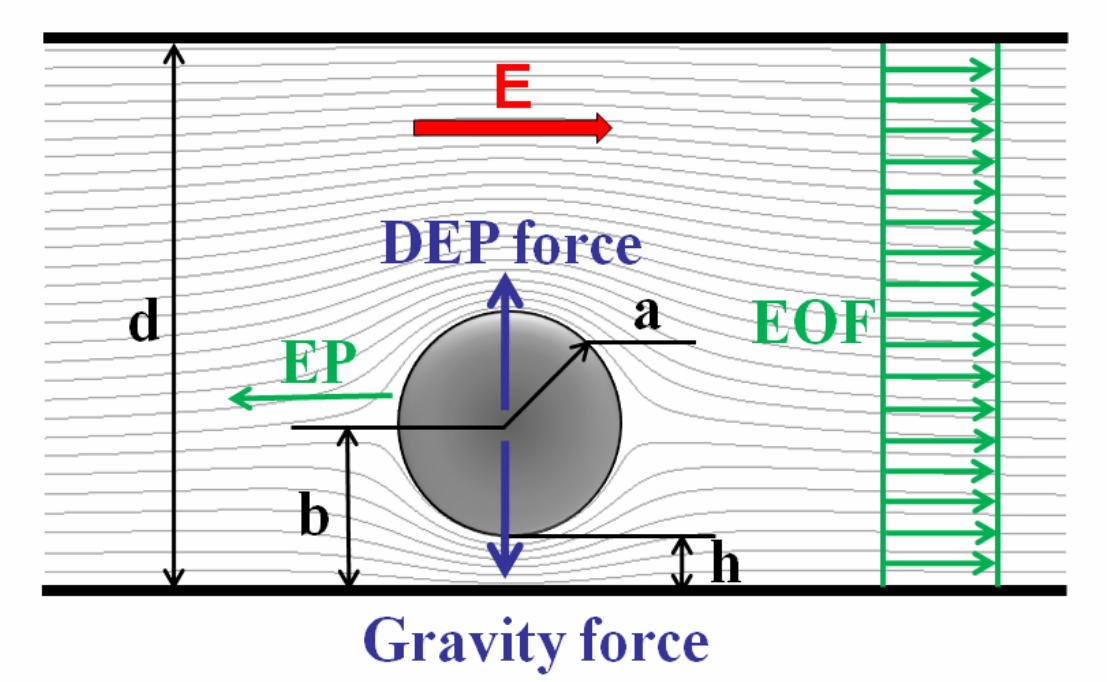

Figure 3.1 Illustration of electrophoretic transport of a microsphere in a bounded microchannel (front view). Light gray lines in the microchannel depict electric field lines with the presence of a nonconducting solid particle. (Not in scale)

The particle-wall separation above the bottom channel surface can be flexible controlled by balancing the gravity with the wall-induced DEP along the vertical direction. When particle motion in a microchannel at the steady state, the net force acting on the particle along the vertical direction is given by

$$\mathbf{F}_G + \mathbf{F}_{DEP} = 0 \tag{3.1}$$

where $\mathbf{F}_G$ and $\mathbf{F}_{DEP}$ are the gravitational force and the DEP force, respectively. The DEP force can be calculated with equation (2.18). The gravity force is expressed as

$$\mathbf{F}_G = \frac{4}{3}\pi a^3(\rho_p - \rho_l)\mathbf{g} \tag{3.2}$$

where ρ_p, ρ_l and $\boldsymbol{g}$ are respectively the densities of the particle and the liquid and the gravitational constant. By substituting equation (2.18) and (3.2) into equation (3.1), we have

$$\frac{(\rho_p - \rho_l)\mathbf{g}}{3\varepsilon \cdot K_{CM}} = \mathbf{E} \cdot \nabla \mathbf{E} \tag{3.3}$$

Notice that the left hand side of equation (3.3) is constant by applying a DC electric voltage. As a result, with increasing externally applied electrical field **E**, the gradient of the electrical field $\nabla\mathbf{E}$ should decline, yielding larger particle-wall separation gap. Therefore as soon as electric field is increased, the DEP force increases accordingly and thus break the force balance established earlier. In order to reach a new balance between DEP and gravitational forces, the particle must move further away from the channel wall to reduce the DEP force. As such, a larger particle-wall separation is reached at the new equilibrium and the balance between DEP and gravitational forces is reestablished.

3.3 Experiment

3.3.1 Experimental setup

A schematic of the experimental setup is shown in Figure 3.2. In order to directly observe particle motion in the vertical plane within rectangular microchannel, a CCD camera was mounted from side view. This is simply achieved by laterally turning an optical microscope (Zeiss, Germany) 90^{o} so that the object stage is perpendicular to the table surface. A DC power supply (Stanford Research, USA) was used to set up the driving electric field through two platinum wires placed into two reservoirs of the microchannel. The particle motion in the microchannel was monitored by the CCD camera and the captured digital images were recorded and processed by a personal computer.

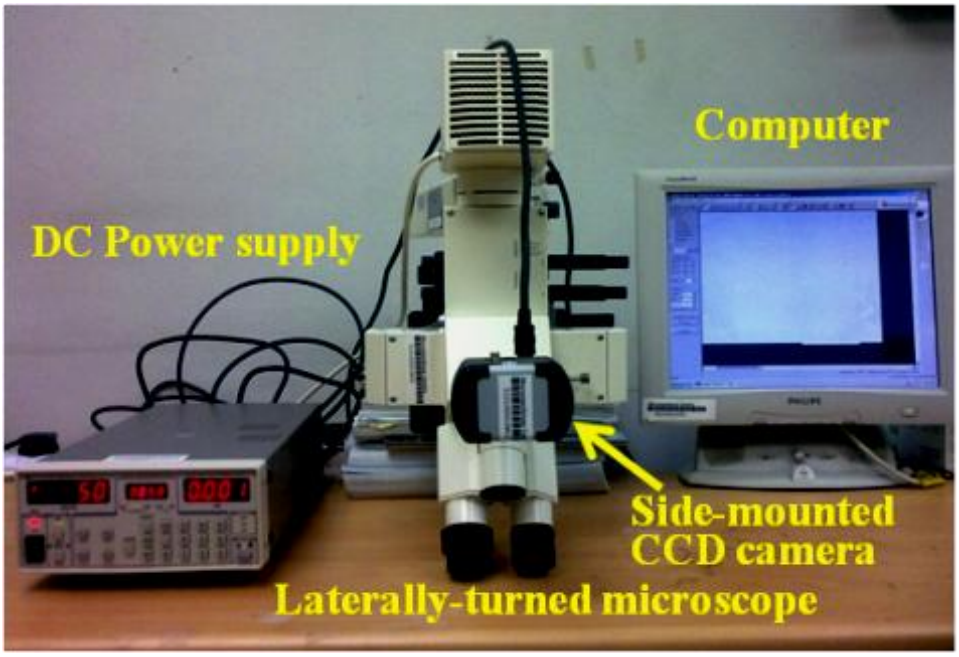

Figure 3.2 The experimental setup for the investigation of wall effects on electrokinetic transport of particles.

3.3.2 Microchannel fabrication

A 2 cm long rectangular poly-dimethylsiloxane (PDMS) microchannel with 100 μm in width and 250 μm in height was fabricated by using the well-established soft lithography technique (Whitesides et al. 2001). First a negative photoresist SU8 pattern was made by using the photolithography technique. Then liquid PDMS was casted on the silicon wafer, and baked in an oven at 85 ^{o}C for 1 hour. Later the cured PDMS slab with microchannel patterns was peeled off from the master mould, and finally bonded with another PDMS slab after with plasma treatment in an oxygen plasma cleaner (PDC-32G, Harrick Scientific, USA).

Due to the limitation of the photolithography technique, the side wall of the SU8 master mould actually is not smooth but rough. Walls of the PDMS channel peeled off from the SU8 mould are also rough and thus have low surface quality which would degrade the accuracy of measurement of particle-wall separation. To improve the surface quality of the channel boundary, we developed a protocol for assembling the microchip so that smooth PDMS surface can be used as the bottom channel wall during the course of experiment (see Figure 3.3). At this situation, the CCD camera was mounted in parallel to the PDMS-PDMS interface and was used for monitoring the physical process within the microchannel from side view. A PDMS slab with microchannel patterns and fluid reservoirs was peeled off from the master mould and bonded with another PDMS slab after plasma treated (Figure 3.3 (a)). The bonded PDMS chip was carefully cut into a cuboid (Figure 3.3 (b)). In order to improve the surface roughness from cutting, the rough surface was placed on a glass slide coated

with a thin film of Liquid PDMS (Figure 3.3 (c)). After baked into an oven at 85 ^{o}C for 1 hour, the PDMS gel was solidified and incorporated into the rough surface. Then the chip was peeled off from the glass slide and the surface quality of rough surface was greatly improved. We smoothed all rough surfaces by repeating the above procedure. Finally, the chip was turned 90^{o} with respect to Figure 3.3 (b) and bounded with a glass slide to form the final version of microchip. To facilitate the measurement of vertical particle-wall separation during the experiment, the entire microchip was turned 90^{o} with respect to Figure 3.3 (c) and observation was performed through an object lens beside the microchip, as illustrated in Figure 3.3 (d). A microchip used in our experiments is shown in Figure 3.4.

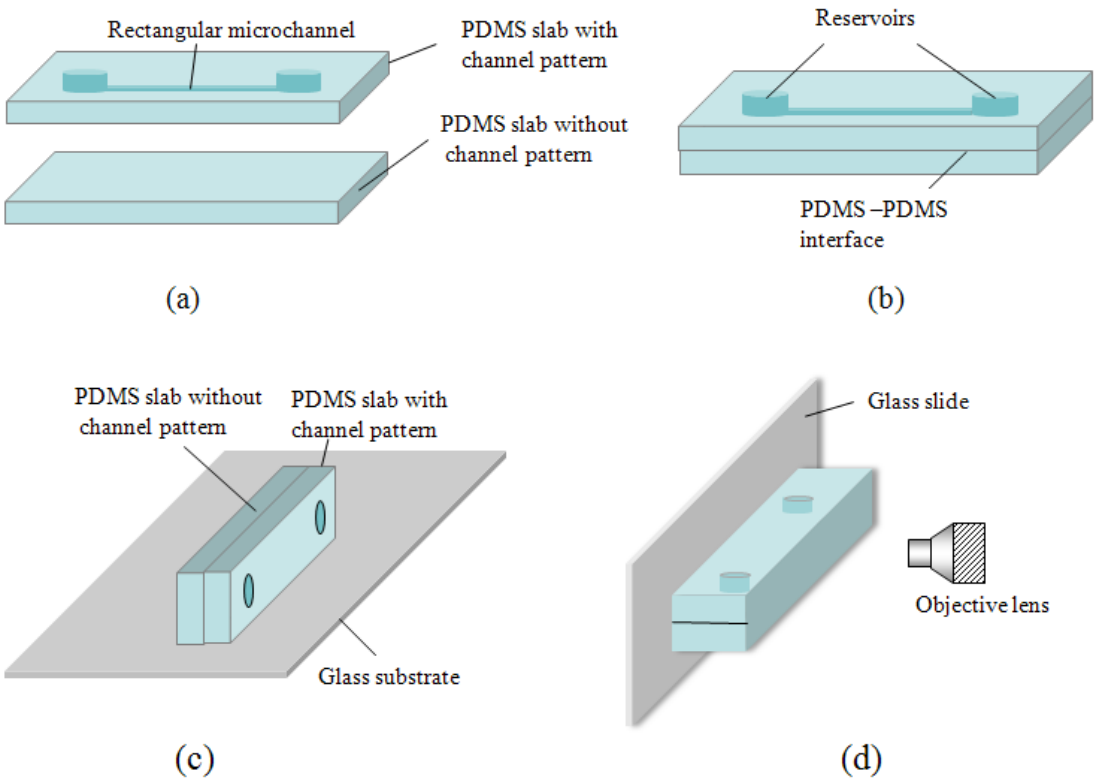

Figure 3.3 Schematic illustration of microchip fabrication. (a) the PDMS slab with microchannel pattern is obtained by soft lithography, (b) the PDMS slab with microchannel pattern is bonded with another PDMS slab, (c) a thin liquid PDMS layer is coated on a piece of glass substrate, and the PDMS slab is placed on the glass slide with its side profile contacted. (d) The PDMS chip is bonded with a glass slide and the device is observed from the side surface. As a result, the PDMS-PDMS interface was employed as the bottom channel wall during the experiment and the physical process within the microchannel could be readily observed from side view.

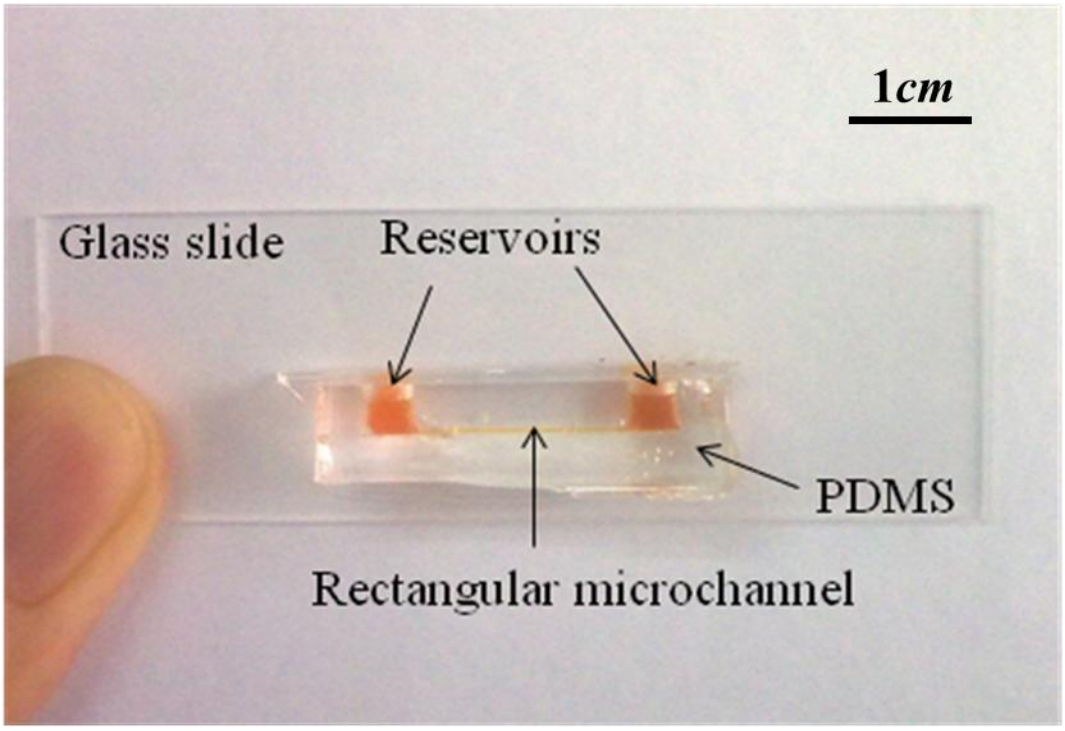

Figure 3.4 A photograph of the microchip used in the experiment.

3.3.3 Materials

Polystyrene microspheres (Duke Scientific, USA) with 15 μm, 30 μm and 40 μm in diameter were used in this study. The mixture of sodium bicarbonate (Sigma-Aldrich, Singapore) and DI water were used as carrier fluid. Prior to the test, the originally purchased particle solution was resuspended and diluted with 1mM sodium bicarbonate solution in order to allow the observation of only a single particle move into the viewing window.

3.3.4 Experimental method

Prior to experimental test, the PDMS microchannel was cleaned by soaking them in Acetone for 10 minutes followed by rinsing several times with DI water in an ultrasonic cleaner. Before apply the electrical voltages, the liquid heights of reservoirs were carefully balanced to eliminate the pressure driven flow motion. During the experiment, the direction of the applied electrical field was switched immediately after the particles velocity was observed and the opposite direction velocity was measured subsequently. By using this approach, the particle motion resulting from the external pressure difference can be further minimized once average the particle velocities in these two competing directions. In addition, to exclude the effects of two side walls on particle motion, an AC voltage with an amplitude of 300V and a frequency of 1kHz, obtained by amplifying the signal from a function generator (Agilent, USA) with an amplifier (EPA-102, Piezo System), were applied for at least 1min prior to each measurement to repel the particle to the centerline of channel by

means of DEP forces induced by side walls. Immediately after that, the particle motion in the microchannel was detected under DC electric voltages to examine the bottom wall effect on the near-wall particle transport. The DC voltages were varied from 20 V to 600 V with intervals of 5 V, 25 V and 50 V in the ranges of 20~100 V, 100~300 V and 300~600 V, respectively.

The particle motion was captured at a rate of 15 frames per second (fps) through the side-mounted camera under a 10× objective lens and was subsequently analyzed using the image processing software. The particle-wall separations were measured directly from the captured images with a resolution of 696×520 pixels. Particle velocities were determined by dividing the distance the particle travels by the corresponding time interval. The electrophoretic mobility of the particle was then obtained by dividing the particle velocity over the corresponding applied electric field.

3.4 Numerical simulation

In order to explain the experiment observation, a 3D numerical simulation is carried out with commercial software Comsol Multiphysics 3.4 (Comsol INC, Sweden). Comsol Multiphysics is a general Partial Differential Equation (PDE) solver using the Finite Element Method (FEM) and has several predefined modules. The geometrical parameters of particle and microchannel are chosen to be identical to those in the experimental conditions. It is assumed that:

(a) The particle and microchannel walls are rigid and non-conducting.

(b) The fluid within the microchannel is incompressible and a Newtonian fluid.

(c) The electric double layers (EDL) on the particle and microchannel boundaries are thin.

(d) The particle rotation is not considered.

The mathematic equations employed in the numerical simulation are provided below. Due to the thin EDL assumption, there is no free charge within the bulk fluid. Therefore, the electric field is governed by the Laplace equation

$$\nabla^2 \psi = 0 \tag{3.4}$$

together with the following boundary conditions,

$$\mathbf{n} \cdot \nabla \psi = 0 \text{, on the channel walls and particle surface} \tag{3.5}$$

$$\psi = 0 \text{, at the inlet} \tag{3.6}$$

$$\psi = \psi_0 \text{, at the outlet} \tag{3.7}$$

As the Reynolds number in the experiment is much smaller than 1 and only particle transport at the steady state is concerned, the Navier-Stokes equation (2.4) can be simplified to the Stokes equation

$$-\eta\nabla^2\mathbf{v}+\nabla p=0 \tag{3.8}$$

The flow field is governed by the Stokes equation and the Continuity equation (2.5), and they are subjected to the following boundary conditions,

$$p=0\text{, at inlet and outlet} \tag{3.9}$$

$$\mathbf{v}=\frac{\varepsilon\varepsilon_0\zeta_w}{\eta}(\mathbf{I}-\mathbf{nn})\cdot\nabla\psi\text{, on the channel wall} \tag{3.10}$$

$$\mathbf{v}=\mathbf{U}+\frac{\varepsilon\varepsilon_0\zeta_p}{\eta}(\mathbf{I}-\mathbf{nn})\cdot\nabla\psi\text{, on the particle surface} \tag{3.11}$$

where ζ_w and ζ_p are respectively the zeta potential of the channel wall and the zeta potential of the particle. $\mathbf{I}$ is the unit dyadic. $\mathbf{U}$ is the electrophoretic velocity of the microsphere, and it satisfies Newton's Second law as

$$m\frac{d\mathbf{U}}{dt}=\mathbf{F}_h \tag{3.12}$$

where *m* and *t* are the particle mass and time. According to the thin EDL model, the net force acting on the particle is the hydrodynamic force $\mathbf{F}_h$ only, which can be

obtained by integrating the hydrodynamic stress tensor $\boldsymbol{\sigma}_h$ with respect to the particle surface.

$$\mathbf{F}_h = \int_S \boldsymbol{\sigma}_h \cdot \mathbf{n} ds = \int_S \{-P\mathbf{I} + \eta[\nabla \mathbf{v} + (\nabla \mathbf{v})^T]\} \cdot \mathbf{n} ds \tag{3.13}$$

Here we neglect the EDL and van der Waals interactions between particle and bottom wall since the EDL thickness is negligibly thin in the present investigation (around 10 nm for 1mM sodium bicarbonate solution) and the van der Waals interaction takes effect only when separation is down to the order of 100nm or less.

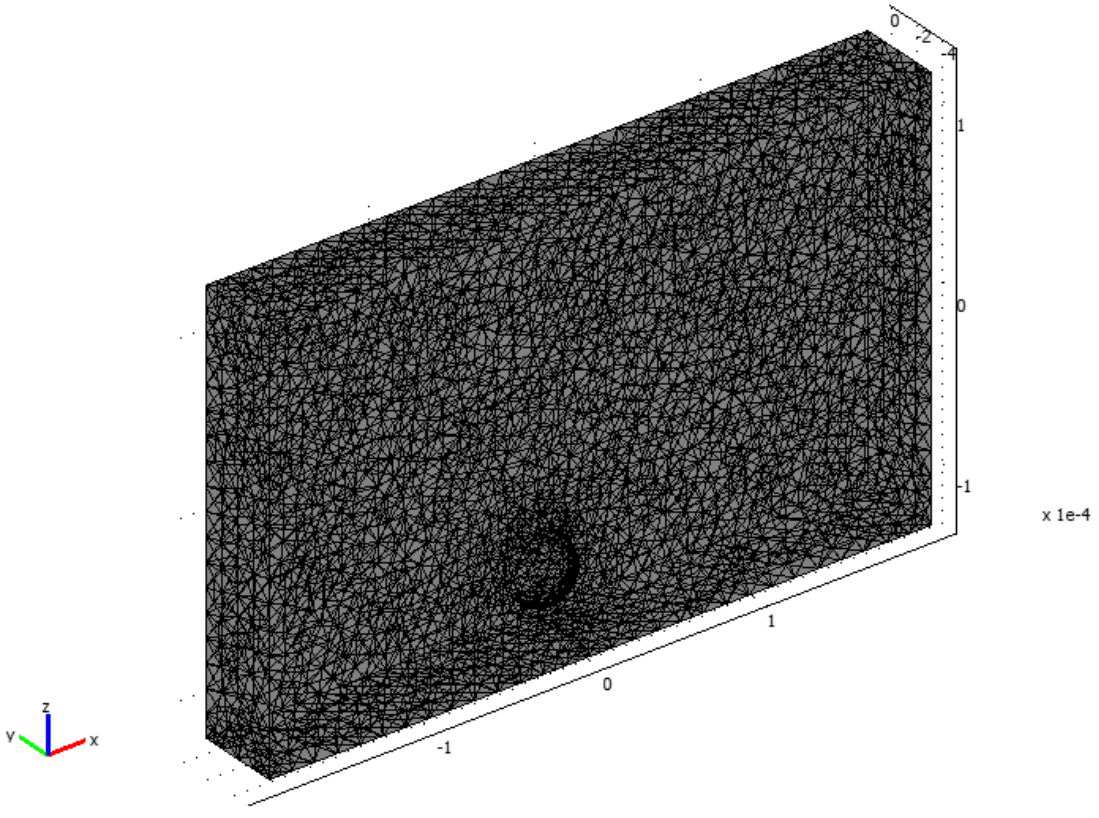

Figure 3.5 An illustration of 3D meshes used in the numerical simulation.

A 3D mathematic model based on above-described equations is established. The model is solved in a workstation with 128 GB RAM. Figure 3.5 shows a three-dimensional mesh generation in the numerical simulation. There are 297,279 tetrahedral mesh elements inside the domain, and the region near the particle surface is meshed more densely to accurately estimate the force acting on the particle. Due to the symmetry along the direction that is perpendicular to side walls, only half of channel was used as the simulation domain. Because the electric and flow fields are decoupled, so we solved the electric field first and then the flow field. The initial velocity of the particle transport is given by using the Smoluchowski equation.

To verify the numerical model, we simulated the electrophoretic motion of a particle in a large domain with dimensions to be 200 times of the particle diameter. The result obtained from the numerical simulation was then compared with the Smoluchowski equation and an excellent agreement was achieved. In addition, mesh independence was tested prior to the computation to ensure that all solutions obtained are fully convergent and independent of mesh density.

3.5 Results and discussion

The effect of the top channel wall on the particle motion vanishes because of the very large separation between particle and top channel wall. In the following, particle-wall separation exclusively refers to the separation between the particle and the bottom

channel wall. The electrophoretic mobility (μ) of the particle obtained in the experiment were normalized by a reference mobility (μ_r) to eliminate the effect of side channel wall, where μ_r is the electrophoretic mobility of the particle motion above the bottom surface at $a/b \approx 0.2$. As a result, the effect of side channel walls on the particle transport was cancelled once obtains the dimensionless electrophoretic mobility.

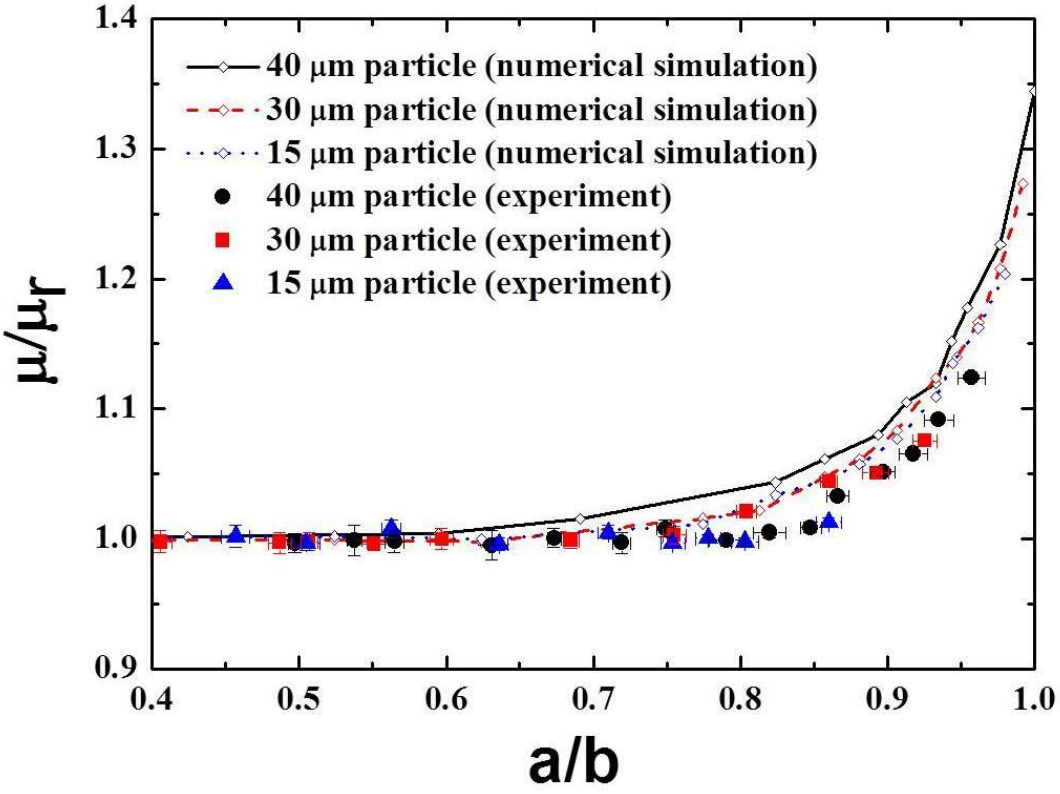

Figure 3.6 The relationship between the particle electrophoretic mobility against the particle-wall separations. Experimental data for 40 μm, 30 μm and 15 μm particles are signified by black circles, red squares and blue triangles, respectively. The black, red and blue solid curves suggest the numerical predictions for 40 μm, 30 μm and 15 μm particles.

Figure 3.6 depicts the variation of the electrophoretic mobility with the particle-wall separations for three sizes of particles. The largest particle-wall separation achievable in our experiment is limited to a/b=0.4. To achieve even larger particle-wall separations, extremely high strength of electric field must be required, and thus the electrophoretic motion of particles becomes too fast to be recorded with the camera used in our experiment. It is readily identified from the plot that at small particle-wall separations ($0.8< a/b <1$), the measured electrophoretic mobility is increased significantly. However, for relatively large particle-wall separations ($0.4< a/b <0.7$), the measured electrophoretic mobility is nearly a constant and rarely depends on the particle-wall separations. The numerical results can well predict the trend of experiment as shown in Figure 3.6, though there are quantative differences between these two. Such differences however could be due to the assumptions made for numerical simulations. In fact, the wall effects on electrophoresis have been attributed to two competing mechanisms: on one hand, the narrow gap between particle and channel wall leads to the enhancement of local electrical field because of the conservation of electric current, therefore accelerating the particle; on the other hand, the solid channel walls viscously retards the flow which in turn slows down the particle. The former effect dominates over the latter effect when the particle is close to the bottom wall, resulting in the increment of electrophoretic mobility due to the dominant enhancement of electric stress within the narrow gap.

The particle-wall separation for a moving particle is directly measured by counting the pixels from pictures captured during the experiment, as shown in Figure 3.7.

Prior to applying an electric voltage, the value of $a+b$ of a particle stay on the bottom surface of the microchannel was measured (Figure 3.7 (a)). For a moving particle above the surface with a separation under an externally applied electric field, the change of the value $a+b$ was then calculated and thus the particle-wall separation can be obtained (Figure 3.7 (b)). By using this method, the small particles-wall separation can be easily obtained. Due to the limitation of the measurement method, for the 15 μm particle, it is very difficult to accurately determine the particle-wall separation with an a/b value greater than 0.860. However, because $a/b = a/(a+h)$, more refined dimensionless particle-wall separations can be obtained by using larger particles. For example, with a 40 μm particle used in the experiment, a dimensionless particle-wall separation as great as 0.957 was accurately measured during the test.

The snap shots of particles transport in the microchannel at various particle-wall separations for 40 μm, 30 μm and 15 μm particles are demonstrated in Figure 3.8 (a), (b) and (c), respectively. By adjusting externally applied electrical voltages, the vertical positions of the particle transport were flexible controlled and could be readily observed by the side-mounted camera. As explained by equation (3.3), increasing applied electric field yields the reduction of $\nabla\mathbf{E}$ and thus enlarging the particle-wall separation. It should be pointed out that since the particle-wall separations were manipulated by varying externally applied electric voltages, stronger electric fields are required to provide an equal DEP force against the relative gravity force at higher equilibrium positions, and therefore yielding faster particle transport speeds as well. At the dynamic particle transport system, due to the limitation of the

camera speed, the particle images tends to a little bit blur at higher transport velocities, as shown in the smaller *a/b* cases.

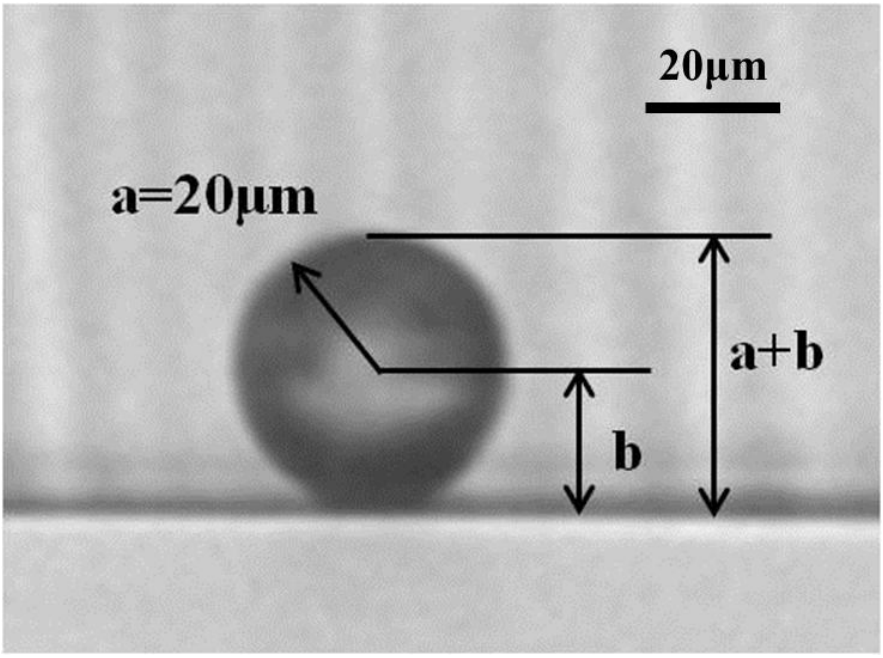

(a) *a/b* = 1

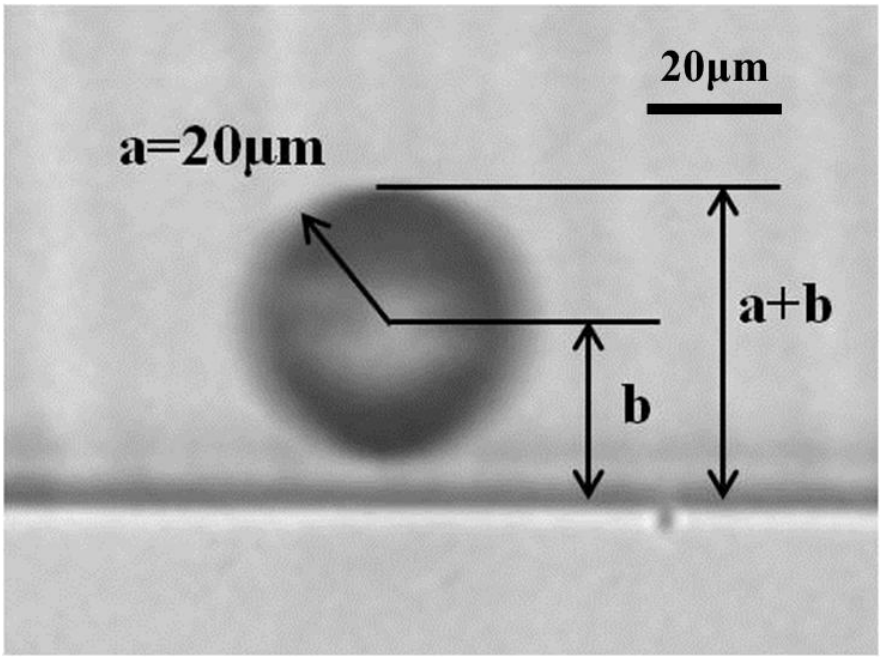

(b) *a/b* = 0.790

Figure 3.7 Measurement of particle-wall separations for a 40 μm particle.

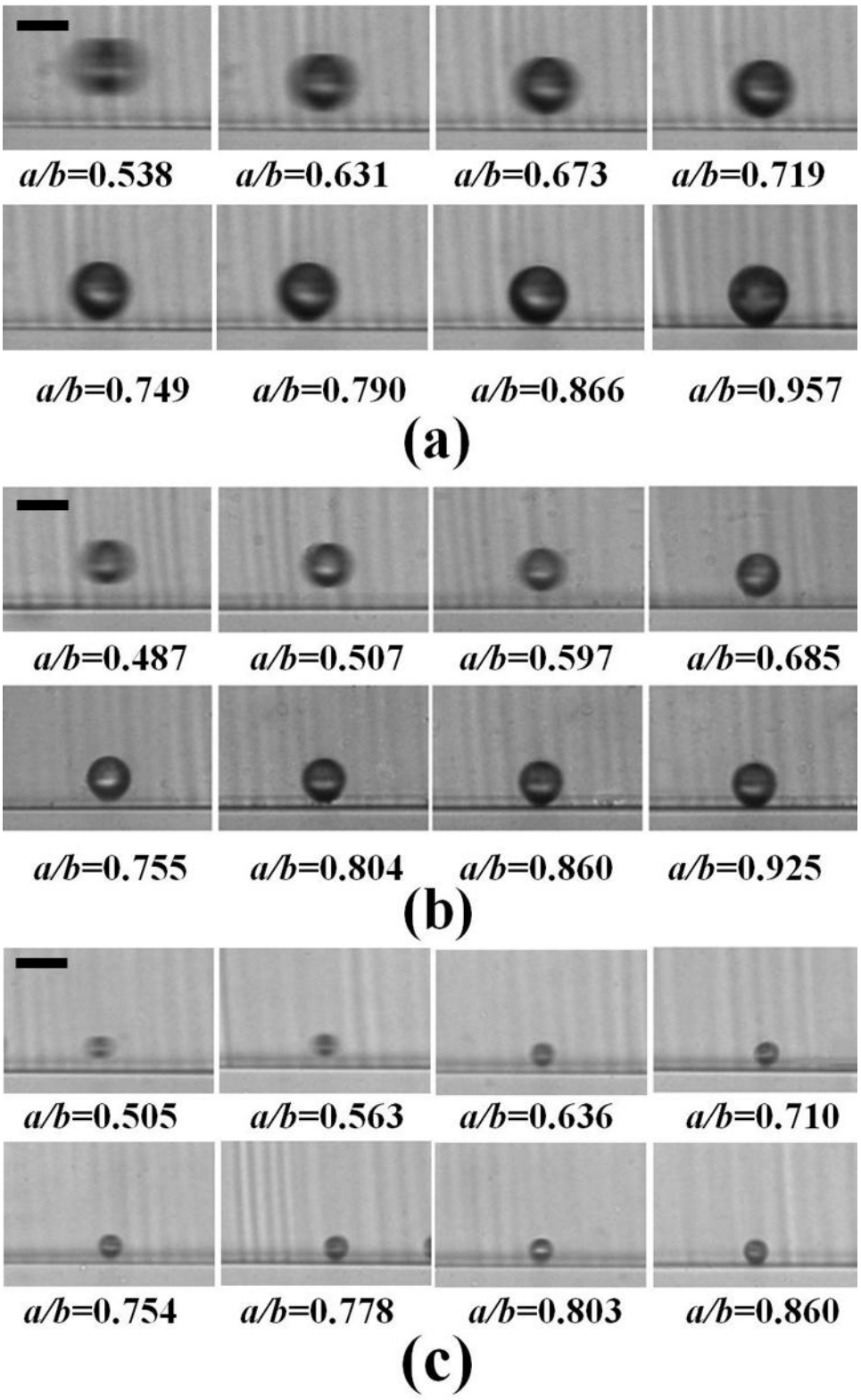

Figure 3.8 Snap shots of particle-wall separations for (a) 40 μm, (b) 30 μm and (c) 15 μm particles transport in a microchannel. Scale bars represent 40 μm. The

corresponding DC voltages are (a): 550V, 350V, 300V, 250V, 200V, 150V, 70V and 25V; (b): 600V, 550V, 450V, 350V, 200V, 100V, 65V and 35V; (c): 550V, 450V, 350V, 250V, 200V, 150V, 100V and 70V.

3.6 Summary

The solid wall effects on near-boundary electrophoretic transport of microspheres in a microchannel have been studied both experimentally and numerically in this chapter. To our best knowledge, this work is the first experimental investigation and observation of the velocity enhancement of electrophoretic transport of a microsphere near a solid boundary with flexible controlled particle-wall separations. In this study the focus was placed on the *x*-*z* vertical plane instead of the *x*-*y* horizontal plane and hence the narrow gap can be accurately adjusted by means of the force balance in terms of the DEP force against gravity. The utiliztion of DEP force to control the partial-wall separation is originated from the following reasons. (1) Electric signals promise high accuracy and much faster feedback than mechanical methods in microfluidic manipulations. (2) The use of DEP force to control the particles position in the microchannel does not affect the channel structure and provides a simple and low cost measurement without increasing the sophistication of the experimental setup. (3) As both DEP and near-wall EP velocity enhancement are introduced due to electric current conservation within the microchannel, the near-wall EP velocity variation can be sensitively modulated by adjusting applied electric voltage. In order to directly observe the particle displacement within the vertical plane, an

experimental setup is employed with a side-mounted CCD camera by laterally turning an optical microscope with 90^{o}.

Experimental results suggested that the electrophoretic mobility of a particle is pronouncedly enhanced with a decrease of the particle-wall separation. This is because as the narrow gap shrinks to a certain value, the effect of electric stress due to the squeezed local electric field can overcome the viscous retardation from the solid boundary, and thus the particle is accelerated. As the particle-wall separation is directly "read" from the images, the use of larger particles can realize the measurement with a smaller particle-wall gap. The experimental results are well described by the numerical simulations with good agreement.

Chapter 4: Continuous concentration of particles in a confined microfluidic chamber

4.1 Introduction

The fast development of microfluidics is due to its promising applications in chemical analyses and biomedical diagnoses such as DNA separation, enzyme assays, immunoassays, PCR amplification etc (Bousse et al. 2000). In most cell-based assays, the preconcentration of sample molecules and micro/nano particulates from the background medium is significant to the success of on-chip biomedical assays. It is well accepted that these particulates/cells in high concentration can not only directly improves the effectiveness of the biochemical detection and chemical reaction, but also facilitates the subsequent analytical and processing steps. Examples can be readily found in microbial analysis of water quality (Greenberg et al. 2005), gene hybridization process (Hames and Higgins 1995) and fluorescence-based bioassays (Visor and Schulman 1981).

Recently, with fast development of micro total analysis systems (μ-TAS) (Reyes et al. 2002) and labs-on-a-chip (LOC) (Stone et al. 2004) technologies, traditional benchtop sample processing methods are no longer satisfy the requirement of concentrating samples in microscale devices. Alternatively, a great many of microfluidic based

approaches regarding the on-chip particulates/cell concentration and manipulation have been addressed, such as hydrodynamic filtration (Yamada and Seki 2005; Aoki et al. 2009; Lee et al. 2010), electrokinetics (EK) (Dhopeshwarkar et al. 2005; Kim et al. 2006), dielectrophoresis (DEP) (Durr et al. 2003; Lapizco-Encinas et al. 2004; Chen and Du 2010) and ultrasonic wave (Li et al. 2007; Shilton et al. 2008; Zhang et al. 2009). In addition, microfluidic concentrators enable concentrating or manipulating particulates/cells in a continuous fluid flow rather than in a stationary medium, because of its potential capacity to process relatively large sample volume in microscale and produce high throughput.

The concept of hydrodynamic filtration relies on the fact that when particle are transported in the channel, the center of the particle cannot be present in a distance equals to particle radius from sidewalls (Yamada and Seki 2005). This method is performed by employing a microchannel network with a number of branch channels. By controlling and adjusting flow rate at each branch point, the particle concentration can be achieved. Nilsson et al. (2004) utilized an ultrasonic standing wave field to manipulate and concentrate suspended particles from the medium in a continuous flow. The particles were formed in lines and collected via the side outlets by means of acoustic frequency control. However, the channel has to be actuated by a piezoceramic plate at the back side of the chip. Electrokinetic approach is used to collect charged molecules/particles in a microfluidic device in terms of the combination of electroosmosis (EO), electrophoresis (EP) and hydrodynamics. To accomplish the concentration of particles, the externally applied electrical voltage

(normally in the order of several hundred to thousands volts) is inevitable. In addition, based upon the principle that particles can motion in a non-uniform electrical field resulting from the unbalanced force acting on the induced dipole of the particle, DEP is widely utilized in microfluidic systems to concentrate, manipulate, separate and sort particles, cells and bacteria (Pethig 2010). Either direct current (DC) (Chou et al. 2002; Chen and Du 2010) or alternative current (AC) (Durr et al. 2003; Chen et al. 2006) electric signal is employed to carry out DEP. The non-uniform electrical field is yielded by patterning asymmetric electrodes in the microchannel (i.e., electrode-based DEP) or using only two simple electrodes that straddle an insulating structures array (i.e., insulator-based DEP). More recently, Shafiee et al. (2010) successfully exhibited the enrichment of biological particles in an insulator-based microfluidic system. This so called contactless DEP system incorporates side liquid electrodes adjacent to the main microfluidic channel and they are separated by a thin dielectric barrier. By applying a high-frequency electric field, they claimed that this method is able to concentrate 2 μm polystyrene beads and THP-1 human leukemia cells from a heterogeneous sample solution.

Although various particles enrichment approaches have been successful developed, instinct limitations are easily found in these methods. The microfluidic configuration in hydrodynamic filtration is so complicated and the precise flow rate control in each branch channel is of vital significance to the concentration performance. Similarly, acoustic method needs a piezoceramic plate to generate ultrasonic standing wave, which increases the cost of the device and complexity of the operation. Electrokinetic

and DEP methods have to work under a strong externally applied electric field either in intensity and or in frequency. In this chapter, a method for rapid and continuous particles concentration in a confined microfluidic chamber is presented. The confined microfluidic chamber consists of a pair of metal electrodes embedded at two side walls. By applying a very low DC electric voltage (a few volts), particles enrichment is achieved in the confined chamber with a short time. The structure of the microfluidic concentrator is very simple and is fabricated using the conventional soft lithography. A novel copper imbedding method is used to create 3D side wall electrodes within the confined microfluidic chamber.

4.2 Experiment

4.2.1 Microchannel configuration

The configuration of microchannel used in the experiment for particles concentration is shown in Figure 4.1. The microchip was fabricated by using a PDMS slab with microchannel structures and it was bonded with a piece of glass slide. The sample flow was fed to the microchannel through plastic tubes connected with needles inserted into the PDMS slab. The entire microchannel configuration is 2 cm in length and 100 μm in depth with a confined microfluidic chamber designed at the center of the channel. The dimension of the confined chamber is 400 μm × 400 μm. Two 40 μm wide “gates” are designed at each side of the confined chamber to facilitate the sample fluid access.

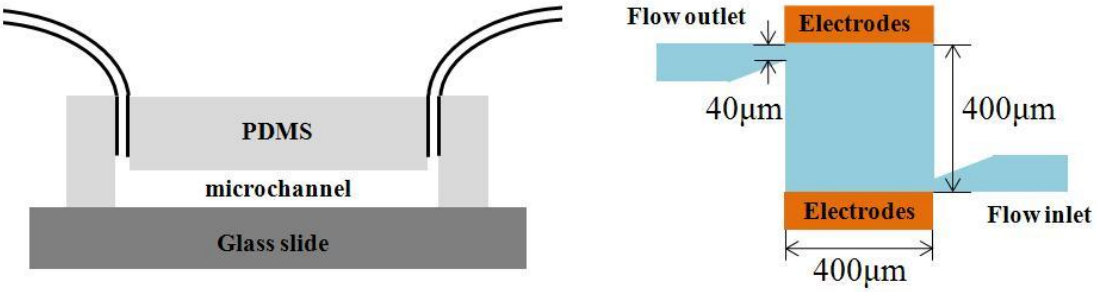

(a) (b)

Figure 4.1 Schematic illustration of microchannel configuration. (a) Cross sectional view of the microchannel along the depth direction. (b) Top view of the section of confined chamber.

4.2.2 Microchannel fabrication

The microchip was fabricated with poly-dimethylsiloxane (PDMS) using the standard soft lithography method. A pair of side-wall copper electrodes was embedded into the microchannel to yield an electric field across the confined microfluidic chamber. The fabrication procedure of the microchannel with copper electrodes is demonstrated in Figure 4.2. The 100 μm thick copper foil (Sigma-Aldrich, Singapore) was carefully incised as small pieces with the dimension of 0.5 mm×8 mm approximately and was folded as L-shape. First, the master (Figure 4.2(a)) was casted with a droplet of liquid PDMS around the SU8 mold to form a thin liquid PDMS layer (Figure 4.2(b)). Subsequently, a pair of L-shape copper foils was emplaced at the designed positions. External forces were provided horizontally in parallel to the wafer surface towards the center (as indicated by the arrows in Figure 4.2(c)) to push the copper foils tightly

connect to the SU8 patterns. The silicon wafer with copper electrodes was immediately baked at 90 ℃ on a hotplate for half minute (Figure 4.2(c)) in order to fix the copper electrodes with the cured PDMS. The mold was then poured over by the PDMS mixture of 10:1 mass ratio of prepolymer and curing agent (Figure 4.2(d)). After being degassed into a vacuum oven for 30 minutes, the liquid PDMS was cured into a convection oven (Binder, Thermal Fisher Scientific, USA) at 80 ℃ for 1 hour. Once cured, the PDMS with the channel portion was peeled off from the mold (Figure 4.2(e)) and two 0.5-mm-diameter holes were punched vertically at each end of the channel to form the inlet and outlet. Finally, the PDMS slab with the channel portion and a clean glass slide were bonded to form the microdevice (Figure 4.2(f)) after plasma-treated in oxygen plasma cleaner (PDC-32G, Harrick Scientific, USA) for 45 s and heating at 80 ℃ for 10 min.

The microchip used in the experiment is shown in Figure 4.3. It is seen that the copper electrodes contact tightly with PDMS microchannel and a confined microfluidic chamber with side-wall electrodes is thus formed.

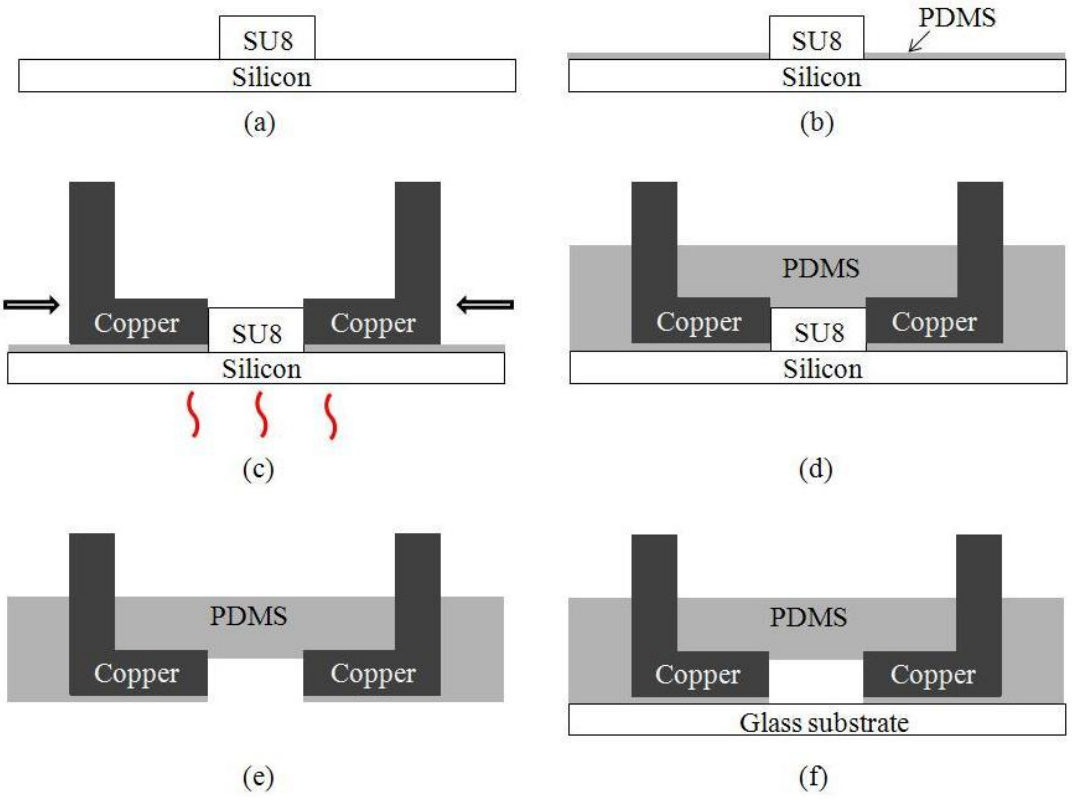

Figure 4.2 Schematic illustration of the fabrication steps for a microchannel with copper electrodes. (a) the master mold including SU8 patterns, (b) a thin PDMS layer was coated on a silicon wafer, (c) L-shape copper foils were emplaced and then heated on a hotplate, (d) liquid PDMS was poured over the mold, (e) Peeling off the PDMS film, and (f) bonding the PDMS slab with a glass slide.

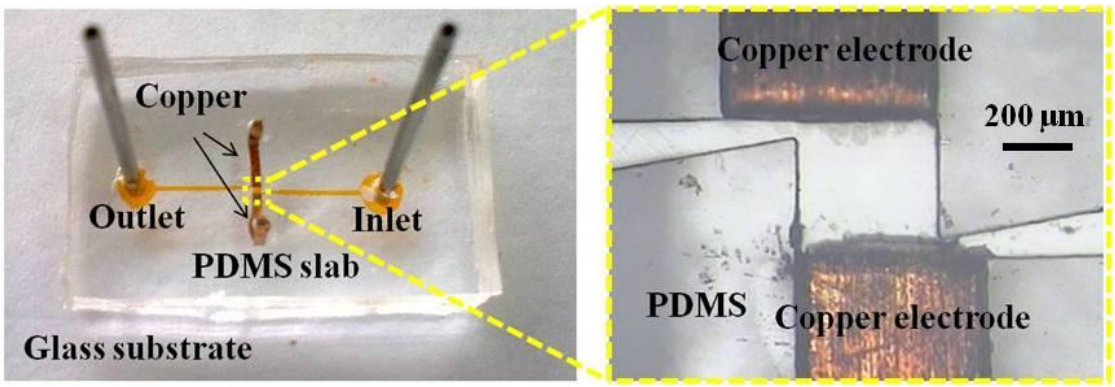

(a) (b)

Figure 4.3 The microchip for particles enrichment used in the experiment (a) A photograph of the PDMS microchannel and (b) A microscopy image of the confined microfluidic chamber.

4.2.3 Materials and method

In order to test the performance of particles concentration in the present device, fluorescent polystyrene microspheres (Duck Scientific, USA) with the sizes of 1 μm, 0.5 μm and 0.1 μm in diameter were used in this experiment. Deionized (DI) water and 0.01mM and 0.1 mM Sodium chloride (Sigma-Aldrich, Singapore) solutions were employed as the medium solvent. Prior to the test, the original particle solution was dehydrated with a centrifuge machine and resuspended in the media solvent to obtain a 500-time-diluted sample solution. Before each experiment, the microchip was treated with 5% bovine serum albumin (BSA) for 4 hours to minimize the particle adhesion to channel walls. Before applying electrical field, the sample solution was transported through the entire test section from inlet to outlet for few minutes to obtain a steady flow rate.

To examine the physical process of microparticles enrichment in the confined microfluidic chamber, 1 μm fluorescent microspheres was firstly used and resuspended in DI water to form a 500 times diluted solution. An 8 V DC electric voltage was provided across the copper electrodes, yielding a 20 kV/m electric filed along the vertical direction within the confined chamber. The diluted sample solution was introduced into the chamber from bottom right corner inlet and went out through the top left corner outlet by the syringe pump at a 0.5mL/h volume flow rate. The fluorescent intensity variation of particles in the confined chamber was recorded after the voltage is turned on. Subsequently, the effects of applied electric voltage, feeding flow rate, electrolyte solution and particle size were studied by varying experimental conditions accordingly.

4.2.4 Experimental setup

The experiment setup is illustrated in Figure 4.4. The electric field was generated by applying a DC voltage across the copper electrodes. The antennas of the L-shape electrodes were connected directly to a constant DC power source (GPS-3030DD, GW Instek, Taiwan) which provides uninterrupted power supply during the course of the experiment. The diluted sample solution was introduced into the test section and fed by using a syringe pump (LSP02-1B, Longer Pump Co, PR China). Plastic tubes were employed to link the syringe pump and needles inserted into the PDMS microchannel. The motion of particles within the test section was imaged and recorded by using an inverted microscope (Nikon TE-2000U, Japan) equipped with a cooled monochrome camera (Retiga Exi) for optical observation and a mercury arc

lamp for fluorescent excitation. The acquired images were transferred to a computer for further analysis and were processed using the image software NIS Elements AR.

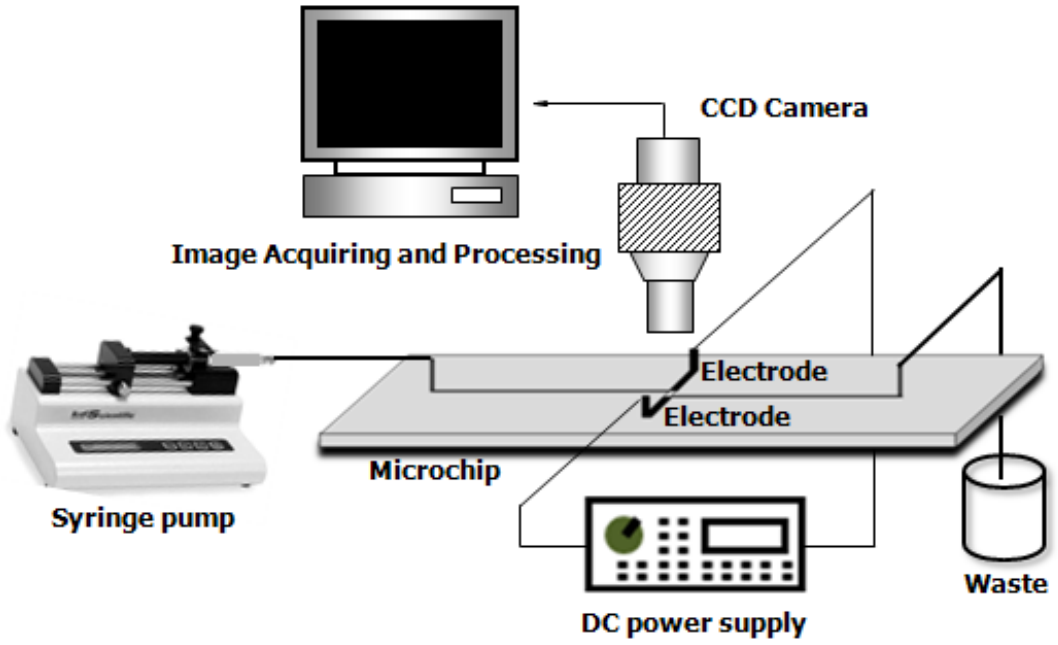

Figure 4.4 Schematic of the experimental setup.

4.3 Mathematical model

A mathematic model is established to describe the physical process of particle enrichment within the confined microfluidic chamber under an externally applied electric field. The physical problem is formulated in *x*-*y* two dimensions only because previous studies have suggested that 2D model can sufficiently capture the transport phenomenon with both good accuracy and economic computational costs. The

computational domain is strictly focused on a rectangular microfluidic chamber as shown in Figure 4.5. Several assumptions are made as follows:

(a) The fluid in the microchannel is incompressible and Newtonian;

(b) The flow is laminar flow and in the steady-state;

(c) The electrical charges on the channel surfaces are uniformly;

(d) The temperature within the microchannel is uniform and constant.

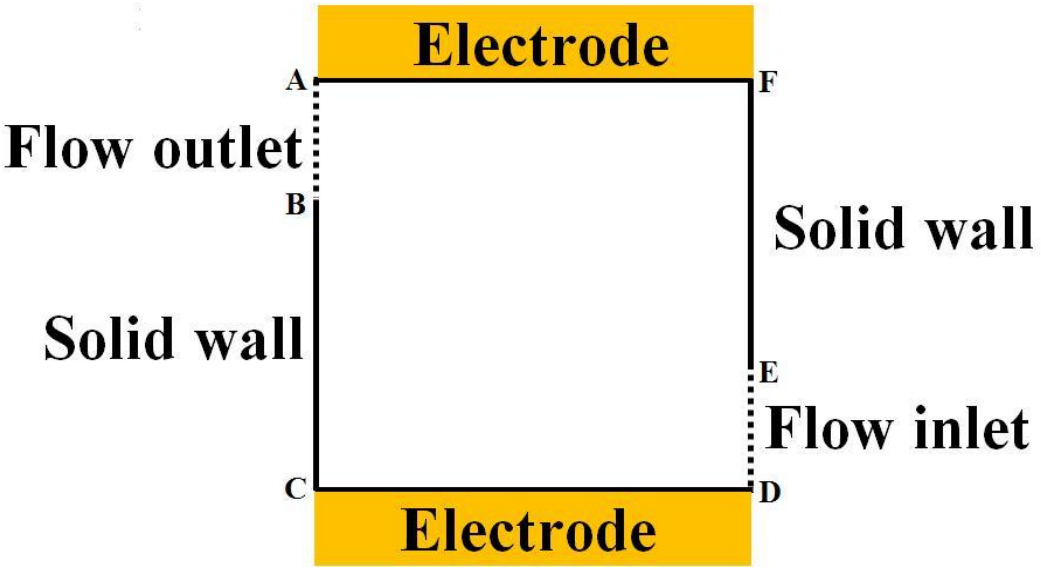

Figure 4.5 Sketch of the computational domain.

As the particle enrichment within the confined microfluidic chamber involves multi-physical problems including electric potential distribution, momentum transport and mass transport, a multi-physical mathematic model is developed to simulate the complex phenomena.

The electric field in the bulk fluid satisfies the Laplace equation

$$\nabla^2 \psi = 0 \tag{4.1}$$

The boundary conditions on the electrodes surfaces AF and CD are set as specified electrical potentials and the rest boundaries are electrical insulation.

Since the flow considered in the microfluidic system is usually of creeping type with very small Reynolds number, the incompressible fluid flow at the steady state can be governed by the Navier-Stokes equation and the Continuity equation,

$$\rho \mathbf{v} \cdot \nabla \mathbf{v} = -\nabla p + \eta \nabla^2 \mathbf{v} \tag{4.2}$$

$$\nabla \cdot \mathbf{v} = 0 \tag{4.3}$$

The non-slip condition $\mathbf{v} = 0$ is employed on the electrodes surfaces AF and CD due to the equipotential and the slip condition $\mathbf{v} = -\varepsilon\varepsilon_0\zeta_w\mathbf{E}/\eta$ is used at the chamber walls BC and EF due to the EOF, where ζ_w denotes zeta potential on the solid walls. The flow is introduced into the confined chamber at inlet DE with a normal inflow velocity $\mathbf{V}_0$ and at the outlet AB the back pressure is set as zero.

Because the microspheres used in the experiment are much smaller than the microchannel, the particle enrichment process within the microfluidic chamber can be described by the mass transport equation,

$$\frac{\partial C}{\partial t} + \nabla \cdot (\mathbf{v} + \mathbf{v}_{ep})C = D\nabla^2 C \tag{4.4}$$

where C, t and D are resepectively the concentration of microspheres, time and mass diffusion coefficient of the particles solution. $\mathbf{v}_{ep}$ is the electrophoretic velocity of charged particles under the externally applied electric field. $\mathbf{v}_{ep}$ can be calculated by using the theory addressed in Chapter 2, i.e. $\mathbf{v}_{ep} = \mu_{ep}\mathbf{E}$ (where μ_{ep} is the electrophoretic mobility of charged particles). The mass diffusion coefficient of microspheres can be estimated from the Stokes-Einstein relation,

$$D_{\mathrm{p}} = \frac{K_b T}{6\pi\eta a} \tag{4.5}$$

where D_{p} is the diffusion coefficient of microspheres calculated with the above equation and a is the radius of the microsphere. However, many studies have suggested that the utilization of D_{p} directly obtained from the Stokes-Einstein relation is hardly to reflect the actual physical process. The underlying reasons can be possibly explained as follows. Firstly, in the mathematic model the particle-particle and particle-wall interactions are not included. Due to the existence of EDL on the particles and solid walls, the EDL repulsive force among particles and chamber walls are extremely significant when the inter-particle distance and particle-wall distance are very small. This is especially true when microspheres are enriched at a very small volume within the confined microfluidic chamber (Zhao 2012). Secondly, in the

mathematic model the viscosity of the particles is assumed constant and identical with the value of water. Indeed, for the solution with microspheres suspended, the viscosity is not a constant value but depends on the particle size and volume fraction of particles. Especially for the small space where microspheres are concentrated, the local viscosity is totally different from that of the pure solution. Thirdly, as the dielectric permittivity of particles is much lower than the medium fluid, induced dipole is therefore generated within the microspheres when an externally electric field is applied. Such induced dipole tends to arrange microspheres as chain structures along the electric field and it is competing to the enrichment effect which accumulates particles at a small space. As a result, correction of equation (4.5) is suggested by introducing a correction factor *c* and then the mass diffusion coefficient of the particle solution can be rewritten as,

$$D = cD_{\mathrm{p}} = \frac{cK_bT}{6\pi\eta a} \tag{4.6}$$

It is quite difficult to determine such correction factor *c* as it can depend on the surface charge density of the particles, the dielectric properties of the particles and the volume fraction of the microspheres. However, since the dependence of *c* on these factors is complicated and unknown, a zero-order approximation is applied in this study by assuming that the correction is constant for a specified particle size.

The governing equation (4.4) is subject to the following boundary conditions. Since the particles are introduced into the confined microfluidic chamber from the inlet

boundary, the particles concentration should be as same as the initial particles concentration at DE. At the flow outlet AB it is assumed that microspheres only go through convectively and hence convective flux boundary condition is employed. At the rest boundaries, particles cannot penetrate through the chamber wall and thus impermeable boundary conditions are applied. Furthermore, at the initial state, the confined chamber is filled with the inflow particle solution, so the initial condition is $C = C_0\big|_{t=0}$. A summary of all boundary conditions specified for solving the three governing equations are listed in Table 4.1.

Table 4.1 Summary of boundary conditions specified in the mathematic model.

Governing equations / Boundaries	Electric field	Flow field	Mass transport
AB	Insulation	Zero pressure	Convective flux
BC	Insulation	EOF	Impermeable
CD	Electric voltage	Non-slip velocity	Impermeable
DE	Insulation	Inflow velocity	Specified concentration
EF	Insulation	EOF	Impermeable
FA	Grounded	Non-slip velocity	Impermeable

The mathematic model is solved by using Comsol Multiphysics 3.4 (Comsol INC, Sweden). The computational domain is meshed with triangular elements. Because the

electric field, flow field and concentration field are not coupled, it is thus reasonable to solve the steady state electric field and flow field firstly. After that, the transient mass transport is calculated subsequently by using the results obtained from the first step. The electrophoretic mobility $\mu_{eo}=3.5\times10^{-4}$ $cm^2V^{-1}s^{-1}$ is used in the numerical simulation. The test of mesh independence is conducted prior to the computation to ensure that all the solution obtained is not dependent on the grid density.

4.4 Results and discussion

4.4.1 Particles enrichment within the confined chamber

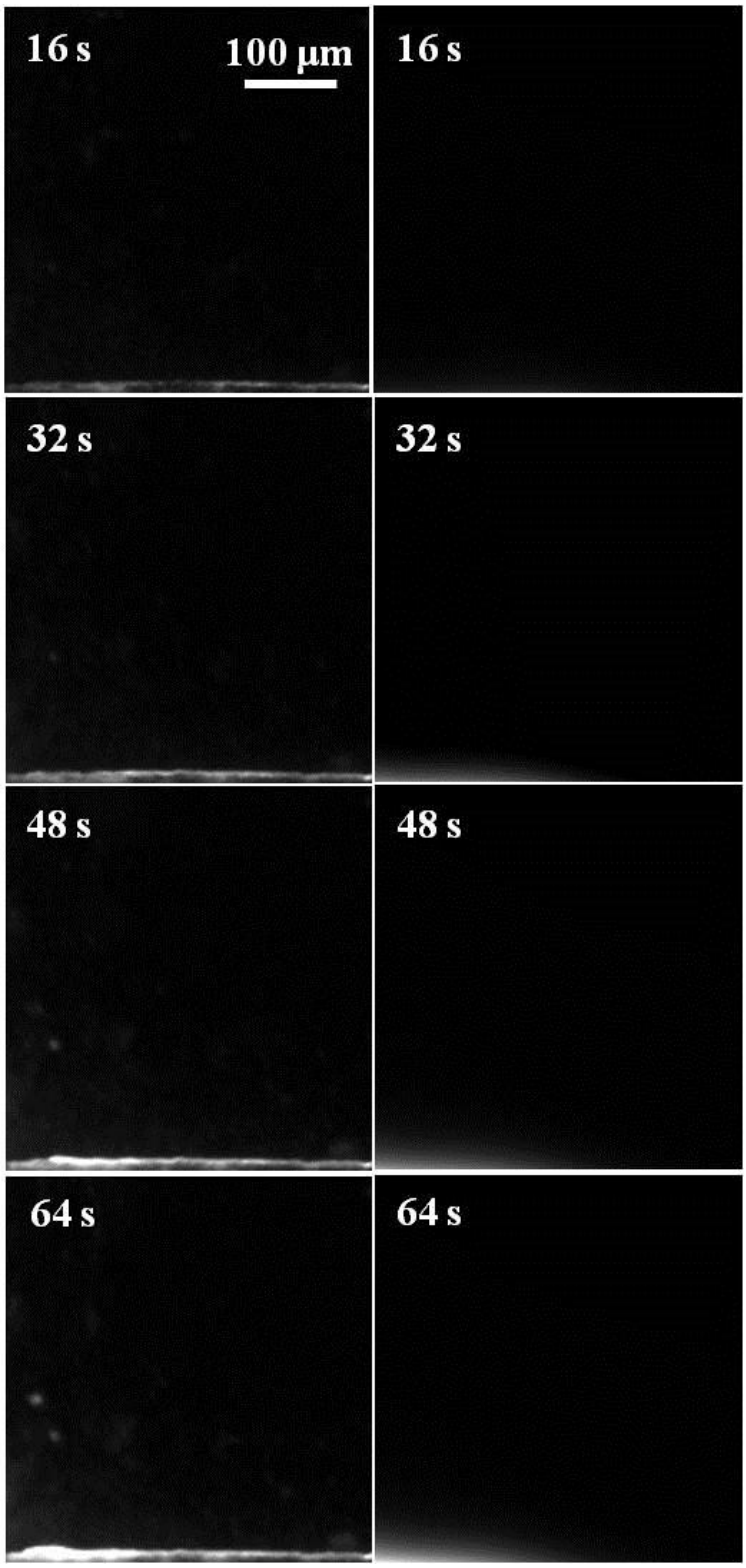

Figure 4.6 Sequential images of the enrichment process of 1 μm particles in the confined microfluidic chamber. Images sets in the left hand side and right hand side

show experimental observations and numerical simulations respectively with a time interval of 16 s. The flow inlet and outlet are emplaced at the bottom right corner and the top left corner respectively. Electric field is applied vertically within the chamber from bottom to top.

Figure 4.6 shows the particle enrichment process with time elapse in the confined microfluidic chamber. The experimental observations and numerical simulations are demonstrated in the left hand side and right hand side, respectively. The flow inlet and outlet are placed at the bottom right and top left of the confined microfluidic chamber, respectively. It is pronouncedly noticed that particles are rapidly enriched at the lower left region within the confined chamber. In fact, once moving into the confined chamber, a strong electrophoretic force towards the bottom anode is added on the particles due to the Coulombic attraction. At the same time, the particles also experience a hydrodynamic force because of the fluid flow. The combination of these two forces, therefore, attracts particles to the lower left corner of the confined chamber and traps them with chamber boundaries.

In order to quantify the trapping efficiency within confined microfluidic chamber, the fluorescent intensity of trapped particles, which reflects the local particles concentration, was measured during the experimental process. Image sequence was capture under the fluorescent microscope and was then analyzed with an in-house code. Because the calibration suggests a linear relationship between the fluorescent intensity and the particle concentration, the particle concentration can be readily

converted from the experimentally measured fluorescent intensity (Ge 2011). Before the device was energized, the mean fluorescent intensity of the 500-time-diluted sample solution was analyzed and set as reference. The maximum fluorescent intensities of particles in the confined chamber at each time step were then detected during the experimental course and were normalized by the reference subsequently, suggesting the particles concentration efficiency as time elapse.

4.4.2 Effect of applied electric voltage

The effect of applied electric voltages on the microspheres enrichment process within the confined microfluidic chamber is depicted in Figure 4.7. The electric voltages of 8V, 6V and 4V are applied and the rest parameters are held unchanged. The results suggest that the trapping efficiency rises dramatically with the increment of the electric field within the trapping region. As applied electric voltages drop, the electrophoretic force acting on the microspheres is weakened, yielding a decline of particles trapping efficiency.

To simplify the computation, numerical results shown in the figure are obtained with a constant correction factor c. It is found that the simulation results can give a close match to most of the experimental observations by setting $c = 466$. As the correction factor c is related to the local microspheres concentration, it can be readily inferred that the actual mass diffusion coefficient D of the microsphere is a space and time-dependent function. At the initial stage of the microspheres enrichment process, the

local concentration of the microspheres at the trapping area is low, resulting in an overestimation of the correction factor *c*. As results, the experimental observations are greater than that of the numerical simulations. However, the difference between experimental and numerical results reduces with time elapse and a good agreement is found once higher microsphere concentrations are achieved.

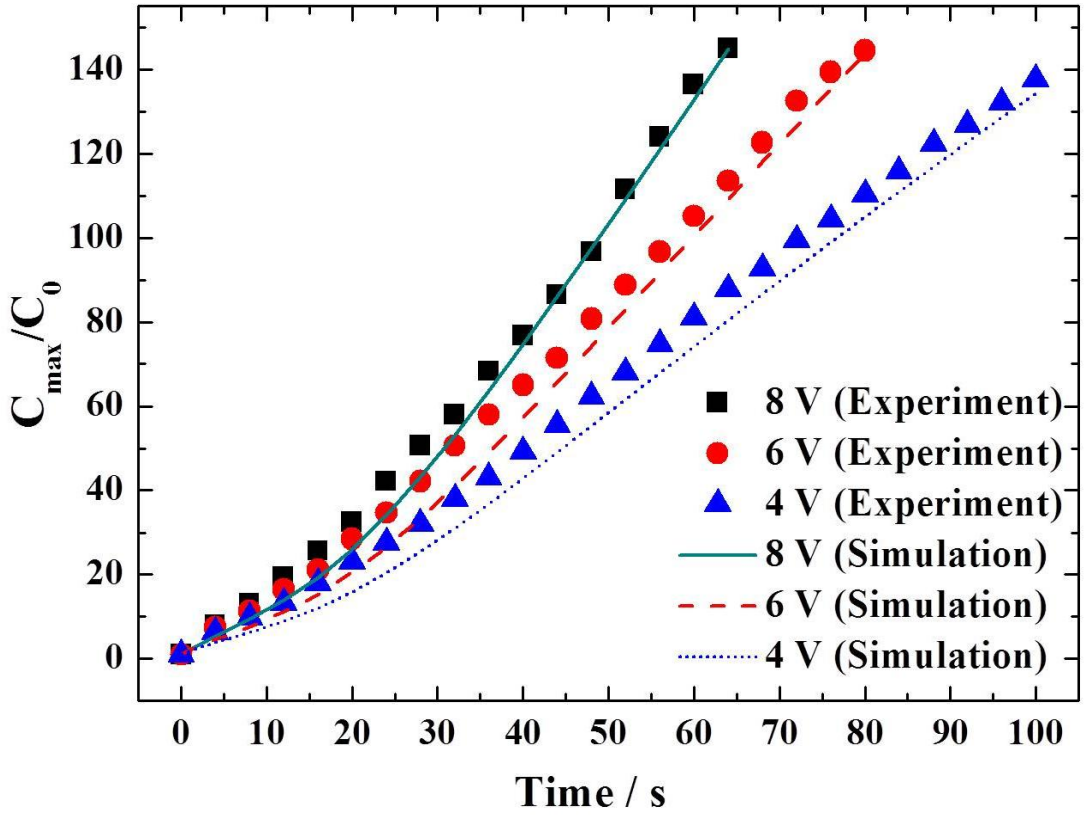

Figure 4.7 The particle enrichment varies with the applied electric voltage. Symbols and curves indicate experimental results and numerical simulations, respectively. Experimental results plotted in the figure were captured every 4 seconds. c = 466.

4.4.3 Effect of feeding flow rate

Figure 4.8 shows the effect of flow rate on the particles concentration within the confined microfluidic chamber. The results suggest that the reduction of feeding flow rate can lead to a significant decline of maximum particles concentration C_{max} within the confined chamber. Indeed, at the region above the bottom electrode, the flow velocity has a very smaller vertical component but a much greater horizontal component. Therefore, the drop of horizontal flow velocity is much pronouncedly than the vertical flow velocity decrease at this region due to the reduction of feeding flow rate. At a lower feed flow rate, the microspheres are concentrated "evenly" on the electrode surface because of a small horizontal flow velocity above the electrode, yielding a lower maximum particles concentration C_{max}. On the contrary, at a higher feeding flow rate, particles above the bottom electrode are swept to the left hand side due to a significant horizontal flow velocity and concentrated at a small volume within the confined chamber, therefore yielding a higher maximum concentration C_{max} (as shown in Figure 4.9). In addition, the flow field within the confined microfluidic chamber is dependent on the combination of externally pressure driven flow and EOF induced by chamber boundaries. As the feed flow rate drops, the effect of EOF on the flow field becomes increasingly significant. The wall induced EOF, especially in the *z* direction (the direction perpendicular to the computational domain), can generate vortex within the confined chamber and therefore weaken the microspheres enrichment effect.

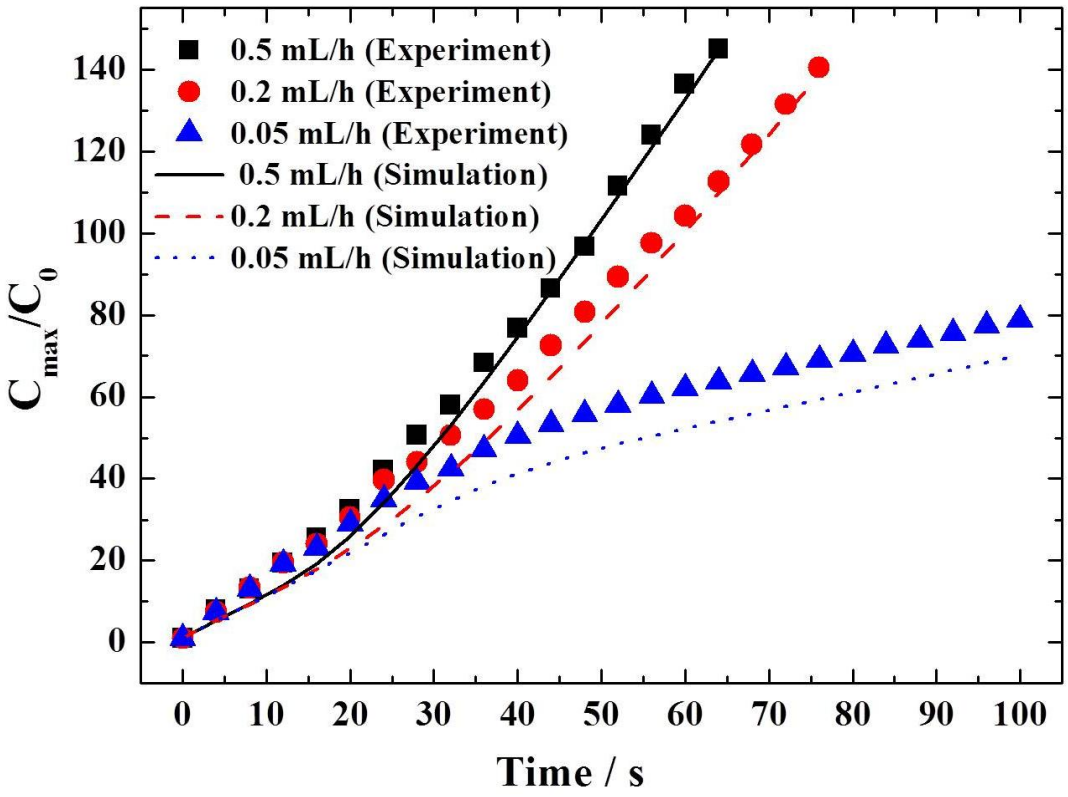

Figure 4.8 The particle enrichment varies with the feeding flow rate. Symbols and curves indicate experimental results and numerical simulations, respectively. Experimental results plotted in the figure were captured every 4 seconds. c = 466.

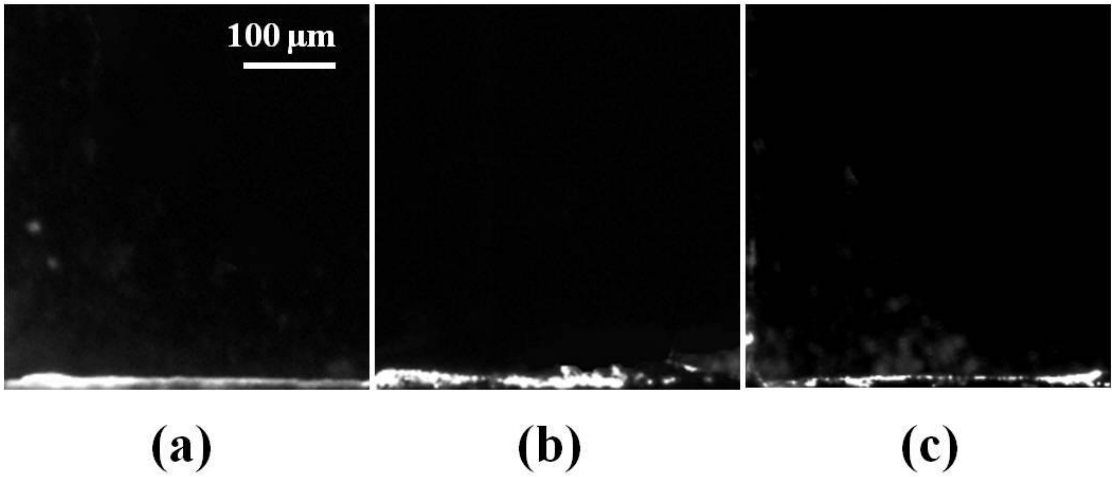

Figure 4.9 Images of 1 μm microspheres enrichment within the confined microfluidic chamber after the electric field is applied for 64 s at a feeding flow rate of (a) 0.5 mL/h, (b) 0.2 mL/h and (c) 0.05 mL/h.

4.4.4 Effect of electrolyte solution

Figure 4.10 describes the effect of electrolyte concentrations on the trapping process of microparticles within the confined microfluidic chamber. It is well acknowledged that the zeta potential is dependent on the electrolyte concentration and typically increases with the decrease of the electrolyte concentration. The variation of zeta potentials on both the solid walls and particles would responsible for the changes of the flow field and the electrophoretic mobility of the particle. The particles suspended in the sample solution with a lower electrolyte concentration experiences a stronger electrophoretic interaction under the applied electric field, and therefore they are more effectively trapped within the confined chamber than that of higher electrolyte concentrations. However, it should be realized that in the present study the 3D electrodes were formed by copper foils, which significantly limit the concentration

range of the electrolyte during the test due to the electrodes corrosion. In the experiment, we found the electrodes corrosion become significant when the electrolyte concentration is greater than 1mM.

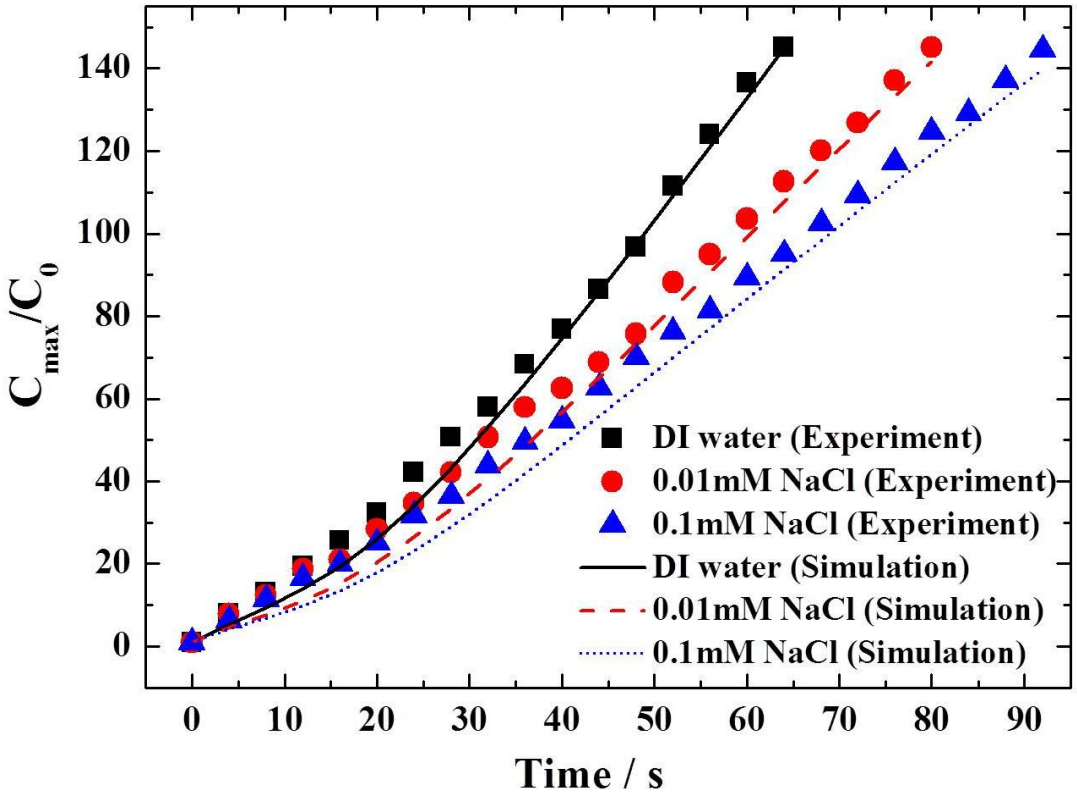

Figure 4.10 The particle enrichment varies with the electrolyte solution. Symbols and curves indicate experimental results and numerical simulations, respectively. Experimental results plotted in the figure were captured every 4 seconds. c = 466.

4.4.5 Effect of particle size

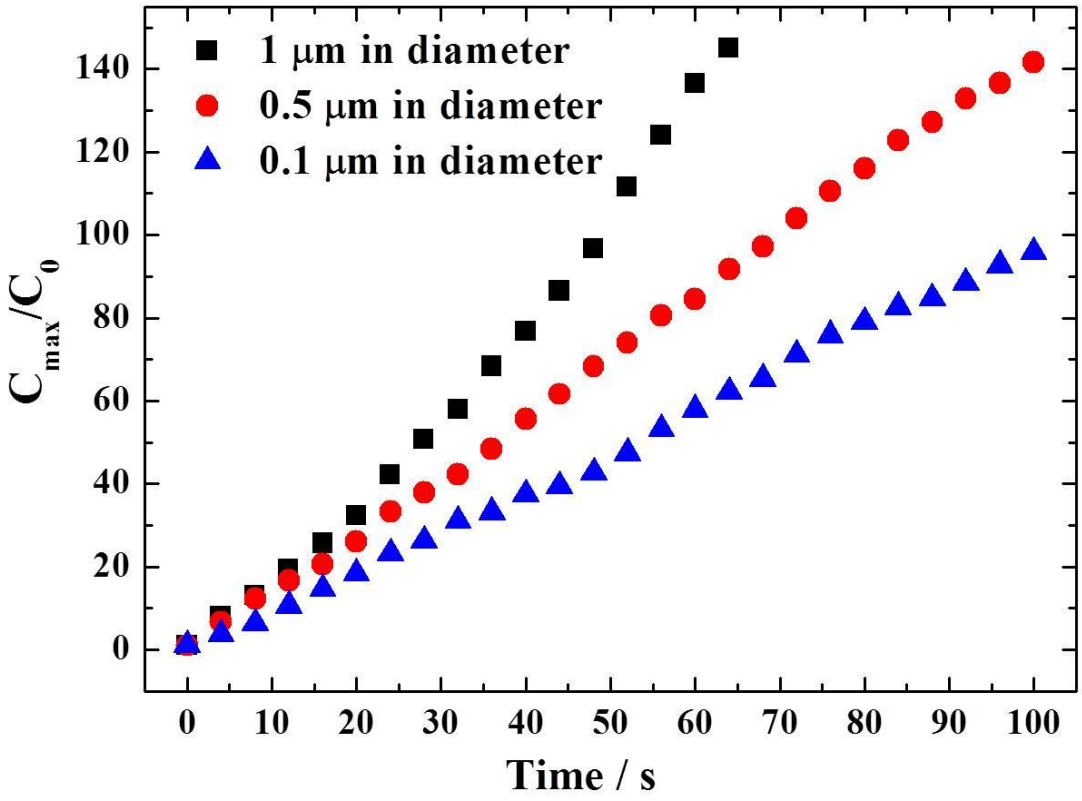

Figure 4.11 The particle enrichment varies with the microsphere size. Experimental results plotted in the figure were captured every 4 seconds.

The effect of particle size on the concentration process of microspheres within the confined microfluidic chamber is investigated and the result is represented in Figure 4.11. It is readily observed that the microsphere size plays a vital role in the particle trapping process. The 1 μm particles are efficiently trapped within the confined chamber, evidenced by a 145 folds maximum concentration enhancement after 64 s

during the experimental course. In contrast, the concentration of 0.1 μm particles within the trapping region grows very slowly, indicating a low trapping performance in this case. The enrichment process of small microspheres is even retarded if the mean concentration is examined, as shown in Figure 4.12. As the particle size reduces, the mass diffusion coefficient raises accordingly based on the Stokes-Einstein relation and thus the microspheres enrichment process is significantly retarded. In addition, because of the complexity of the correction factor, it is difficult to find a constant factor *c* matching all experimental and numerical results. Therefore, only experimental observations are demonstrated in the figure.

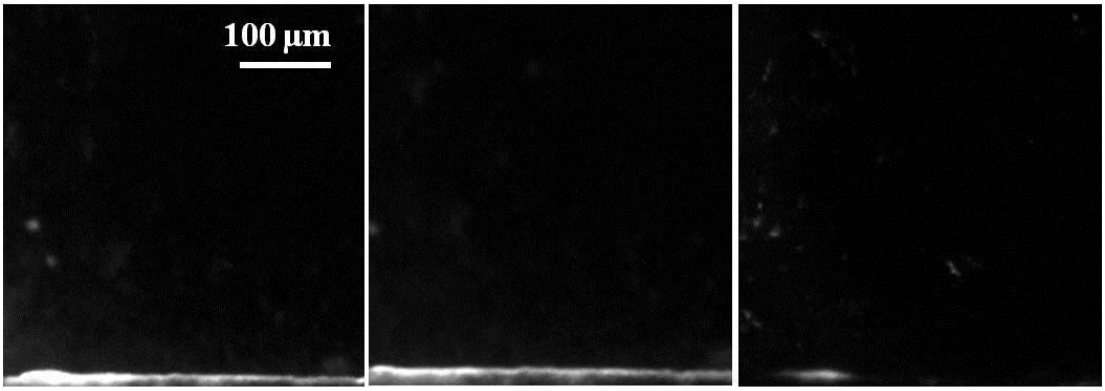

Figure 4.12 Images of microsphere enrichment within the confined microfluidic chamber. (a) 1 μm and t = 64 s, (b) 0.5 μm and t = 100 s and (c) 0.1 μm and t = 100 s.

4.5 Summary

In this chapter, a method for continuous concentration of microspheres in a confined microfluidic chamber was proposed and systematically studied. By applying very low DC electric voltage across a pair of copper electrodes and feeding the particles solution with a syringe pump, successful microsphere enrichment has been demonstrated. The study of experimental parameters suggests that higher electric voltage and feeding flow rate, electrolyte solution with lower concentration, and larger particle size are favorable to such particles enrichment process within the confined microfluidic chamber. A numerical model is developed to simulate the particle enrichment process and reasonable agreement with the experimental observations is obtained.

The major advantage of this method is that since the separation between two electrodes is in microscale and the device is energized by very low DC electric voltage, it is envisioned to implement this method for Lab-on-a-chip devices, especially for those mobile devices operated by batteries. However, restrained by its operation principle, the efficiency of such method degraded dramatically once the particles size drops to submicron. In addition, a novel 3D electrodes fabrication approach in microfluidic channel is proposed and experimentally demonstrated. PDMS microchannel with 3D copper electrodes can be created within 2 hours without involving clean room facilities when surface roughness of the electrodes and channel boundary is not specifically required.

Chapter 5: A novel electronic paper display based on in-plane dielectrophoresis

5.1 Introduction

Nowadays, particle-based displays rely on the electric polarity and charge distribution of the particles, i.e. the Electrophoretic Display (EPD), have been developed for a long period because of their high contrast and low power consumptions. EPD is a reflective display technology based upon the phenomenon of electrophoresis. In a typical EPD, dyed micro/submicro-particles with surface charges are suspended into a dielectric carrier fluid and they are encapsulated within an electronic display cell with transparent electrodes patterned on the inner surfaces of front and back planes. The desired information is displayed on the front plane by transporting pigment particles toward the top electrodes under an external applied electric field.

Since the information display on EPD is realized by means of the rearrangement of particles with an electric impulse, the optical performance of EPD is significantly depends on the electric and physical properties of the particles and fluid. The fabrication of pigment particles and electrophoretic suspension is a complicated process. For instance, pigment particles are firstly atomized from an organic suspension and sieved to obtain an approximately uniform size. The white and black pigment particles used in EPD cells are made of different materials in order to yield different zeta potential with opposite signs on the particles surface, and thus they can

electrophoretically move to the opposite directions in response to an applied electric field. The microparticles are then dispersed in an organic mixture with a lower viscosity and a density equals to the particles so as to enhance the particle transport velocity and eliminate the effect of gravitational force (Comiskey et al. 1998; Kim et al. 2005). Polymeric adsorbed layers are coated on the particles surface to prevent them from coagulating. In some cases a charge controlling agent is added into the suspension fluid as well in order to yield higher surface charges on the particles.

In recent years, several new electronic paper display technologies by using neutral particles instead of charged pigment spheres (Wen et al. 2005; Chiu et al. 2007; Chiu et al. 2008; Hsu et al. 2008; Chen et al. 2009) have been reported. Since the surface charge on pigment particles is no longer essential, the manufacturing process of these electronic displays can be greatly simplified. These devices can be realized either by suspending polystyrene microparticles into deionized (DI) water or mixing toner particles with oil. However, the operation of these electronic paper display technologies normally rely on high electric voltages input and therefore the energy consumption of these technologies are significantly. In addition, limited by their working principles, the optical transmittance of these technologies are still in lower levels.

In this chapter, a novel electronic paper display technique by using neutral particles directly suspend in aqueous medium is presented. The particles rearrangement within the electronic display panel is realized by using an in-plane dielectrophoretic force.

Because dielectrophoresis (DEP) (Pethig 2010) is a physical phenomenon independent of the surface charge of particles, the advantage of using DEP as particles driven force is that either charged or neutral pigment particles can be used in this new technology. As a result, the manufacturing cost of the current electronic paper display could be much reduced since the complicated chemical processes on both pigment particles and the carrier medium are not necessary. In addition, the use of aqueous medium, like water, instead of organic mixture can also yield a faster particles transport within the device as the viscosity of water is typically lower than most oils used in electronic display technologies.

5.2 In-plane dielectrophoresis

Normally, a non-uniform electric field can be formed by applying an electric field across a pair of co-planar electrodes. The inhomogeneity of the electric field between the two co-planar electrodes is significantly dependent on the inter-electrode separation if the dimension of the electrodes is fixed, and it is enhanced by reducing the inter-electrode gap, as shown in Figure 5.1. As a result, an electric field gradient along the longitudinal direction is created when the inter-electrode gap varies along the electrodes length and a DEP force is thus yielded parallel to the back plane. This DEP force can be used for particles/cells manipulation in microfluidic devices (Choi and Park 2005; Chunag et al. 2009). Because the direction of the DEP force created

by the co-planar electrodes is longitudinally parallel to the electrodes, we term this effect in-plane DEP.

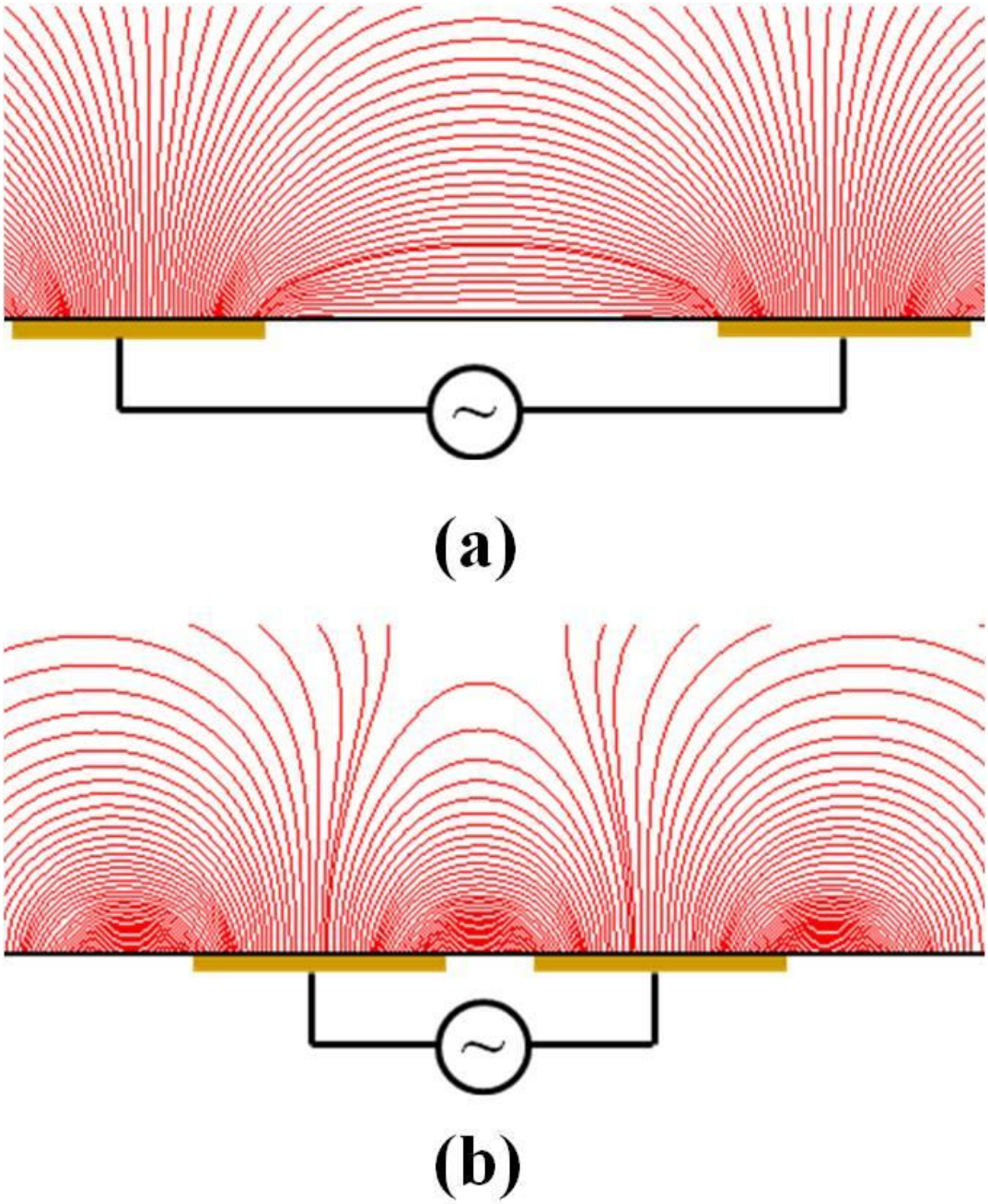

Figure 5.1 A non-uniform electric field yielded by a pair of co-planar electrodes with (a) a wider and (b) a narrower inter-electrode separation. The curve lines above the electrodes denote electric field.

5.3 Operation principle

Figure 5.2 illustrates the operation principle of the electronic paper display developed in this study. As shown in the figure, an electronic display unit/cell consists of a transparent frontplane and a backplane with electrodes patterns as well as a spacer for separating the front and back planes. The display cell is filled with pigment particles suspended in a dielectric fluid. In the absence of electric field, pigment particles are evenly distributed throughout the display panel, and thus light is scattered by the uniformly dispersed particles to represent a dark state in display situation (Figure 5.2 (a)). When an AC electric voltage is imposed, the pigment particles subject to in-plane DEP forces are repelled to desired regions, and the rest regions without presence of particles are transparent to light to represent a bright state (Figure 5.2 (b)). Consequently, light is reflected by the background underneath the display unit and a reflective electronic paper display is therefore created.

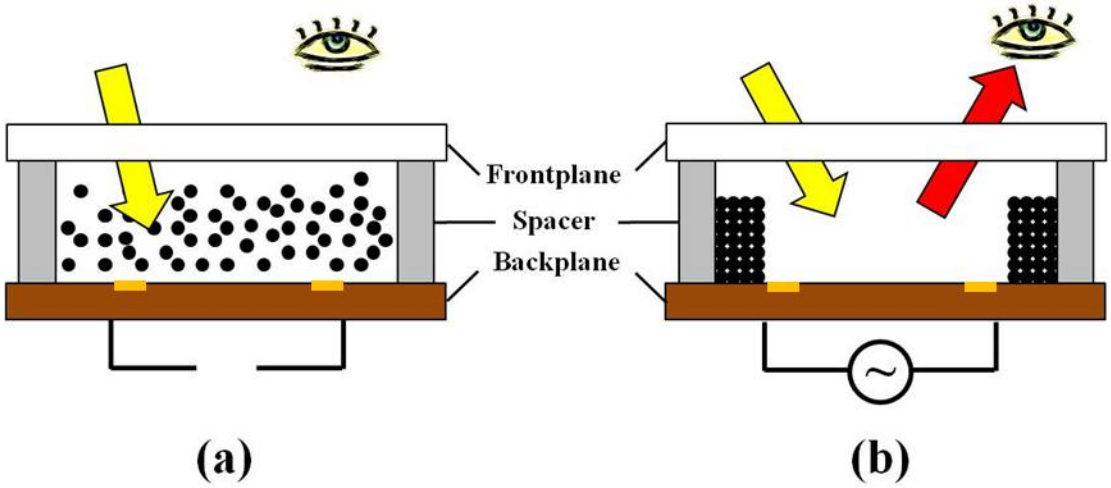

Figure 5.2 Schematic diagram for illustrating the operation principle of the electronic paper display based on in-plane DEP (a) without any electric voltage applied (dark state) (b) with an electric voltage applied (bright state).

In order to realize the electronic paper display by using in-plane DEP, co-planar electrodes are symmetrically patterned with varied inter-electrode separations on the backplane of the display cell. Figure 5.3 represents four different designs of electrodes configurations on the backplane. In design I, the electrodes are designed as wave-shape array with 30 μm in width and each strip consists of quarter-circular arcs with an inner radius of 100 μm. The minimum separations between electrodes are 30 μm and they are enlarged with the electrodes length. In design II, the minimum inter-electrode separation is reduced to 20 μm. Design III uses 30 μm wide straight electrodes instead of the wave-shape negative electrodes and the minimum inter-electrode separation is maintained as 30 μm. In design IV the inner radius of the quarter-circular arcs is increased to 170 μm while the minimum inter-electrode separation is still 30 μm.

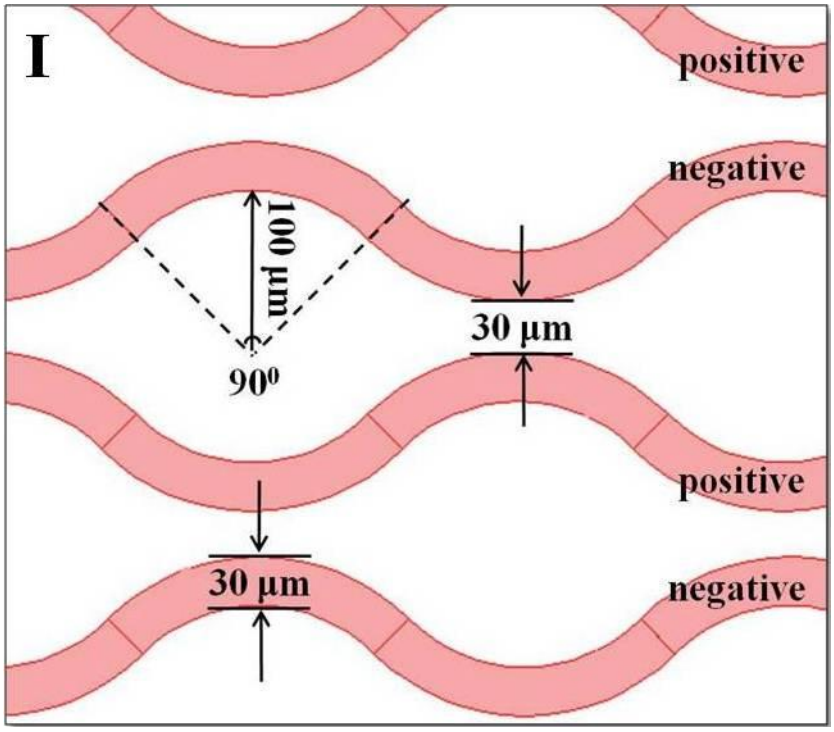
I
positive
negative
100 µm
90⁰
30 µm
positive
30 µm
negative

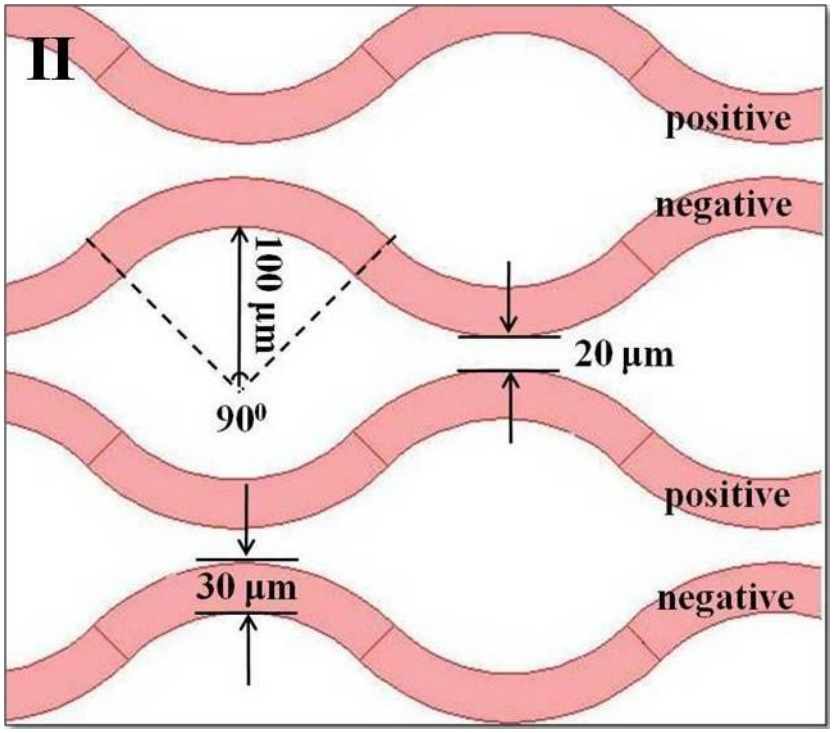
II
positive
negative
100 µm
90⁰
20 µm
positive
30 µm
negative

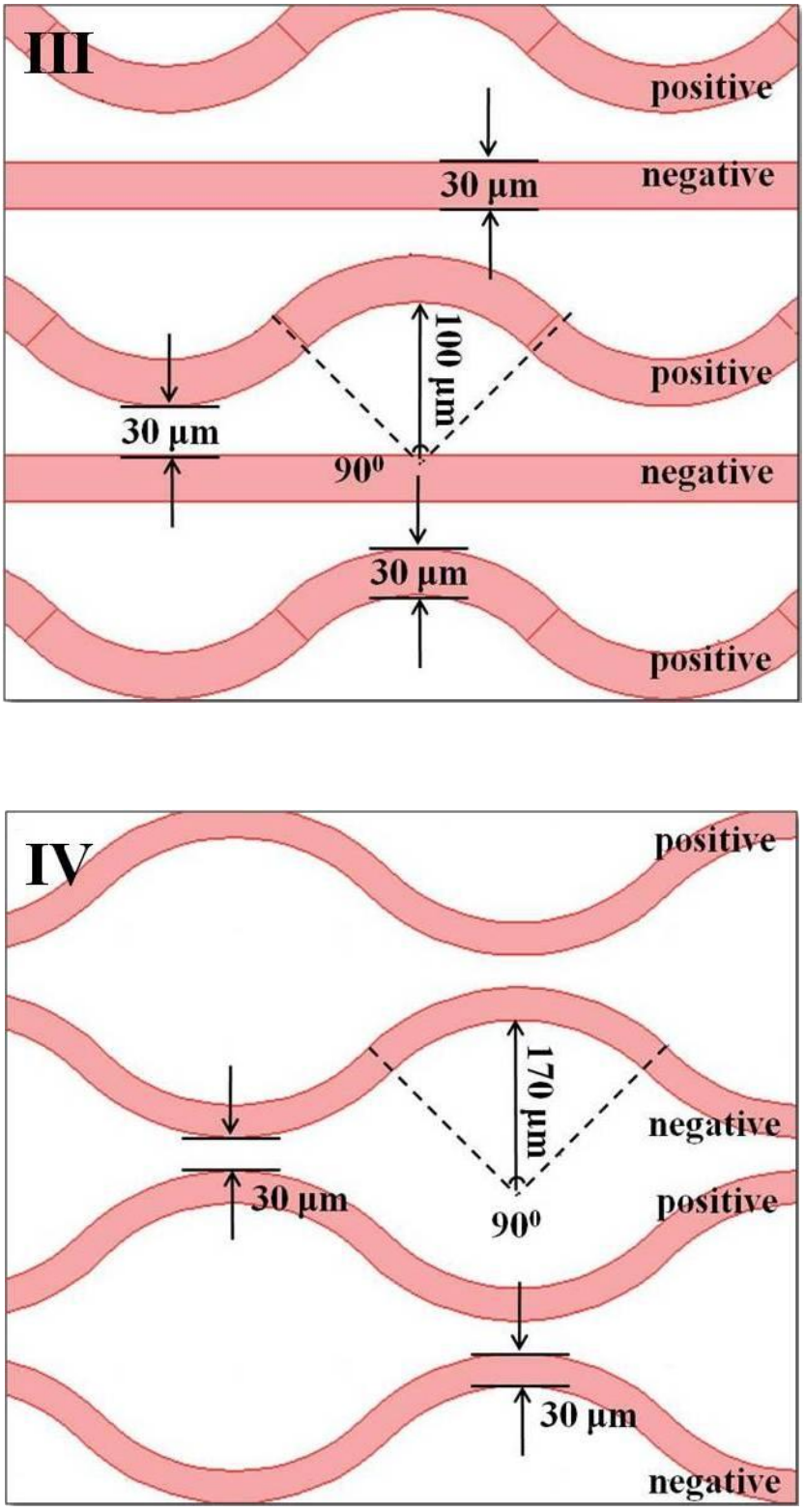

Figure 5.3 Four different designs of electrodes configurations patterned on the backplane of the electronic display panel.

5.4 Experiment

5.4.1 Microdevice fabrication

The transparent electrodes were patterned on 0.7 mm thick Indium Tin Oxide (ITO) glass with an electric resistance of 10 ohm/sq. The microdevice was then fabricated using a piece of plain silica glass (without any electrodes) covered on the ITO glass. A 60 μm thick dry adhesive layer (Arclad 8102 transfer adhesive, Adhesives Research, Inc.) was used to separate these two glasses. Two 1 mm holes were drilled using diamond drill bits at corners of the display panel in order to facilitate filling of particle solution. The prototype used in the present study is illustrated in Figure 5.4.

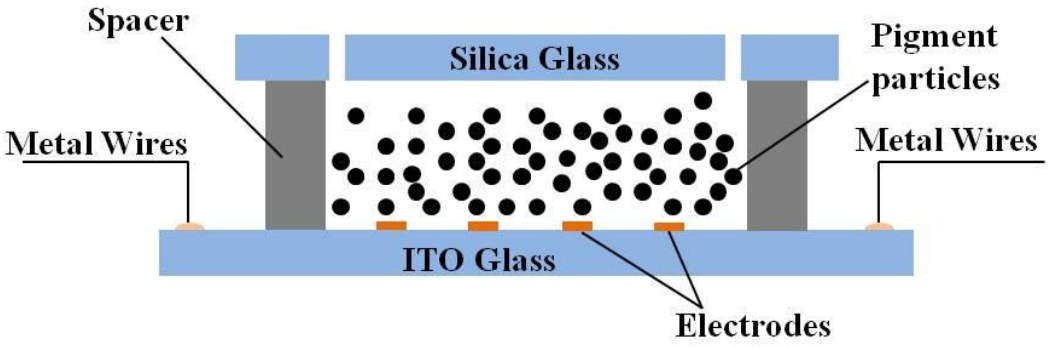

(a)

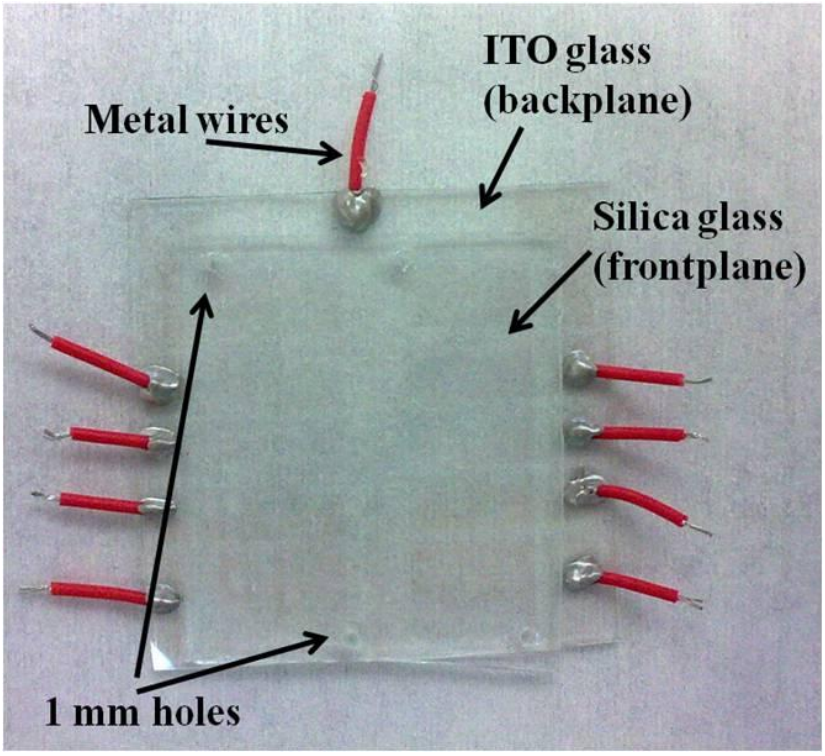

(b)

Figure 5.4 (a) the schematic illustration (cross-sectional view, not in scale) and (b) photograph (top view) of a prototype of the electronic paper display.

5.4.2 Materials

In order to investigate the electronic paper display, polystyrene particles (Duke Scientific, USA) with 2.9 μm and 1.0 μm in diameter (white color) were chosen as pigment particles, and they were re-suspended and mixed with deionised (DI) water at a weight/weight concentration of 3%, corresponding to 2.6×10^{8} and 6.3×10^{9} particles/ml approximately, respectively.

5.4.3 Experimental setup

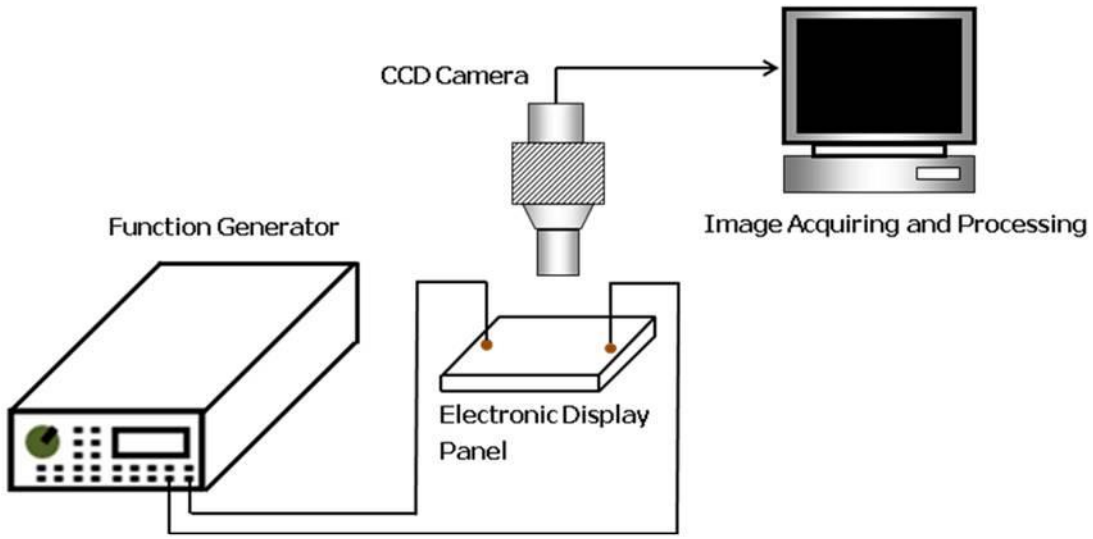

Figure 5.5 Experimental setup used for testing the performance of the prototype of the electronic paper display.

The AC electric signal applied on the electronic display panel was provided by a function generator (Agilent 33250A, USA). The information screened on the electronic display panel was captured by a digital camera with a rate of 25 frames per second (fps). The microscale particles rearrangement within the electronic display cell was captured by an optical microscope (Zeiss, Germany) equipped with a CCD camera (Sensovation, Germany) at a rate of 15 fps and the results were processed subsequently by using the image processing software. During the experiment, the particles solution was introduced into the electronic display cell by a syringe through a hole on the front plane and the cell was hence filled automatically by capillary forces.

5.5 Numerical simulation

Numercial calculation of the electric field gradients squared $\nabla \mathbf{E}^2$ is conducted to analyze the performance of the electronic paper device. The electric field distribution can be obtained by numerically solving the Laplace equation with finite element method based software Comsol Multiphysics 3.4 (Comsol Inc., Sweden). The boundary condition on the electrodes is specified as given electric potential and the rest boundaries are defined as zero charge/insulation.

5.6 Results and discussion

5.6.1 Information display on the electronic paper panel

A prototype of the electronic paper display with design I electrodes configuration shown in Figure 5.3 was tested in the experiment. Particles solution with 2.9 μm polystyrene microspheres suspended in DI water was filled into the cell and the device was tested with a 10 Vpp, 1 MHz AC electric voltage. The experimental results are shown in Figure 5.6 and Figure 5.7. Figure 5.6 demonstrates sequential images of the information display on the electronic display panel with time lapse. It is observed that after the electric voltage is turned on within 200 ms, a word "NTU" appears on the electronic display panel. As the electric voltage is kept loading, the word becomes increasingly clear and a considerable contrast is created after the voltage is applied for 1000 ms. The line width of each letter on the screen is 500 μm

approximately and the dimension of letters is about 2 mm, indicating a remarkable resolution for reading. This dimension is known at the same level of most printed materials.

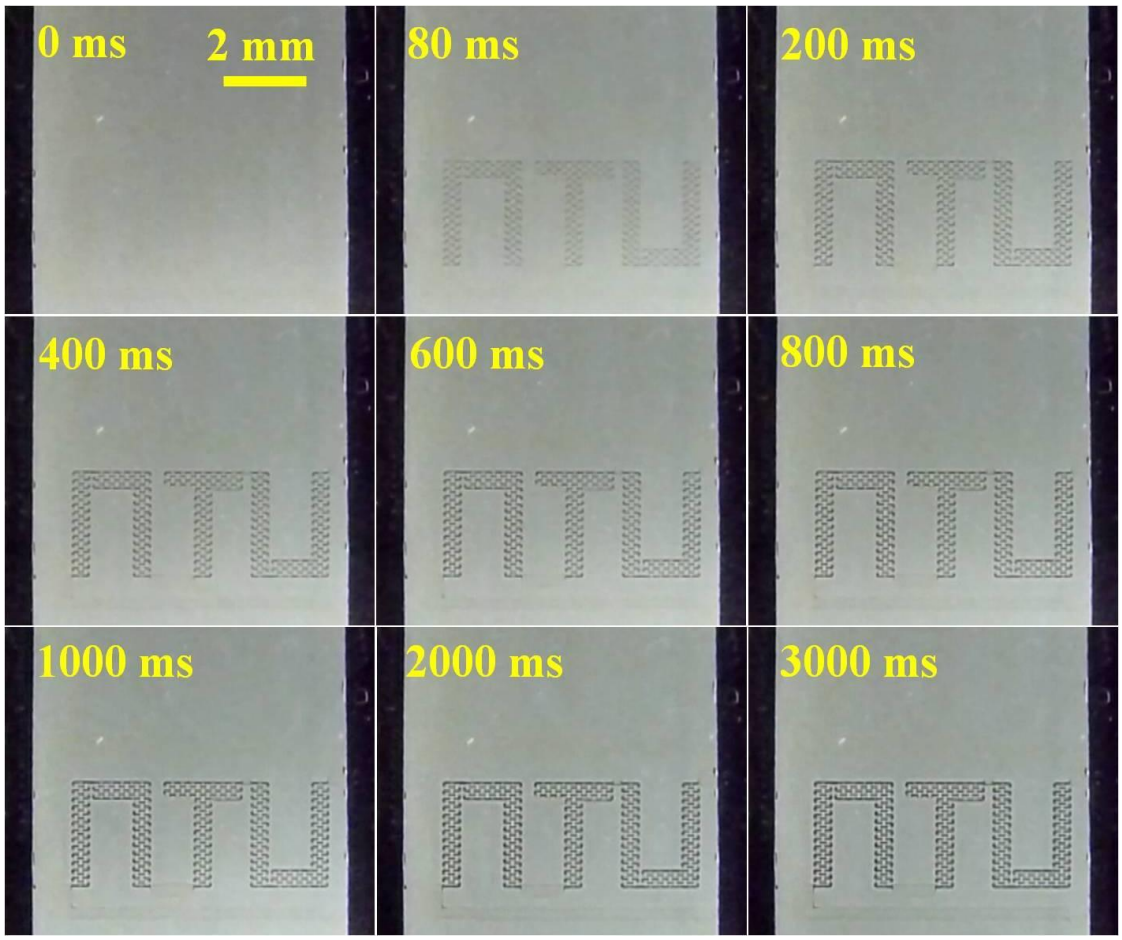

Figure 5.6 Sequential images taken for a prototype of the electronic paper display with design I electrodes configuration. An AC electric signal of 10 Vpp, 1MHz was used in the experiment.

In order to explore the microscale particles movement, the microdevice was also detected under a microscope lens with a 10× magnification. Figure 5.7 shows the

microscopy images of microspheres rearrangement under the AC electric field with time lapse. According to the theory of DEP, a 10 Vpp, 1 MHz AC electric voltage provides negative DEP forces on particles, and thus particles are repelled to the regions with lower electric field after the voltage is turned on. Numerical simulations suggest that both the electric field and the gradient of the electric field squared are much greater near the regions of minimum inter-electrode gap, and therefore a strong DEP force is yielded to push particles toward the regions with larger inter-electrode gap (Figure 5.8). The experimental observation confirms that prediction. It is seen that pigment particles move to the low electric field regions immediately with an electric voltage is turned on. With the electric voltage is applied for 1000 ms, the regions around minimum inter-electrode separations have been cleared, showing the bright state screened on the electronic display panel. After that, the particles are observed keep moving to the low electric fields, however, the response is much retarded and the particles pattern changes very slowly due to low electric field gradients as well as weak DPE forces at these regions.

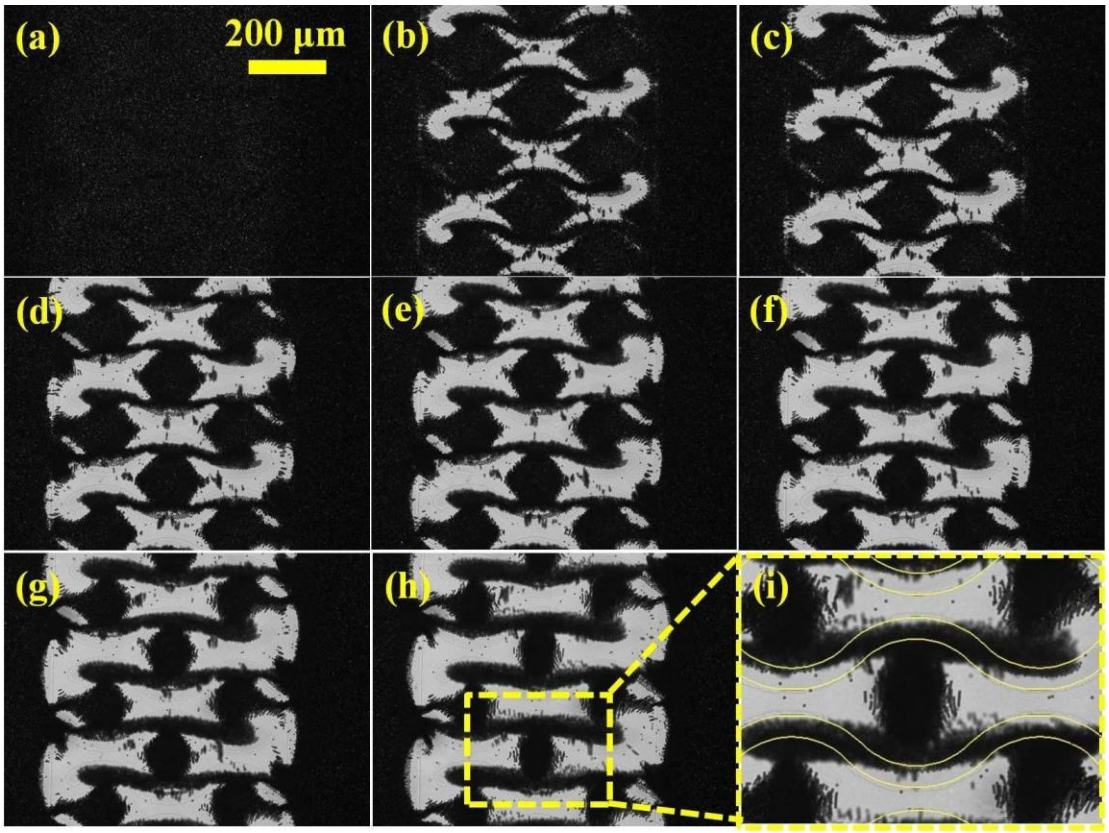

Figure 5.7 Microscopy images illustrating particle patterns in the electronic display cell with design I electrodes configuration. (a): The dark state without applying the electric voltage. (b) ~ (h): The bright state after the electric voltage is turned on for 134 ms, 200 ms, 400 ms, 600 ms, 800 ms, 1000 ms and 2000 ms, respectively. (i): A magnified microscopic image showing the rectangular area of (h). The light-colored curves in (i) represent the positions of electrodes patterns on the backplane. An AC electric signal of 10 Vpp, 1MHz is used in the experiment. All images are taken under a microscope lens with a 10× magnification and the microscope lens is focused on the vertical strip of the letter "T".

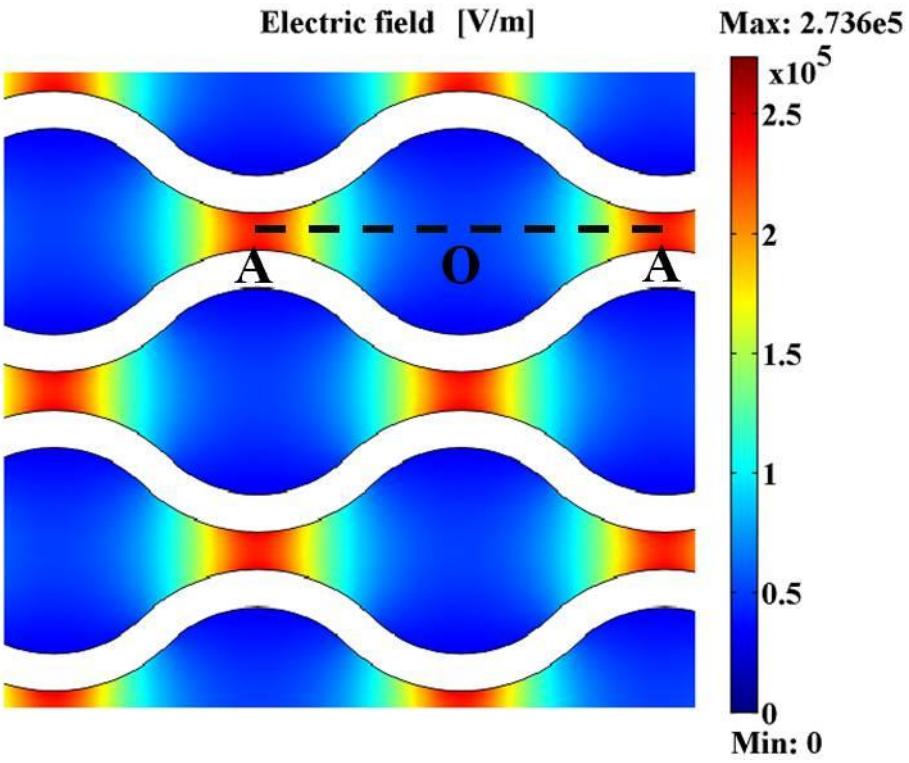
Electric field [V/m]
Max: 2.736e5
x10^5
2.5
2
1.5
1
0.5
0
Min: 0
A
O
A

(a)

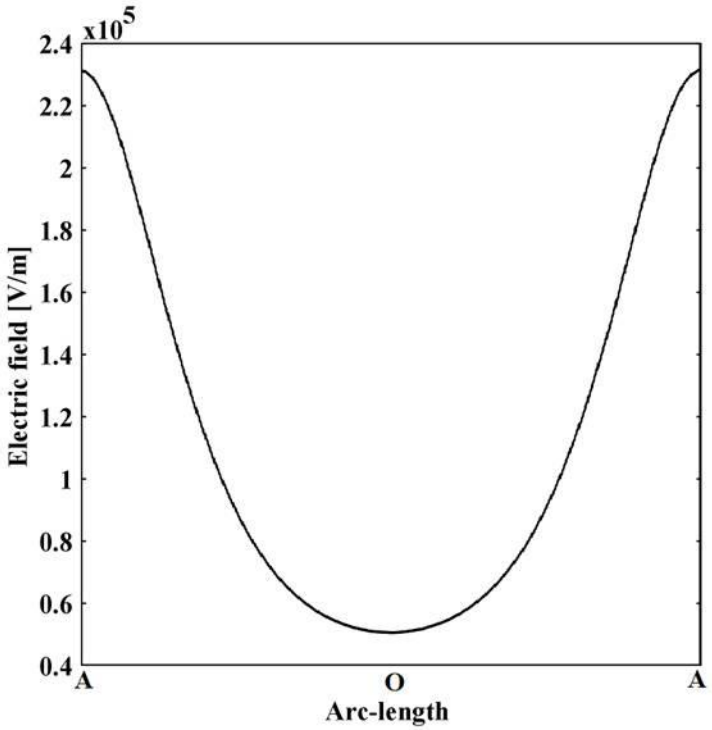
x10^5
2.4
2.2
2
1.8
1.6
1.4
1.2
1
0.8
0.6
0.4
Electric field [V/m]
A
O
A
Arc-length

(b)

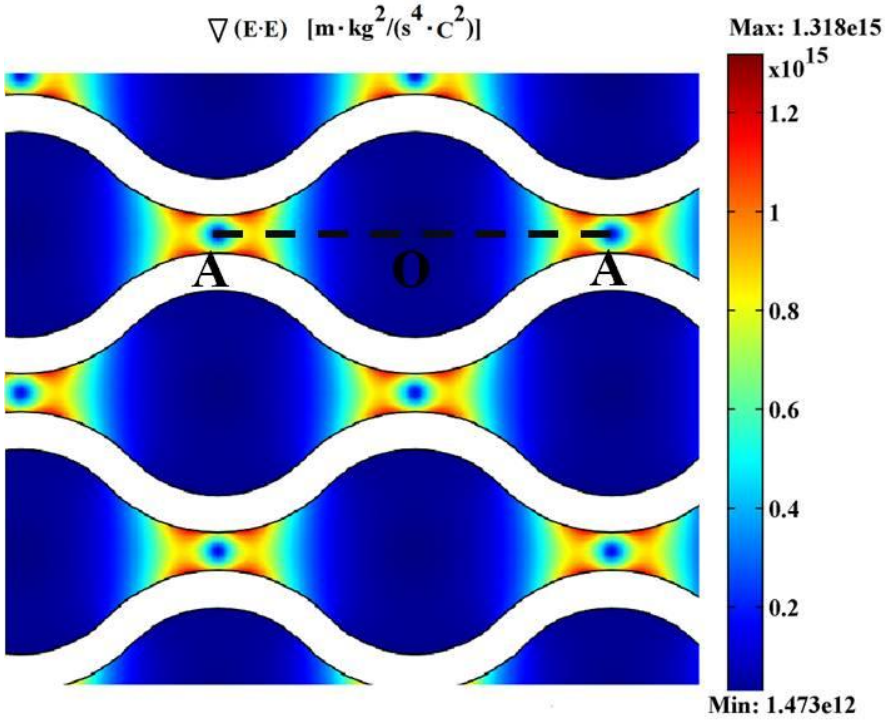
∇(E·E) [m·kg²/(s⁴·C²)]
Max: 1.318e15
x10¹⁵
1.2
1
0.8
0.6
0.4
0.2
Min: 1.473e12
A
O
A

(c)

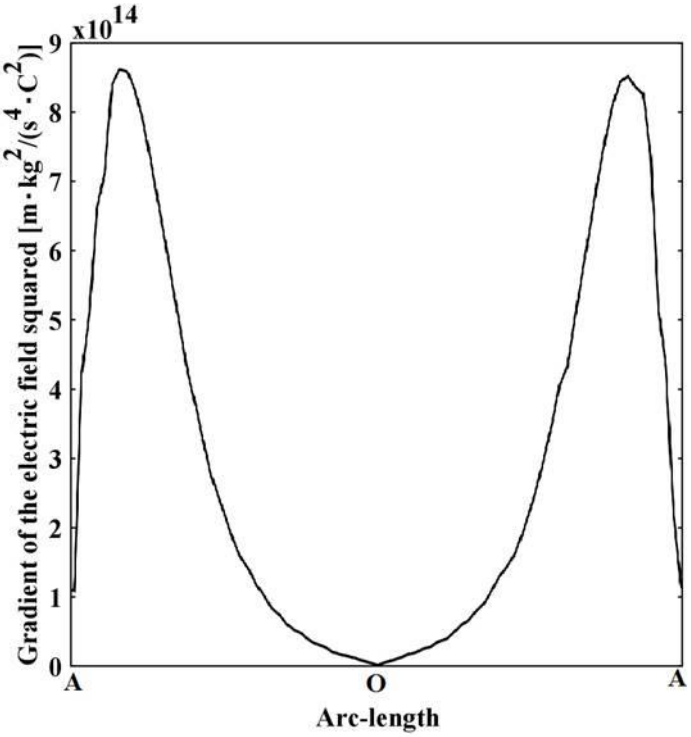
x10¹⁴
Gradient of the electric field squared [m·kg²/(s⁴·C²)]
9
8
7
6
5
4
3
2
1
0
A
O
A
Arc-length

(d)

Figure 5.8 Computational results of design I electrodes configuration: Surface plots of (a) electric field intensity and (c) the gradient of the electric field squared. Line plots of (b) electric field intensity and (d) the gradient of the electric field squared along the dashline "AOA" in Figure 5.8 (a) and (c).

5.6.2 Optical performance of the electronic paper display

To further analyze pigment particles rearrangement responses to the electric field, we studied the transmittance of the electric paper display with design I electrodes configuration under AC electric field of 10 Vpp, 1MHz. The electronic display cell was filled with 2.9 μm microspheres solution. Transmittance of the electronic paper display is defined as the proportion on the backplane with electrodes patterns that incident light can pass through the electronic display cell and was obtained by processing microscopy images captured during the experiment with an in-house code. The 8 bits images taken from the experiment were firstly converted to binary images with a threshold values setting as the average of the maximum and minimum intensities of the image. Subsequently the areas of black and white regions on the image were calculated respectively with the in-house code. Figure 5.9 demonstrates an example of images processing by using the proposed method for a microscopy image shown in Figure 5.7 (g). By counting the ratio of white areas to the total area of the image, the transmittance was thus acquired.

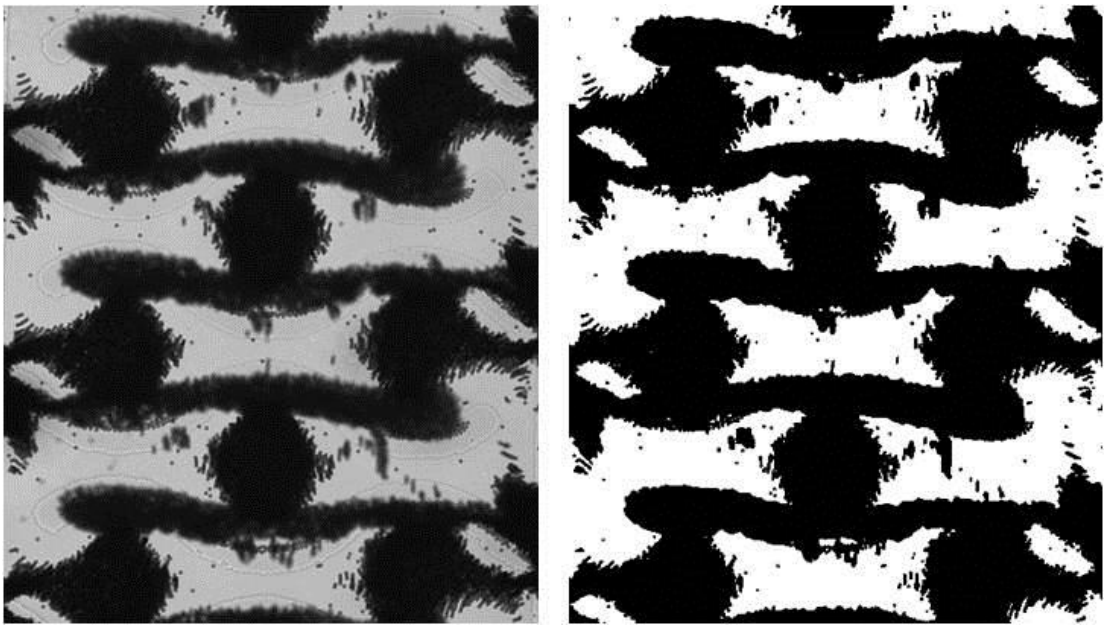

(a) (b)

Figure 5.9 Images processing for illustrating the conversion of a grayscale microscopy image (a) to a binary image (b). The microscopy image is captured with a 10× magnification after the electric voltage is applied for 1000 ms.

Figure 5.10 shows the transmittance of the electronic paper display with design I electrodes configuration under an AC electric field of 10 Vpp, 1MHz. It is readily found that the transmittance rises dramatically right after the electric voltage is applied. The value keeps approximately constant after the electric field is imposed for 2 s following a slow increment period between 1 s and 2 s. This is because pigment particles experience a strong DEP force around the "A" regions as indicated in Figure 5.8 (c) and they are repelled from "A" regions toward "O" regions along the dashline immediately after the electric field is turned on. However, with the particles movement, the DEP force drops sharply along the "AO" dashline and the effect is

much weakened near the regions of "O" because both the intensity and gradient of the local electric field are low. The response time of the proposed electronic paper display, which is defined as the time required for a 90% change in the transmittance after the electric field is applied (Ahn et al. 2008), is then estimated. It is suggested that the electronic paper display with design I electrodes configuration has a response time about 850 ms.

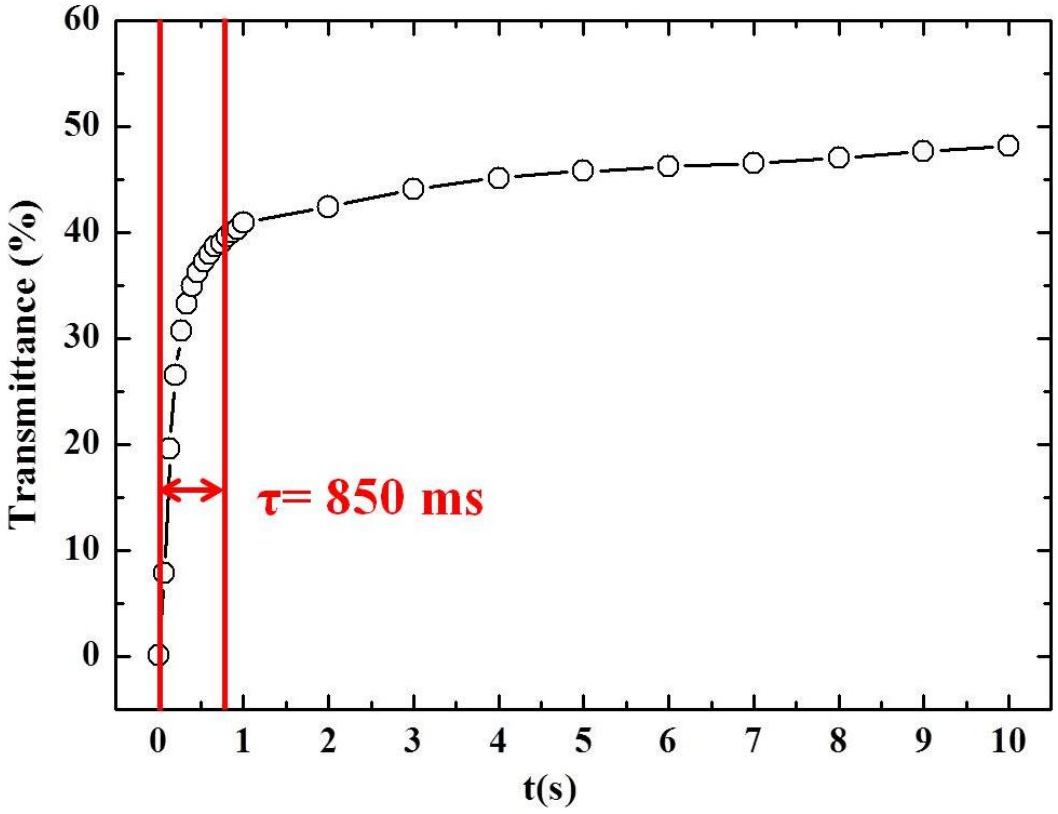

Figure 5.10 The transmittance of the electronic paper display with design I electrodes configuration vary with time.

5.6.3 Effect of electrodes configuration

Figure 5.11 shows the effect of electrodes configurations on transmittance of the electronic paper display. The electronic paper device with design I electrodes configuration demonstrates a fast switching response within less than 1 s and shows almost a constant transmittance after the electric voltage is applied for 2 s. With a smaller minimum inter-electrode gap, the DEP force is greatly enhanced, therefore the response of electronic paper display with design II electrode configuration is even faster than design I. The transmittance of electronic display with design III electrodes configuration is much lower than the others. As the wave-shape electrodes are replaced by straight electrodes, the areas of low electric field are hence reduced. Therefore, the regions for pigment particle "storage" are less than which in the rest designs, resulting in a lower transmittance at the bright state. Similarly, the electronic display with design IV electrodes configuration shows a higher transmittance at the bright state as it provides much areas for particles "storage". However, due to the growth of particles displacement from high electric field regions to low electric field regions, it takes a longer time until the transmittance rise to a stable value. In addition, as the numerical simulations suggested (Figure 5.12), the gradient of the electric field squared of design III and IV are low, and thus the electronic paper display with electrodes configurations of design III and IV demonstrate slower responses compared with which by using design I and II electrodes.

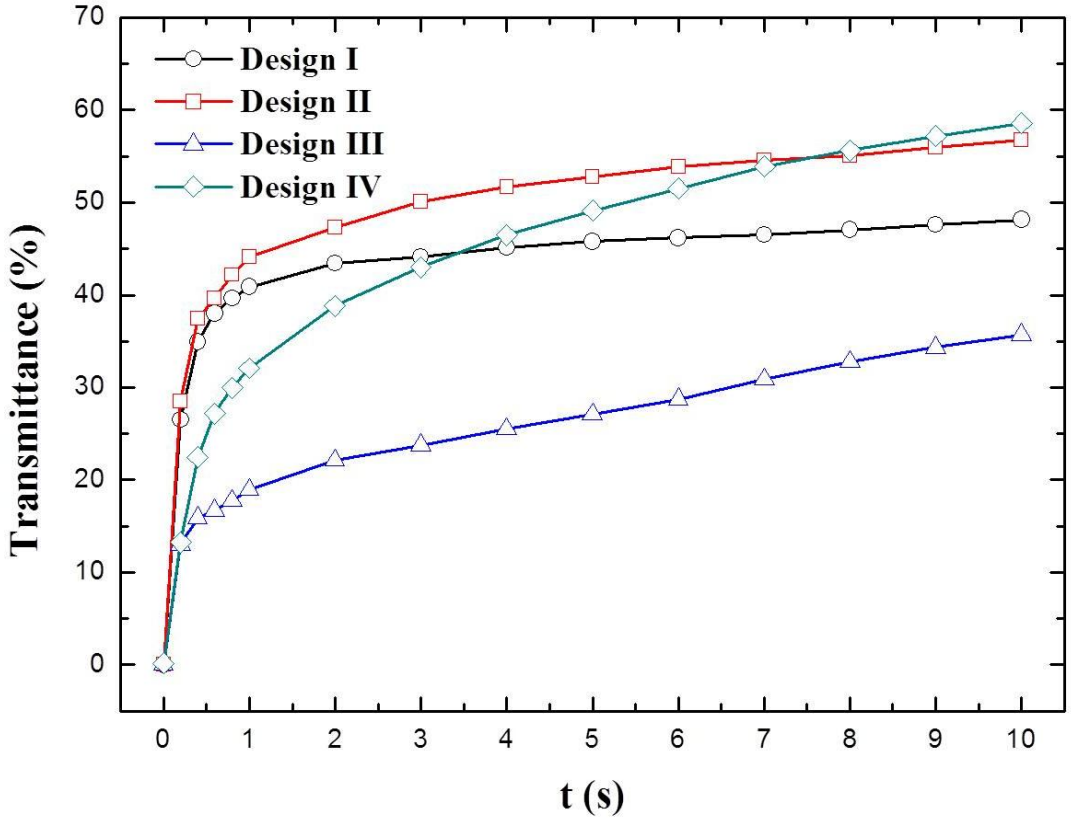

Figure 5.11 Effect of electrodes configurations on the transmittance of the electronic paper display.

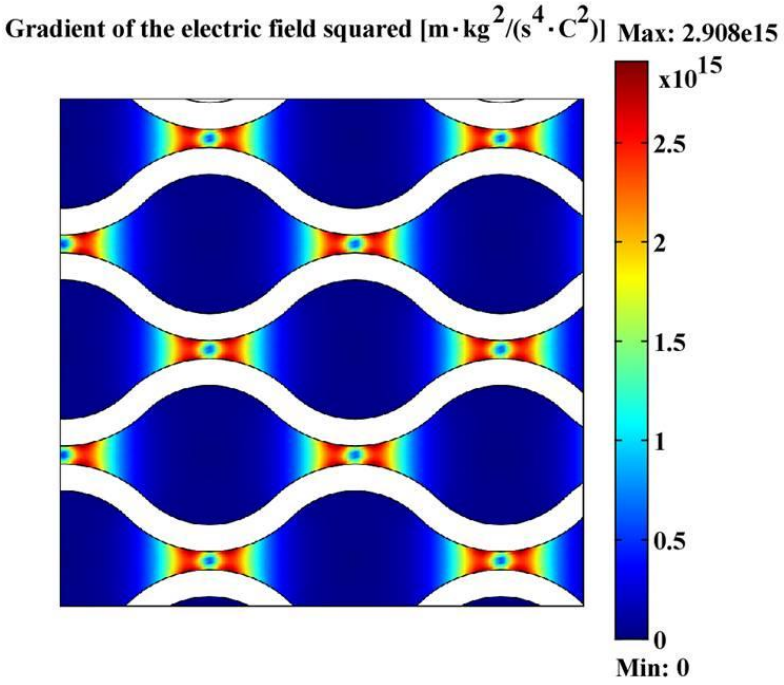
Gradient of the electric field squared [m·kg²/(s⁴·C²)]
Max: 2.908e15
x10¹⁵
2.5
2
1.5
1
0.5
0
Min: 0

(a)

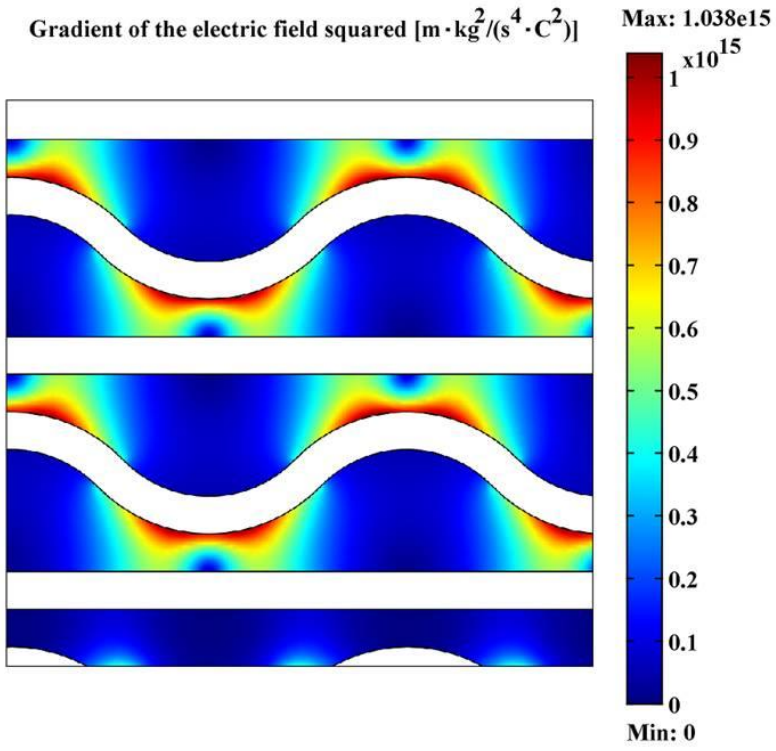
Gradient of the electric field squared [m·kg²/(s⁴·C²)]
Max: 1.038e15
x10¹⁵
1
0.9
0.8
0.7
0.6
0.5
0.4
0.3
0.2
0.1
0
Min: 0

(b)

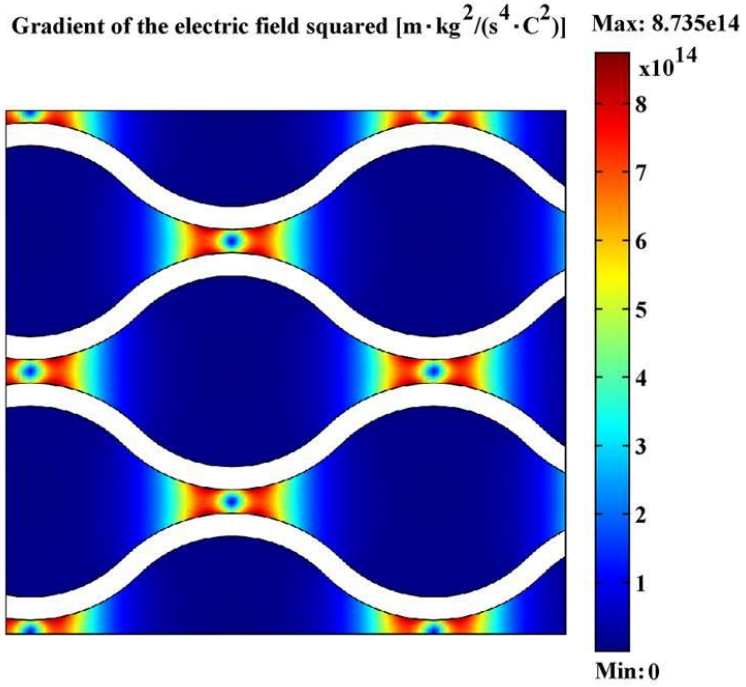

(c)

Figure 5.12 (a), (b) and (c): numerical simulation illustrating the gradient of the electric field squared for electrodes configurations of design II, III and IV, respectively.

5.6.4 Effect of electric signal

DEP is critical to the performance of the present electronic paper display as the pigment particles rearrangement within the display panel is relies on the in-plane DEP force. Therefore the effects of operating parameters on the transmittance of the electronic paper display are studies. In each experiment one parameter was tested and the rest were maintained unchanged.

Figure 5.13 (a) and (b) represent the experimental results of the effect of AC electric field on the transmittance of the electronic paper display with design (a) electrodes configuration and 2.9 μm microspheres solution. As the DEP force is proportional to the gradient of the electric field squared, the transmittance of the electronic paper display reduce pronouncedly with the drop of electric voltages. Similarly, by modulating the frequency of the AC electric signal from 1 MHz to 300 KHz, a sharply transmittance drop is observed due to the reduced driven force on the pigment particles. We did not lower down the frequency below 100 KHz as it may induce unwished positive DEP to be involved.

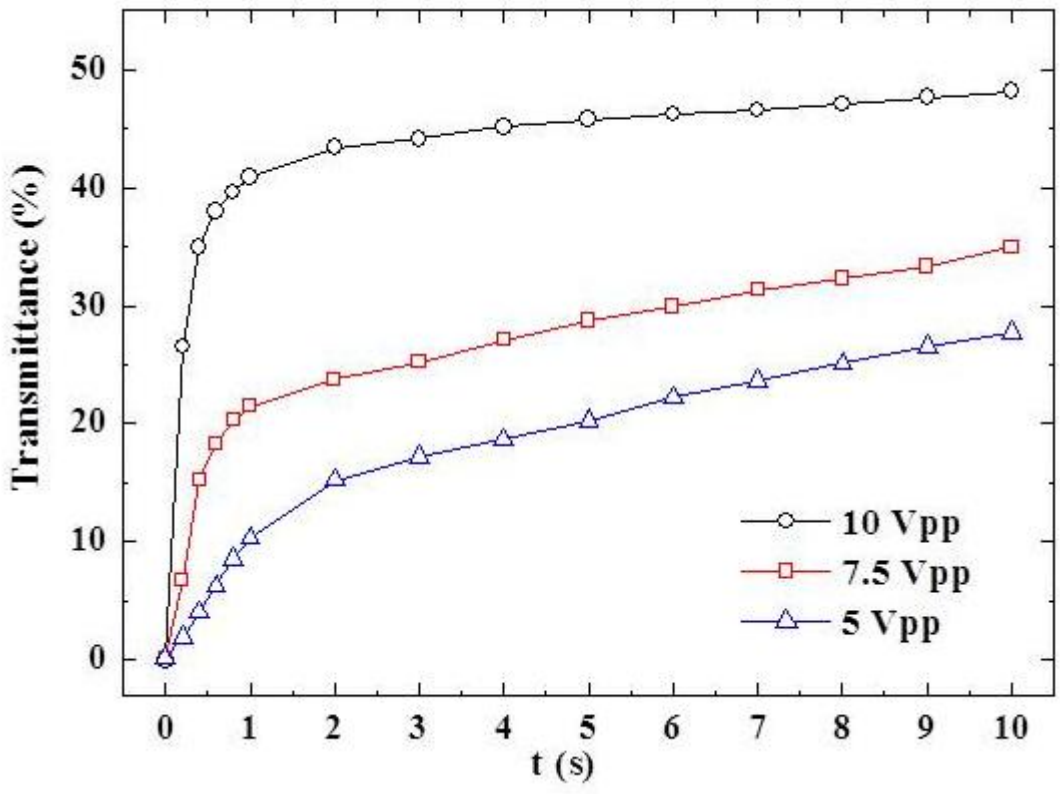

(a)

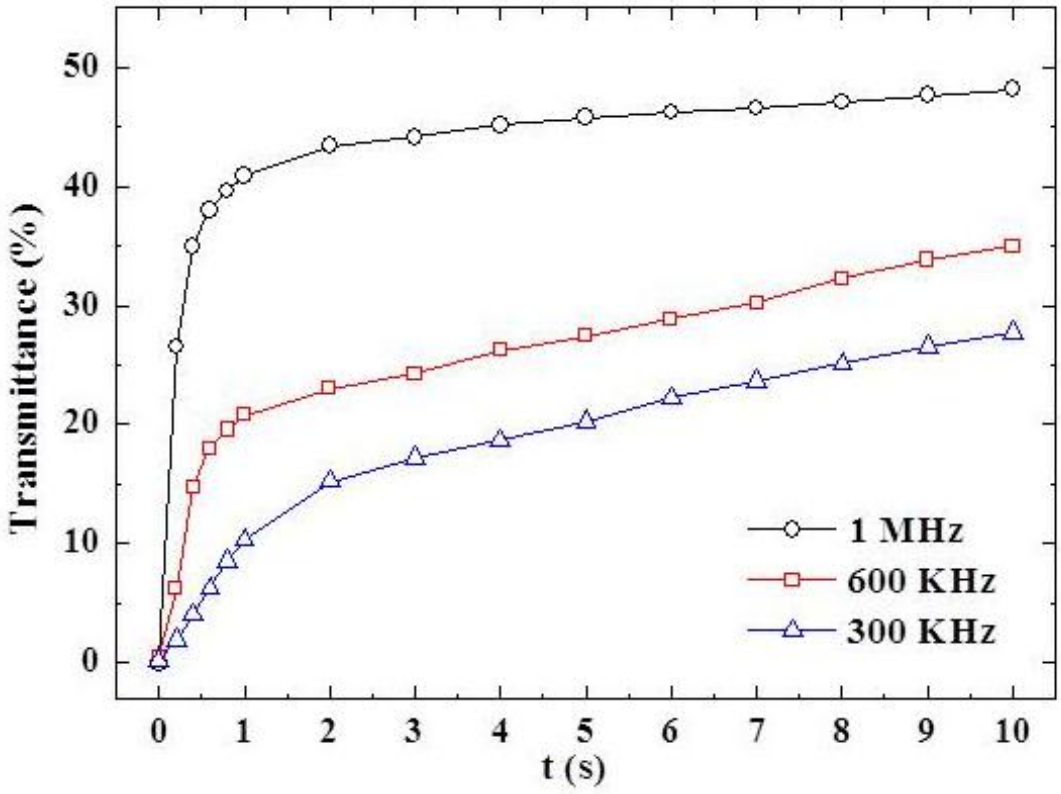

(b)

Figure 5.13 The effects of (a) electric voltages and (b) frequency of the electric field on the transmittance of the electronic paper display.

5.6.5 Effect of particle size

Figure 5.14 (a) shows the effect of pigment particles size on the transmittance of the electronic paper display with a 10 Vpp, 1MHz AC electric field. It is seen that with a small pigment particles filled into the display panel, the transmittance of the device is extremely degraded. Actually, once reduce the pigment particles size, on the one hand, the value of CM factor drops (Figure 5.14 (b)), yielding a smaller driven force

on the particles; on the other hand, since the magnitude of DEP force is proportional to a^3, smaller pigment particles can significantly weaken the in-plane DEP force. As a result, although the same electric field is maintained, the transmittance of the electronic paper display with 1 μm pigment particles is much inferior to which with large pigment particles.

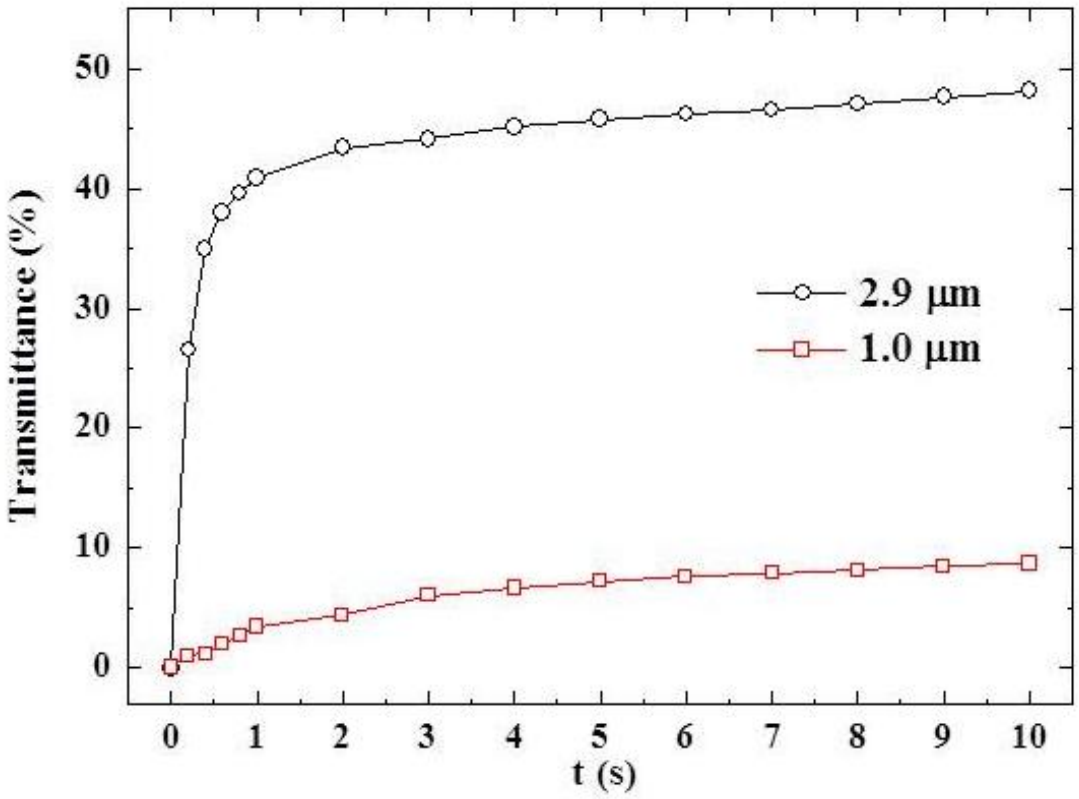

(a)

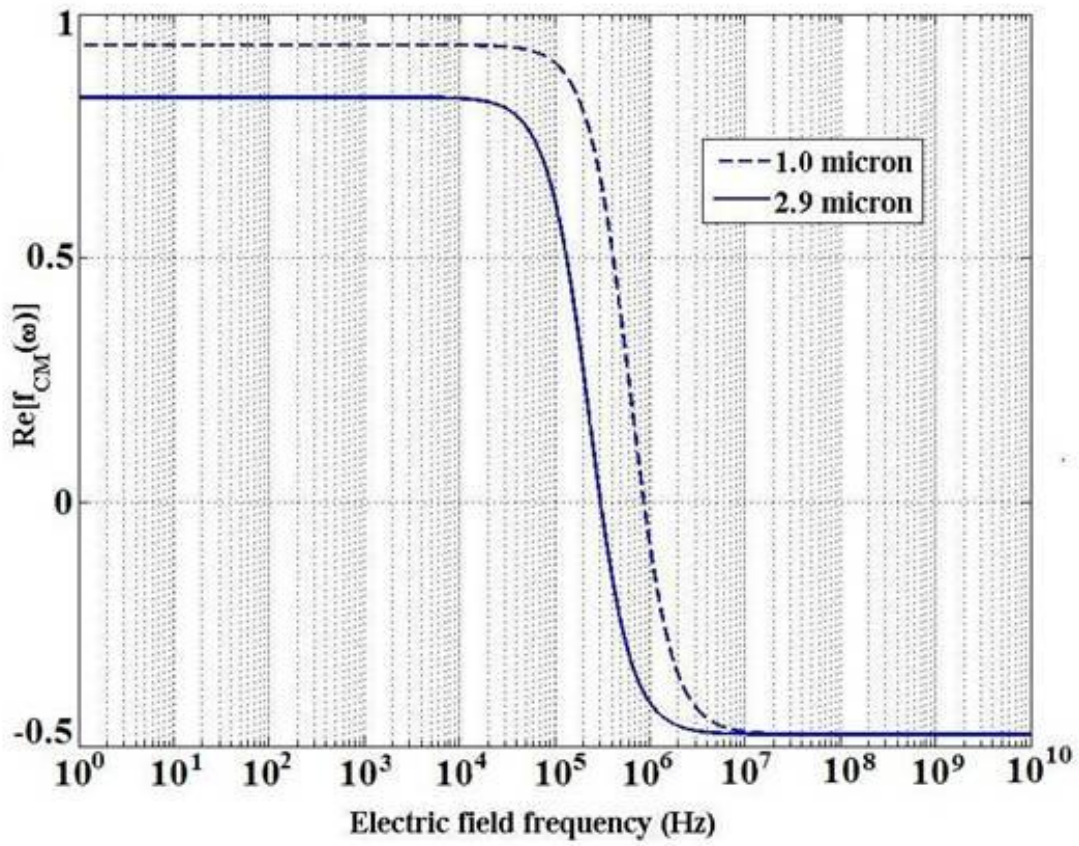

(b)

Figure 5.14 (a): The effects of pigment particles size on the transmittance of the electronic paper display. (b): Plot of the CM factor versus electric field frequency. Re[f_{cm}] denotes the real part of the CM factor.

5.7 Summary

In this chapter a novel electronic paper display technology is developed by using dielectrophoresis for patterning polystyrene particles suspended in DI water. A prototype of the proposed electronic paper display relies on in-plane DEP is fabricated. The in-plane DEP force is created by applying an AC electric field across

co-planar wave-shaped electrodes with varying inter-electrode separations, and the display on the panel is achieved within 850 ms after the voltage is turned on. The particle displacement within the electronic display cell is experimentally and numerically studied. The performance of the electronic paper display with four different electrodes configurations is tested. It is found that the switching response of the electronic paper is enhanced by reducing the minimum inter-electrode gap. A higher transmittance of the electronic paper display is observed by enlarging the low electric field region. Therefore, optimization of electrodes configuration is of vital importance to the optical performance of the present electronic paper display. It is believed that the present electronic paper display can be further improved by patterning well-designed electrode configurations and scaling down the dimension of electrodes with advanced microfabrication methods. In addition, it is also shown that by modulating the input electric signal, the transmittance of the electronic paper display is controllable, suggesting the potential multi grayscale display with a programmable electric circuit. As the operation principle of the present electronic paper display is based on DEP, the optical performance would be degraded by using smaller pigment particles. The present electronic paper display does not have specific requirements on the pigment particles and carrier fluid, and therefore is expected to create a low-cost electronic paper in future.

Chapter 6: On-chip particle assembly by co-planar electrodes induced non-uniform electric field

6.1 Introduction

The investigations of the assembly of micro- and submicro- sized particles have been rapidly grown in the past decades. Particles can be manipulated and assembled by various approaches including hydrodynamic drag, electrostatic interaction, van der Waals force, capillary force as well as gravitational force. The recent advancements in microfluidics, lab-on-a-chip systems and electrokinetics allow for the manipulation of microparticles directly with aid of electric field. The utilization of electric field to manipulate particles through on-chip electrodes has several advantages over the rest approaches. Firstly, use of electric field provides precise control and adjustment of driven forces acting on the particles. This is hardly possible with any other approaches such as using fluid flow, evaporation or mechanical manipulations. The electric field related parameters characterizing an AC electric signal including amplitude, frequency and wave shapes can be readily controlled and can affect the behaviors of particles in different ways. Secondly, the rapid development of micromachining technologies and Micro-electromechanical Systems (MEMS) enables relative simplicity and availability of the experimental detections and microchip fabrications. The microlithography facilities used in microelectronic

devices fabrication allow the ease fabrication of microelectrodes for the required investigation (Velev and Bhatt 2006).

In most microfluidic chips, the fabrication of 2D co-planar electrodes is much preferred because of its lower cost and ease fabrication. The application of an AC electric signal across a pair of co-planar electrodes can yield a non-uniform electric field existed above the electrode surface and hence lead to the emergence of dielectrophoretic (DEP) force (Bhatt 2006). The sign and magnitude of the DEP force acting on a particle in the suspension above the co-planar electrodes can be either positive or negative, depends on the effective polarizability of the particle, which is described by the real parts of the Clausius-Mossotti (CM) factor.

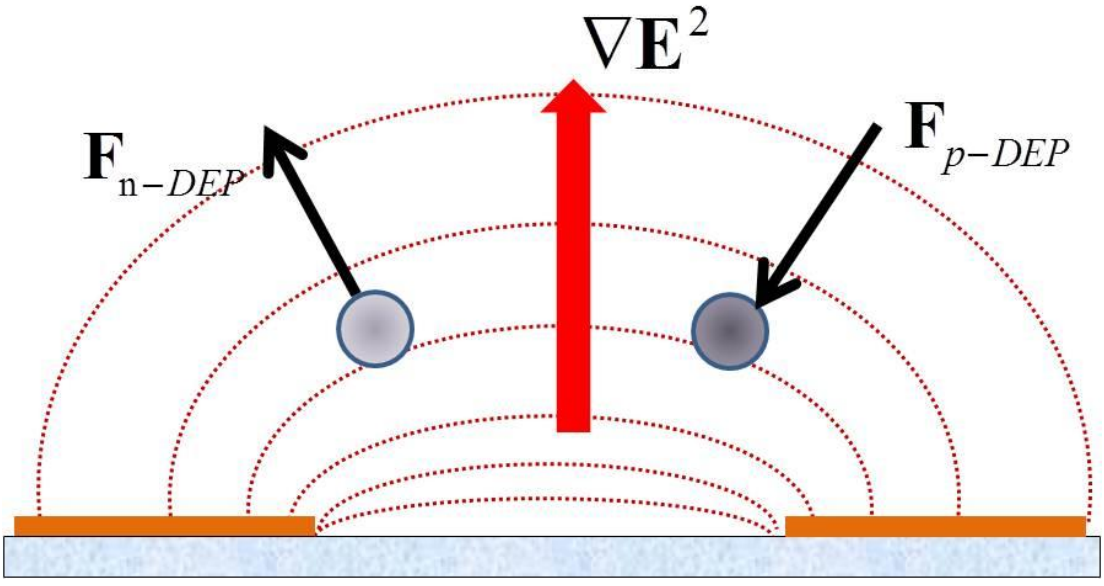

Figure 6.1 Dielectrophoretic (DEP) force acting on a particle in a suspending liquid above the co-planar electrodes. $\mathbf{F}_{p-DEP}$ and $\mathbf{F}_{n-DEP}$ represent the positive and negative DEP forces, respectively. The dash lines indicate the electric field lines yielded by the

co-planar electrodes. The black arrows suggest the direction of the DEP force acting on the particle.

DEP has become a very popular tool for on-chip microparticles control, manipulation and assembly in microfluidics. Many pioneering works and recent researches in DEP are focused on the sorting, trapping and manipulation of DNA (Washizu and Kurosawa 1990; Washizu et al. 1994; Washizu et al. 1995; Suzuki et al. 1998; Kawabata and Washizu 2001; Asbury et al. 2002; Chou et al. 2002; Dalir et al. 2009), carbon nanotubes (CNTs) (Chen et al. 2001; Krupke et al. 2003; Krupke et al. 2003; Lee et al. 2005), cells (Fiedler et al. 1998; Brisson and Tilton 2001; Gascoyne et al. 2002; Heida et al. 2002; Huang et al. 2002; Minerick et al. 2002; Manaresi et al. 2003; Minerick et al. 2003; Gray et al. 2004; Prasad and Ozkan 2004; Lewpiriyawong et al. 2011; Lewpiriyawong et al. 2012), droplets (Washizu 1998; Schwartz et al. 2004; Wang et al. 2009; Wang et al. 2010; Wang et al. 2010) as well as polymer microspheres (Fuhr et al. 1992; Pethig et al. 1992; Fuhr et al. 1994; Green and Morgan 1999; Huang et al. 2002; Lewpiriyawong et al. 2008; Lewpiriyawong et al. 2010). Moreover, DEP is also synergistically combined with other techniques in lab-on-a-chip and microfluidic devices, such as optoelectronic tweezers (Chiou et al. 2005)and electrowetting (Yeo and Chang 2005; Yeo and Chang 2006).

In addition, the use of AC electric field to manipulate and assemble particles has been intensively studied. New materials can be developed by directly assembly of particles with electric functionality in microfluidics (Trau et al. 1995; Trau et al. 1996; Trau et

al. 1997; Velev 2004; Zhang and Liu 2004; Zhang and Liu 2006; Xie and Liu 2008; Xie and Liu 2009). Under the application of AC electric fields, the effect of DEP force becomes much complex when a large amount of particles are suspended into the carrier medium. The induced dipole on particles can not only interplay with the externally applied electric field, but also with each other if the neighboring particles are close enough. It has been reported that rapid and switchable assembly of 2D colloidal crystals is realized by using AC electric fields applied to co-planar electrodes with a gap (Lumsdon et al. 2004; Velev 2004; Velev and Bhatt 2006; Simon and Orlin 2008). The micro-sized particles are attracted to the surface between electrodes by a positive DEP force and subsequently 2D crystals are oriented along the electric field due to the inter-dipole chain force (attractive force). However, in these studies the separation gap between electrodes is in millimeter scales, and hence the electric field gradient at the middle regions of the inter-electrode gap is very weak. In addition, a greater separation between electrodes requires a higher electric voltage input to yield a sufficient electric field.

In this chapter, on-chip particles assembly in non-uniform electric field is demonstrated by using combined effects of DEP and dipole attractive force. Specifically, a remarkable electric field gradient is created by applying AC electric field to co-planar electrodes with microscale separation. A negative DEP force is employed to relocate particles in the inter-electrode gap toward electrode surface and thus push the particles away from the gap between electrodes in a short period. In addition, a hypothesis is proposed to explain the experimental observation.

6.2 Experiment

6.2.1 Microchip design and fabrication

The microchip used for investigating on-chip particles assembly in a non-uniform electric field is similar to which used in chapter 5. Briefly, it consists of a piece 0.7 mm-thick Indium Tin Oxide (ITO) glass with electrodes patterns, a 60 μm thick dry adhesive layer and a piece of 1 mm-thick silica glass. To protect the electrodes from dissolving in electrolyte solution, a 1.5 μm thick SU8 dielectric layer was spin-coated on the ITO glass surface. Two 1 mm holes were drilled on the corner of the top silica glass in order to feed the particle solution. A photograph and schematic illustration of fabricated microchip are shown in Figure 6.2.

Straight electrodes array were patterned on the bottom ITO electrodes. Each electrode was designed with a 200 μm width and arranged parallel to each other with separations of 50 μm, 100 μm and 200 μm, respectively (Figure 6.2 (c)).

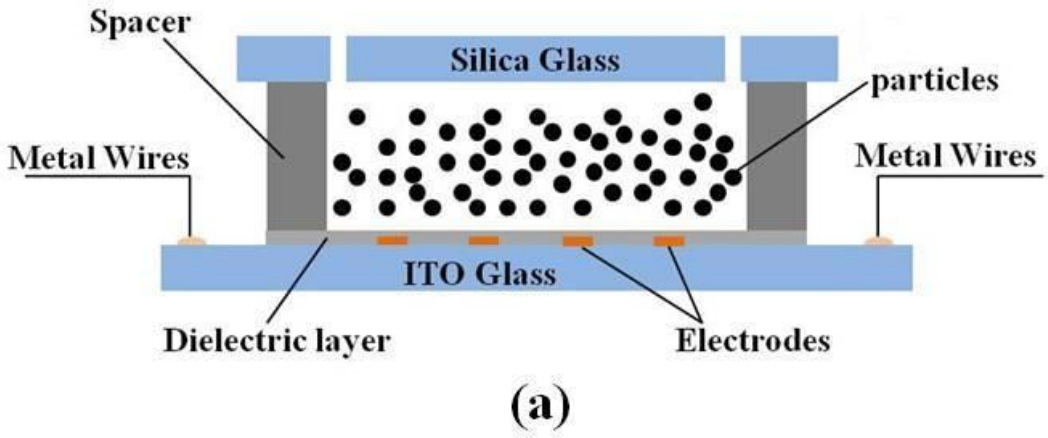

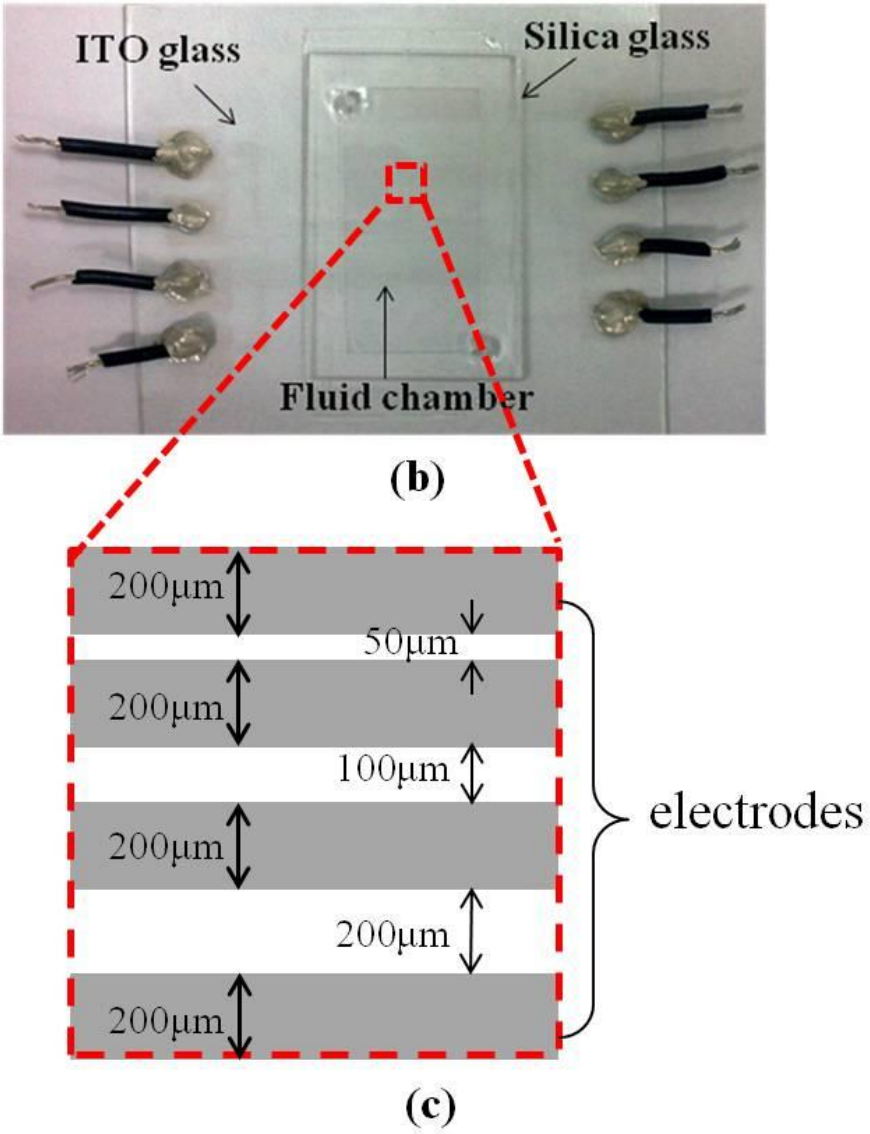

Figure 6.2 Microfluidic chip used for investigating on-chip particles assembly in a non-uniform electric field, (a) a cross-section view of the structure, (b) a photograph of the microchip (top view) and (c) design of electrodes array on the bottom ITO glass. The grey rectangular strips in Figure 6.2 (c) represent the ITO electrodes and white areas between electrodes denote inter-electrode gaps.

6.2.2 Materials and methods

Polystyrene microspheres with 2.9 μm, 1 μm and 0.5 μm in diameter were used in this study. The original particle solution was dehydrated and resuspended in DI water. During the experiment, the particles solution was introduced into the electronic display cell by a syringe through a hole on the front plane and the cell was hence filled automatically by capillary forces. The AC electric signal was provided by a function generator (Agilent 33250A, USA). The microscale particles displacements were captured by an optical microscope (Zeiss, Germany) equipped with a CCD camera (Sensovation, Germany) at a rate of 15 frames per second (fps).

6.3 Results and discussion

6.3.1 On-chip particles assembly by non-uniform electric field

On-chip assemble of 2.9 μm polystyrene microspheres suspended in DI water at a concentration of 5% w/w were first tested in the experiment. An AC electric field of 10 Vpp, 1MHz was applied across the co-planar electrodes with a 100 μm inter-electrode separation. The physical process of on-chip particles assembly in a non-uniform electric field is demonstrated in Figure 6.3. Immediately after the electric signal is turned on, two defect bands are clearly seen along the electrode edges. Particles in the inter-electrode gap assemble compactly to form a rectangular strip

parallel to the co-planar electrodes. With the time elapse, particles in the middle strip are gradually lifted and transported to each side above the electrodes. The image of particles in the middle strip in Figure 6.3 becomes blurring, suggesting the particle lifting process. Particles in the middle strip move to electrodes with bridge-like continuous chains, like fiber drawing form a silk. Since the particles are relocated from the middle strip to the electrodes at each side, the width of middle particles strip within the gap reduces gradually. At the same time, the distance between the outer boundaries of the two defect bands is enlarged with time elapse. With increasingly particles relocate from middle gap to electrodes, the middle particle strip tends to disconnected, as shown in Figure 6.3 from 20 s to 50 s. After the voltage is applied for half a minute, the bridge-like particle chains detach with particles motion due to the sharply reduction of particle numbers in the middle gap (Figure 6.3 30 s), leading to the retardation of the particles relocation. The middle gap between co-planar electrodes is emptied and almost no particle is observed within the gap after the AC electric field is applied for 50 s approximately, as seen in the figure.

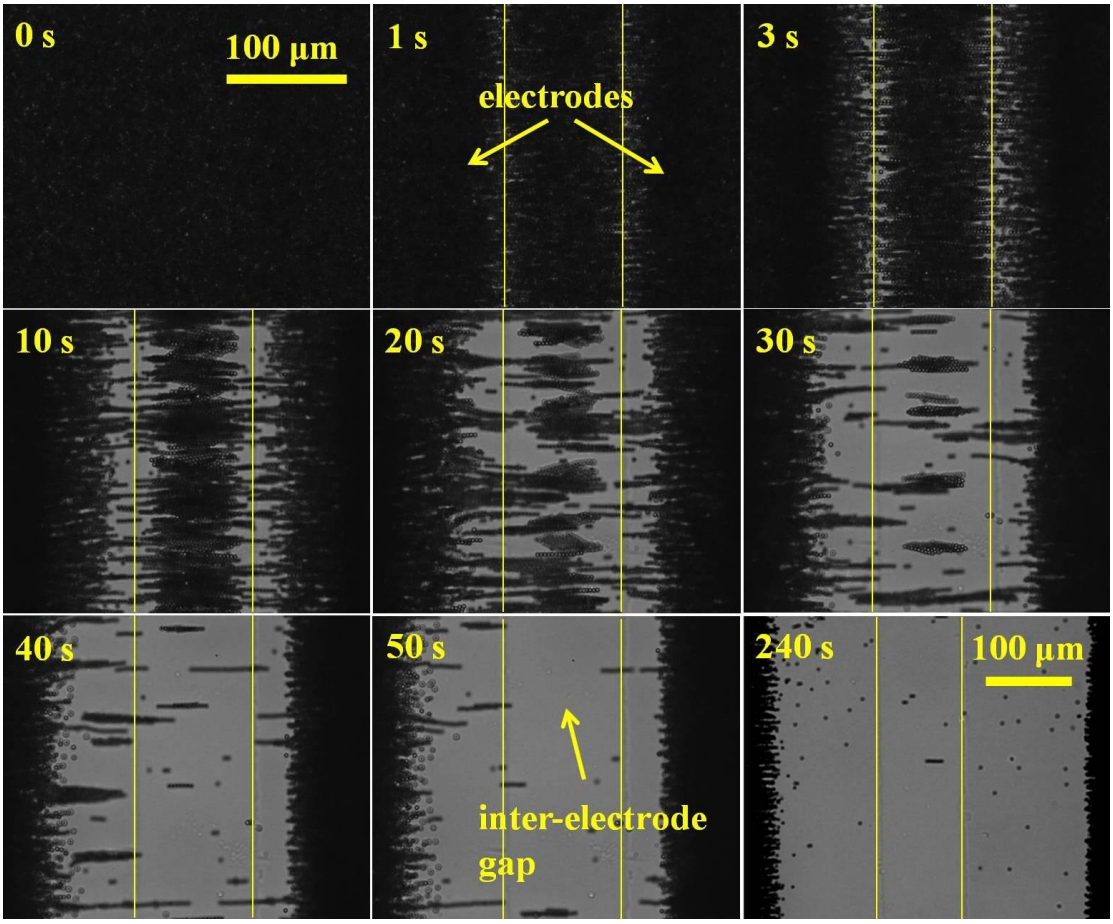

Figure 6.3 The physical process of 2.9 µm microspheres assembly under a non-uniform electric field. An AC electric field of 10 Vpp and 1 MHz is applied across the co-planar electrodes with a 100 µm inter-electrode separation. The scale of last picture is different from the rest. The light lines in the figure indicate the edges of electrodes.

Experimental observation suggests that the on-chip particles assembly in a non-uniform electric field involves two stages, as shown in Figure 6.4. As the non-uniform electric field is yielded by applying AC electric voltages across the co-planar electrodes, it is believed that the highest electric field exists at the inner edges of both electrodes. The physical mechanism of stage I of particles assembly in a non-uniform

electric field is illustrated in Figure 6.4 (a). Once the electric voltage is switched on, the non-uniform electric field yields a very strong DEP force at the electrode edges and particles are hence repelled away from the highest electric field regions. Simultaneously, because of the chain force (attractive interaction among particles) resulted from the interaction of induced dipoles under an externally electric field, the particles in the co-planar electrodes gap are further compacted result in the formation of a close-packed particles strip in the gap between the co-planar electrodes. In stage II, with the electric voltage keep loading, particle chains in the middle gap are gradually lifted by DEP force until they reach a metastable position at which the net force acting on particle chains along the vertical direction (*y* direction in the figure) is balanced by *y*-component DEP force against gravity. However, the net force acting on particle chains along *x* direction due to *x*-component DEP force and chain interaction drive particles relocate from the metastable position above the middle gap to the electrode surface at each side, as shown in Figure 6.4 (b).

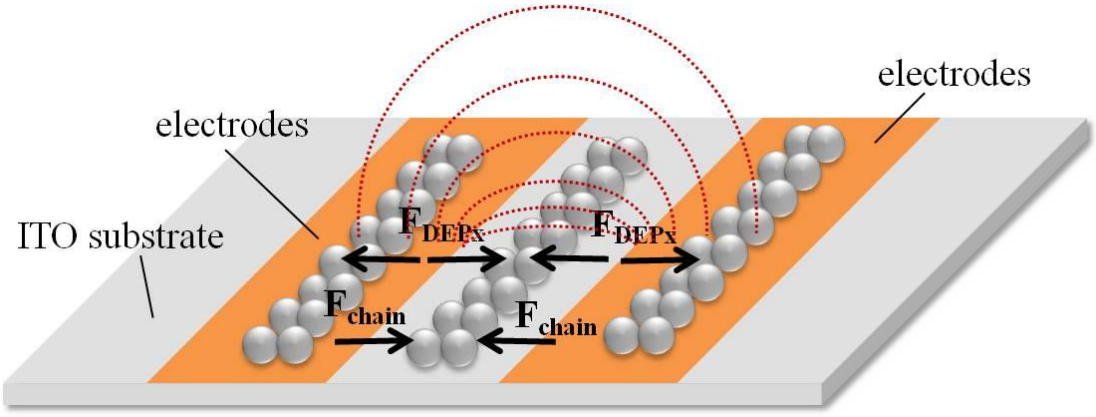

(a)

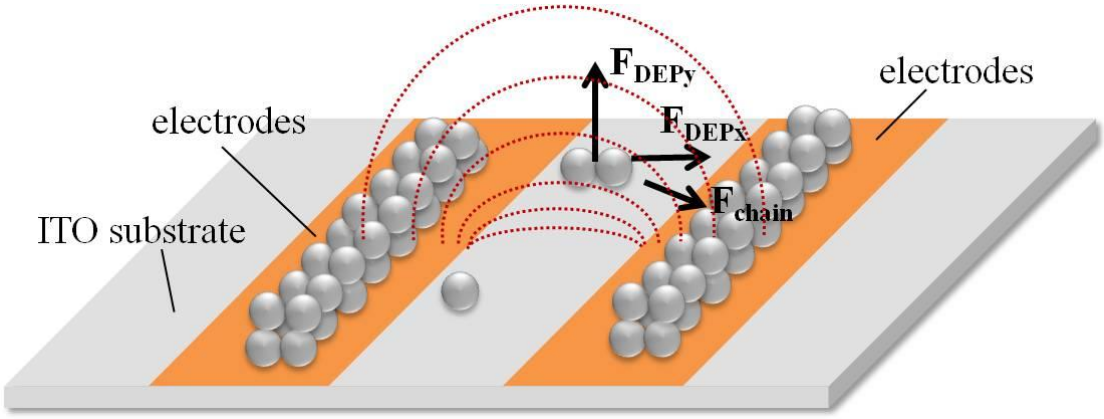

(b)

Figure 6.4 Schematic illustration of the physical mechanism of on-chip particles assembly in a non-uniform electric field for (a) stage I and (b) stage II. The dash curves indicate the electric field lines.

Both the DEP force and chain attractive force are related to the induced dipole in dielectric particles resulted from the mismatch of electric and dielectric properties of the particle and the carrier medium. The use of non-uniform electric field generates non-homogeneously distributed dipole moment over the particle-liquid interface, giving rise to a net DEP force exerting on particle,

$$\mathbf{F}_{DEP} = 2\pi\varepsilon_{\mathrm{m}} a^3 \,\mathrm{Re}\left[f_{CM}(\omega)\right]\nabla E^2 \tag{6.1}$$

where ε_{m} is the dielectric permittivity of the fluid and $\mathrm{Re}\left[f_{CM}(\omega)\right]$ is the real part of the Clausius-Mossotti factor. The induced dipoles in the particles by applied electric field also exert attractive forces between particles and cause them to align into chains.

The chain force is given by (Lumsdon et al. 2004; Velev 2004; Velev and Bhatt 2006; Gupta et al.; Kim et al. 2011)

$$\mathbf{F}_{chain} = -C\pi\varepsilon_{\mathrm{m}}a^2\,\mathrm{Re}\left|f_{CM}(\omega)\right|^2 E^2 \tag{6.2}$$

where the coefficient *C* ranges from 3 to > 1000 depending on the distance between the particles and the length of the particle chain (Jones 1995).

6.3.2 Effect of particle concentration

In order to systematically study the on-chip particles assembly in a non-uniform electric field and explore the underlying physical mechanism accounting for this phenomenon, several operational parameters are further studied.

The effect of particle concentration on the process of particle assembly was investigated. The physical process of 2.9 μm particles assembly under an AC field of 10 Vpp, 1MHz applying across the co-planar electrodes with a 100 μm inter-electrode separation was tested. The 2.9 μm polystyrene microspheres were re-suspended into DI water with three different concentrations (w/w) 5%, 1% and 0.2 %. The experiment results are shown in Figure 6.5. With a 5% particle concentration, stage I and stage II of the on-chip particle assembly process almost effect at the same time. However, with lower particle concentrations, i.e. 1% and 0.2%, particles along the electrodes edges are firstly repelled and arranged in the middle gap to form a compact

particle strip, showing the stage I. With time elapse, the particles in the middle strip are gradually lifted and move to electrodes, indicating the stage II particles assembly process.

It is observed that, at stage I with a high particle concentration a wider middle particle strip is formed but narrower defect bands. In addition, a much faster on-chip particles assembly process is observed for the 5% particle solution. This is because at stage I the formation of the middle particles strip is mainly attributed to the DEP force at the inner electrode edges and chain attractive force. The distance between neighboring particles reduces sharply with the significant increment of particle concentration, resulting in the greatly enhancement of the chain attractive force acting on the particles. Once the electric voltage is turned on, the DEP forces at the electrodes edges repel particles toward the middle gap and they are closely packed due to a strong chain interaction along the direction of the electric field. As a result, particles form a rectangular strip immediately after the electric field is applied for the 5% particle solution. In contrast, because the chain force is significantly weakened in response to the sharply decline of particles number, the compact particles strip in the middle gap is still uncompleted even the electric signal is turned on for 3 s with the 0.2% particle solution.

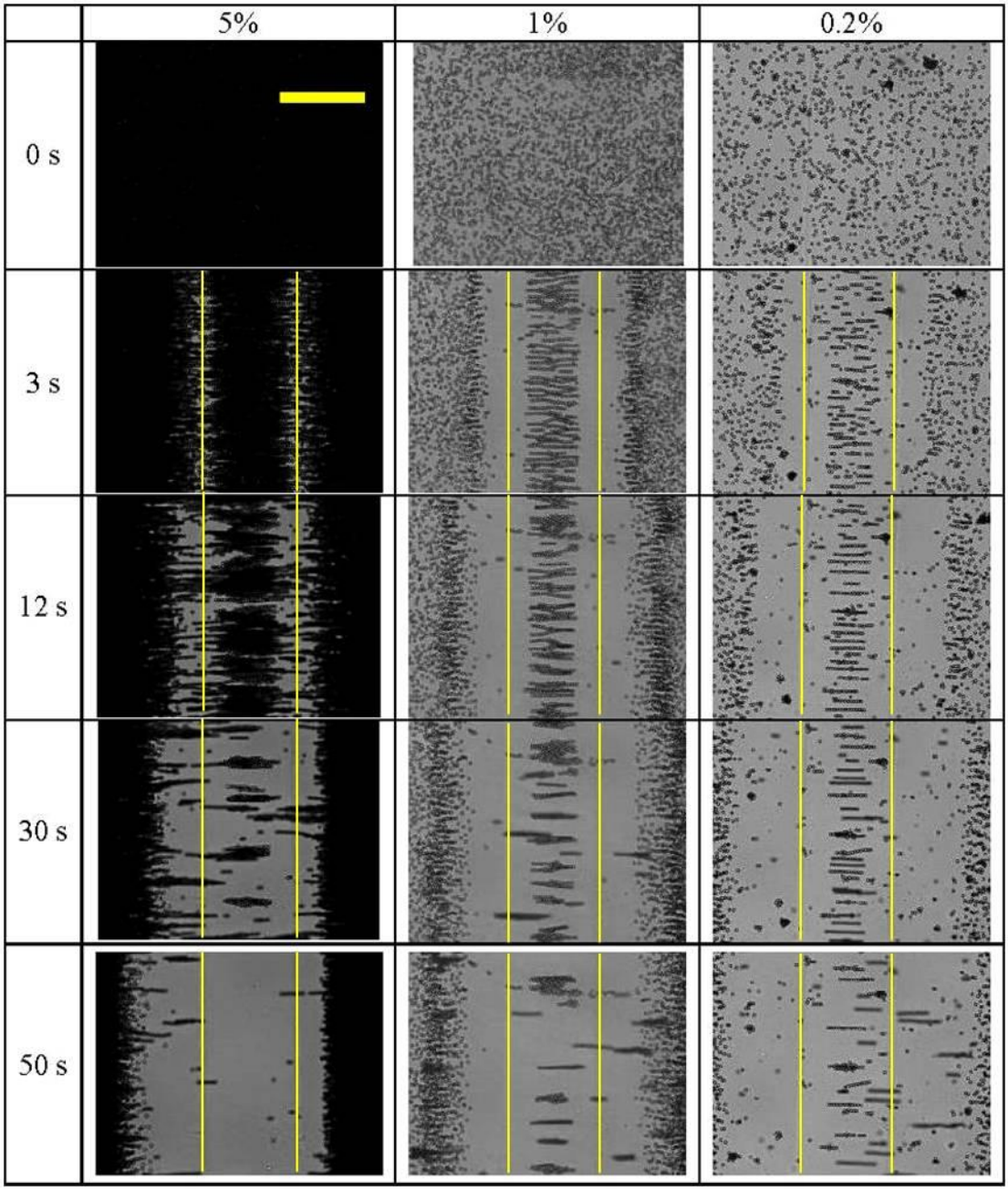

Figure 6.5 Images of the on-chip particle assembly under non-uniform electric field with particle concentrations (w/w) of 5%, 1% and 0.2 %. The scale bar represents 100 μm. The light lines in the figure indicate the edges of electrodes.

At stage II, the particles assembly process is also found enhanced with a higher particle concentration. As seen in the Figure, for a 5% particle solution, most particles have relocated from the middle gap to aside electrodes after the electric field is applied for 30s. The middle gap between the co-planar electrodes is cleared with almost no particles after the electric voltage is loaded for 50 s. However, for lower particle concentrations (for instance, 0.2 % particle solution), as the chain force acting on the particles is much weakened due to a larger inter-particle separation, there are a large number of particles staying in the middle gap even after the electric field is applied for 50 s, as shown by the pictures at the last row in Figure 6.5. The faster response of particles assembly process at stage II with a higher particle concentration is resulted from the high volume fraction of the particles. On one hand, with a higher particle concentration, the reduced inter-distance can enhance the chain interaction among neighboring particles. On the other hand, because DEP is dependent on the volume of the dielectric object, with the increasing number of particles within the micro chip, a greater chain force can in turn form longer particle chains, and thus strengthening the DEP force.

The contribution of chain force on the particles assembly process could also be discovered by comparing the particles assembly process at stage I and stage II. For example, for the 5% particle solution, the particles relocate from the middle strip toward the electrodes with bridge-like continuous chains from 0 s to 30 s. Due to the great chain attractive force, most particles have accumulated at the electrodes within 30 s after the electric field is applied. However, once the continuous chains structures

are broken, the particle assembly process is highly retarded due to the significant reduction of chain force. Although only a small group of particles in the middle gap, it takes 20 more seconds for the completion of the stage II.

6.3.3 Effect of applied electric voltage

In order to quantify the process of on-chip particles assembly in a non-uniform electric field, we define parameters l_1 and l_2 signifying the distance between the outer edges of these two defect bands and the width of particles strip in the middle gap, respectively. l_0 is the inter-electrode separation. l_1 and l_2 are normalized by l_0, giving the dimensionless parameters L_1 and L_2, namely, $L_1 = l_{1/} l_0$ and $L_2 = l_{2/} l_0$.

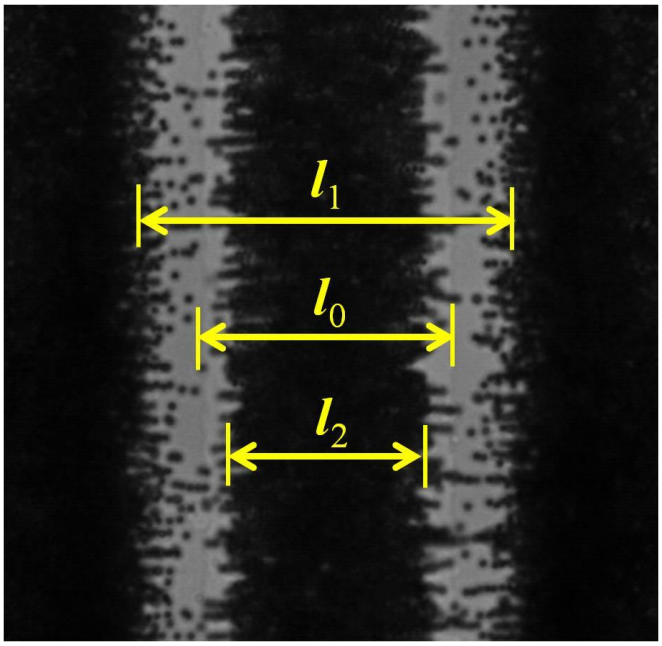

Figure 6.6 Illustration of the parameters defined for analyzing experimental results.

Figure 6.7 represents the effect of applied electric voltage on the particle assembly process in a non-uniform electric field. The particle assembly process under AC electric voltages of 10 Vpp, 7.5 Vpp and 5 Vpp were tested and the rest parameters are kept unchanged. Because both the DEP and chain forces are functions of applied electric field, with the drop of the applied voltage, the particle assembly is retarded dramatically. The dash line in the figure representing an intermediate period at which the middle particles strip is detached so that it is difficult to exactly examine the value of L_2 (corresponding to images of 20 s, 30 s and 40 s demonstrated in Figure 6.3). After a longer time, i.e., t = 50 s, it is no particle in the middle gap and thus L_2 drop to 0 indicating the completion of stage II in the particle assembly process.

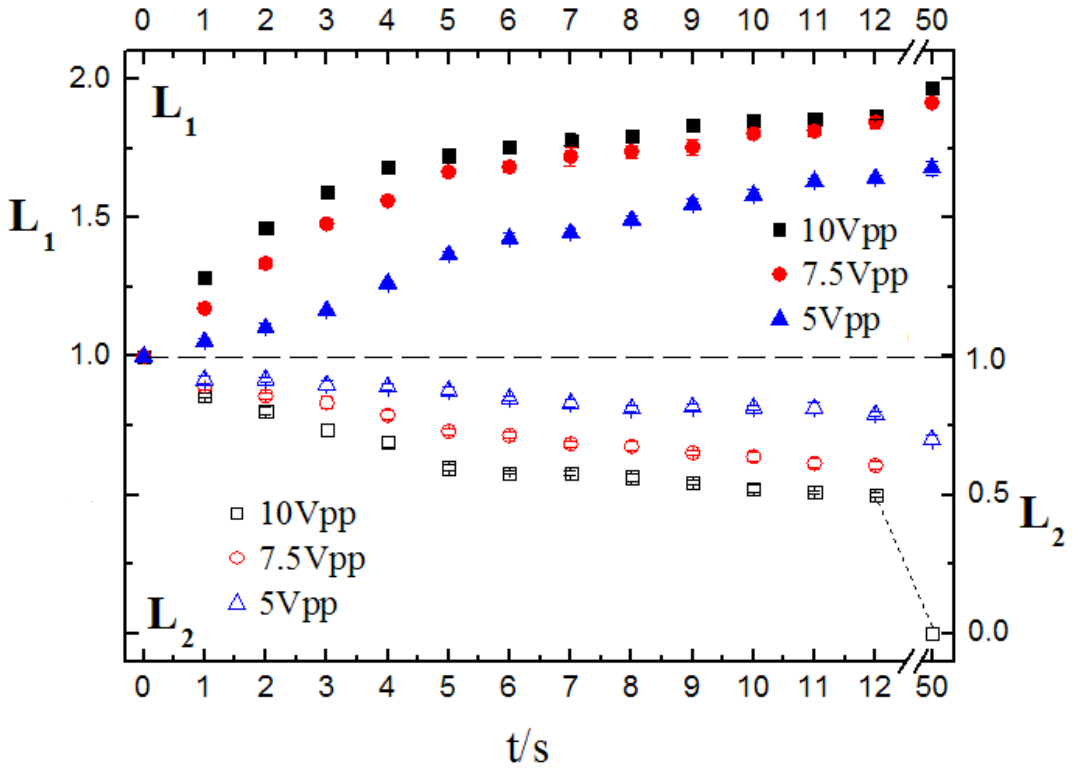

Figure 6.7 Effect of applied electric voltage on the process of particle assembly in non-uniform electric field. Experimental date showing L_1 and L_2 are represented by

solid and hollow symbols, respectively. The dash line indicates the intermediate period.

6.3.4 Effect of the inter-electrode separation

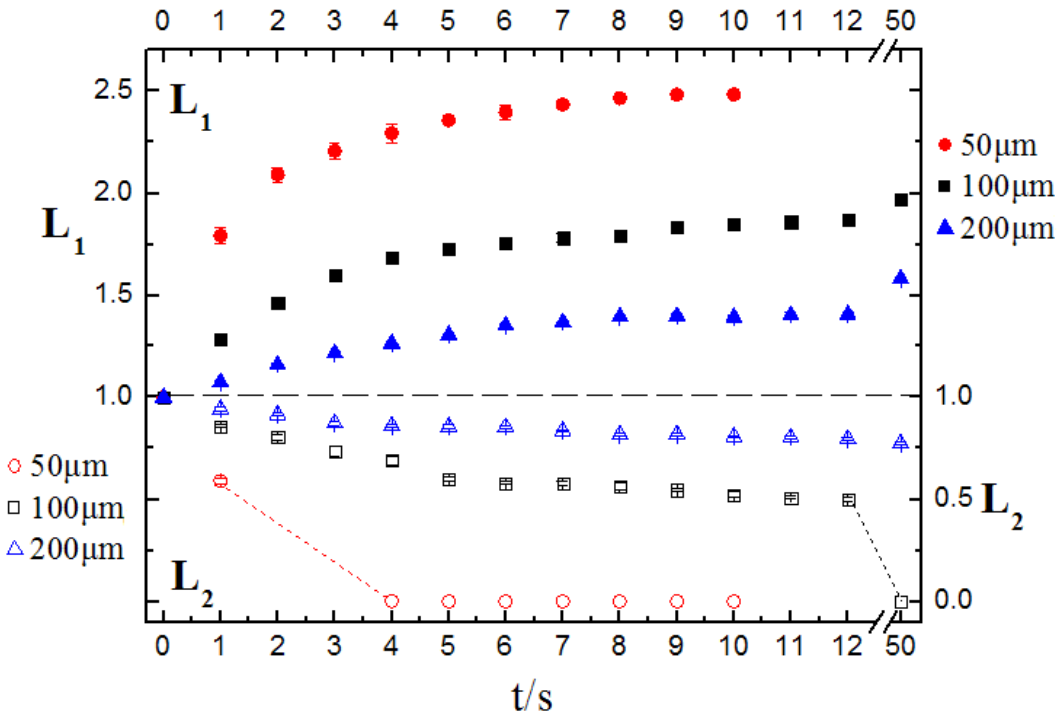

Figure 6.8 Effect of inter-electrode separation on the process of particle assembly in non-uniform electric field. Experimental date showing L_1 and L_2 are represented by solid and hollow symbols, respectively. The dash line indicates the intermediate period.

Figure 6.8 represents the effect of inter-electrode separation on the on-chip particles assembly in a non-uniform electric field. The inter-electrode separations of 50 μm, 100 μm and 200 μm were studied during the experiment and all other parameters are

held constant. It is observed that the particles assembly process is enhanced dramatically with the shrinking of inter-electrode separation. In fact, a narrower inter-electrode separation can enhance both the intensity and gradient of the electric field and therefore significantly increasing the DEP and chain forces during the particles assembly process. As a results, particles assembly with a 50 μm inter-electrode gap response rapidly and L_2 drop to 0 within 4 s after the voltage is turned on (as shown in Figure 6.9) compared with 50 s with that of the 100 μm inter-electrode gap. At a 200 μm inter-electrode separation, both the intensity and gradient of the electric field in the middle gap are very weak, therefore, the width of the particles strip in the middle gap almost unchanged after the electric field is applied for 5 s (Figure 6.10).

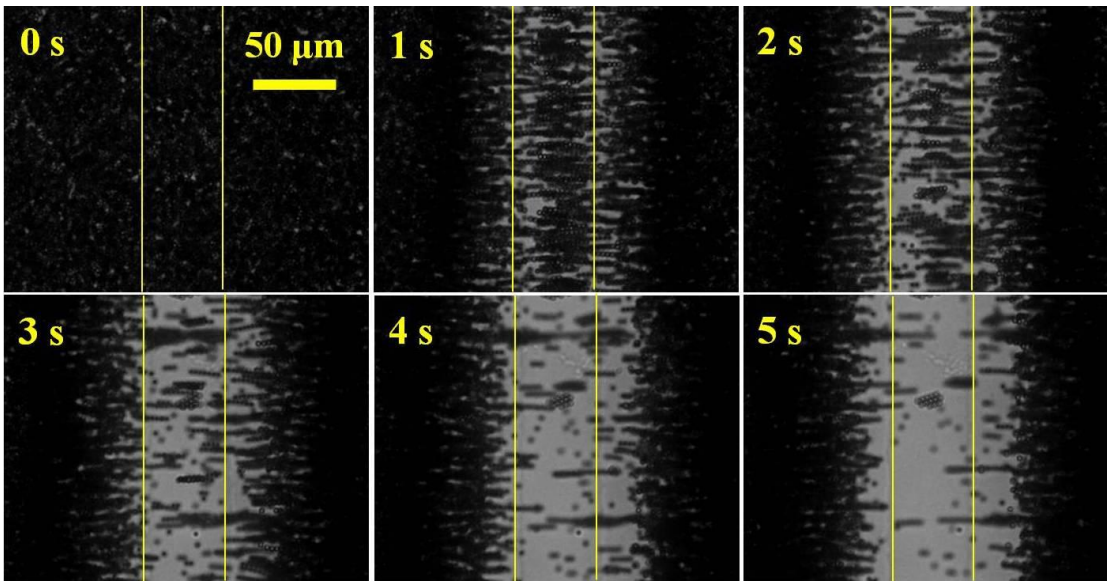

Figure 6.9 The physical process of 2.9 μm microsphere assembly under non-uniform electric field with a 50 μm inter-electrode separation. An AC electric field of 10 Vpp and 1 MHz is applied across the co-planar electrodes. The light lines in the figure indicate the edges of electrodes.

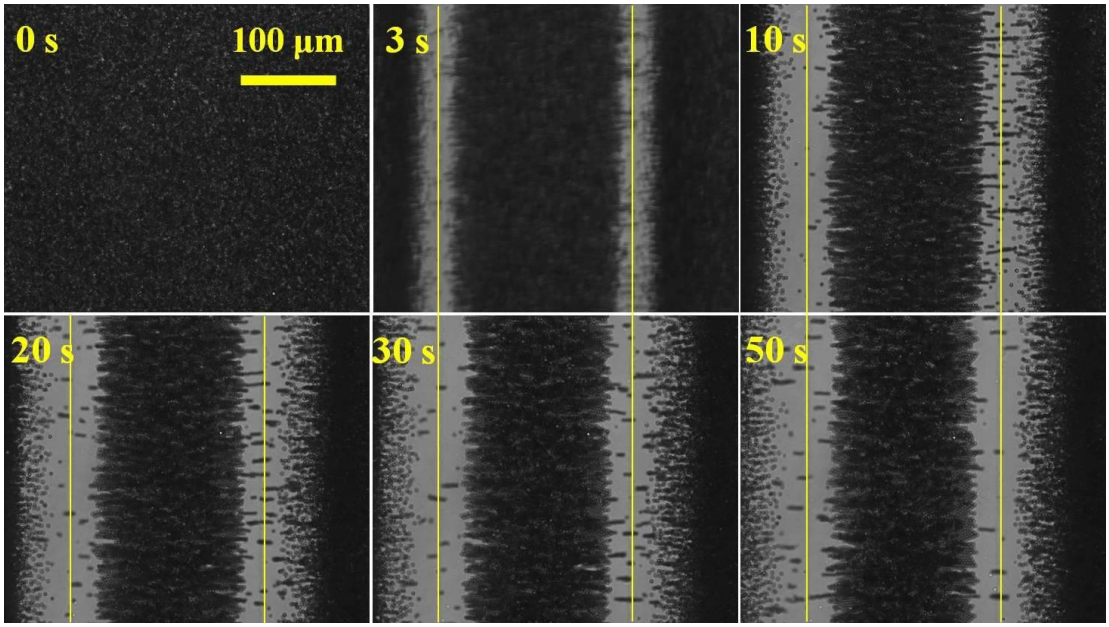

Figure 6.10 The physical process of 2.9 μm microsphere assembly under non-uniform electric field with a 200 μm inter-electrode separation. An AC electric field of 10 Vpp and 1 MHz is applied across the co-planar electrodes. The light lines in the figure indicate the edges of electrodes.

6.3.5 Effect of the frequency of the electric field

Figure 6.11 shows the effect of the frequency of the applied AC electric field on the particles assembly in a non-uniform electric field. The frequency of 1MHz, 500 KHz and 100 KHz were studied during the experiment and all other parameters are held constant. At a 500 KHz, both L_1 and L_2 grow very slowly with time elapse, indicating the drop of driven force acting on particles. Actually, for 2.9 μm particles suspend in DI water, the real part of the Clausius-Mossotti factor $\mathrm{Re}\left[f_{CM}(\omega)\right]$, which is a measure of the effective polarizability of particles, reduce significantly when the frequency drop from 1 MHz to 500 KHz (as shown in Figure 6.12). At 100 KHz,

according to the prediction of the plot of CM factor, the value of $\mathrm{Re}\left|f_{CM}(\omega)\right|$ is above 0 which suggest a positive DEP force at this frequency. The experimental observations are demonstrated in Figure 6.13. The particles assembly is significantly retarded by the reduced DEP and dipole chain force at 500 KHz frequency. With the frequency keeps dropping to 100 KHz, particles are observed assemble in the middle gap without any defect band, suggesting the positive DEP force acting on the particles. We did not test the frequency at the order of ~10 KHz because the electrohydrodynamic flow (EHD) becomes significant at such frequencies range.

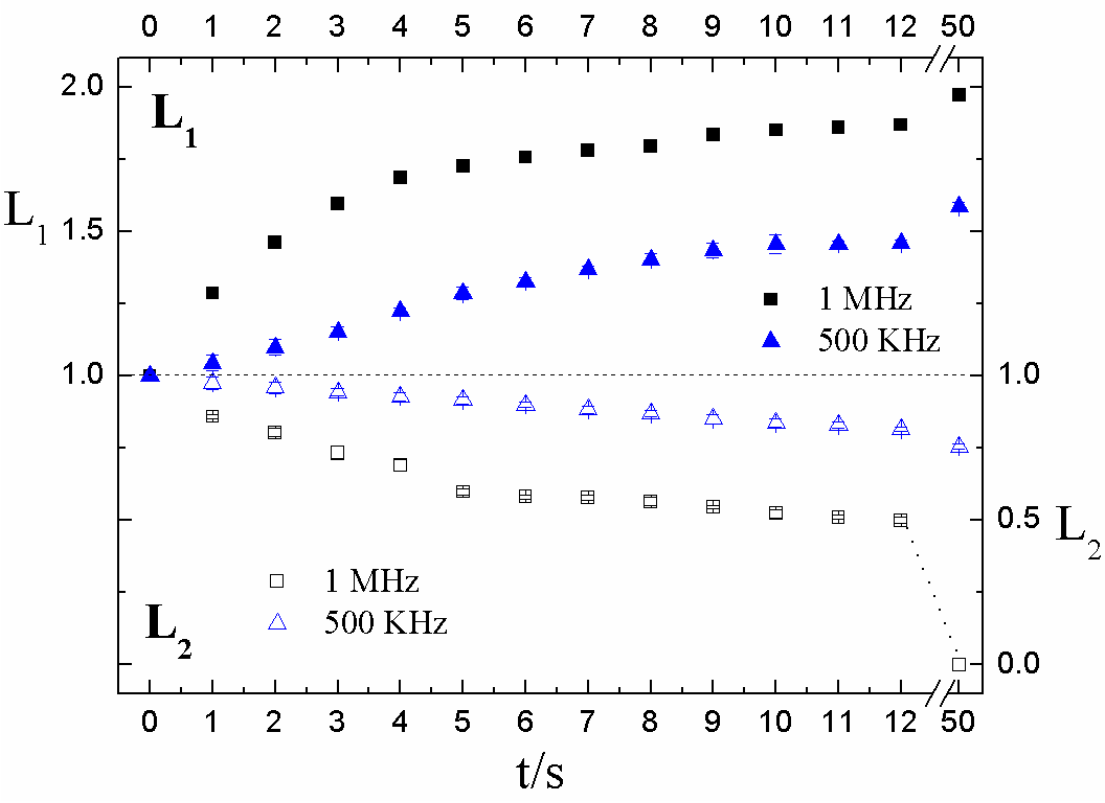

Figure 6.11 Effect of the frequency of the applied AC electric field on the process of particles assembly in non-uniform electric field. Experimental date showing L_1 and L_2 are represented by solid and hollow symbols, respectively. The dash line indicates the intermediate period.

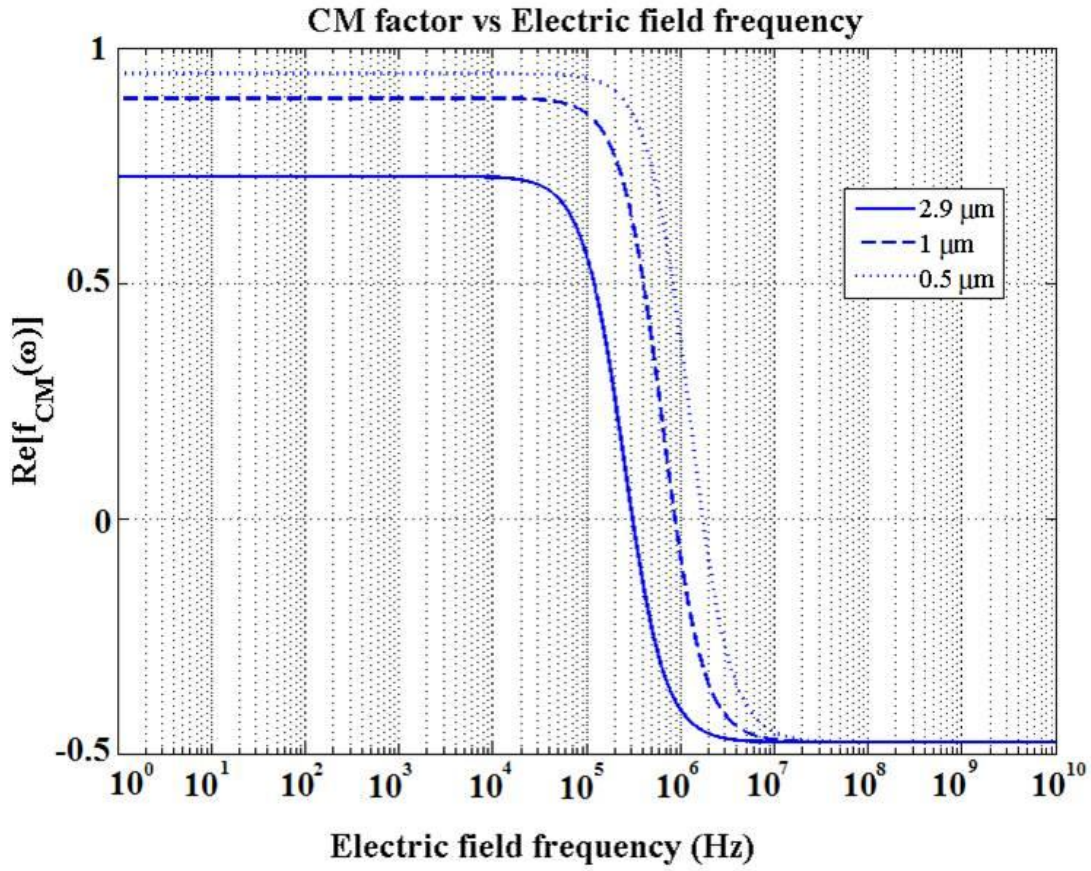

Figure 6.12 Plot of the CM factor versus frequency for particles with different size.

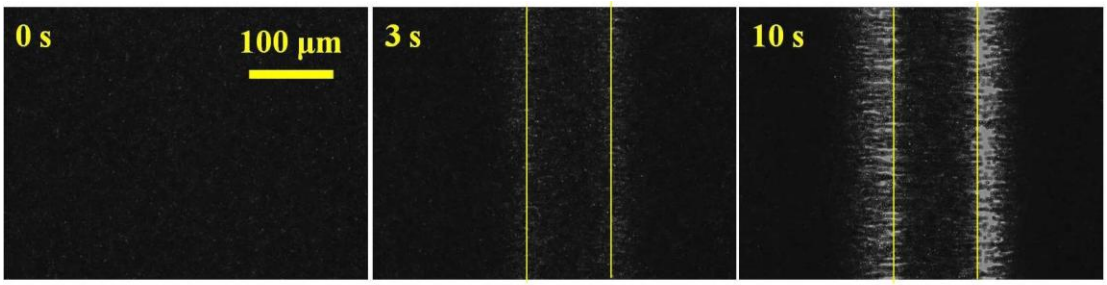

(a) $f = 500$ KHz

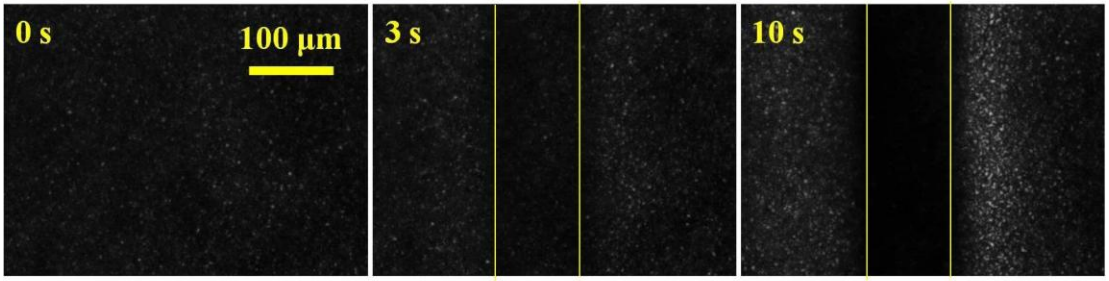

(b) $f = 100$ KHz

Figure 6.13 The physical process of 2.9 μm microsphere assembly under non-uniform electric field with applying an AC electric field of 10 Vpp , (a) 500 KHz and (b) 100 KHz. The electric field is applied across the co-planar electrodes with a 100 μm inter-electrode separation. The light lines in the figure indicate the edges of electrodes.

6.3.6 Effect of particle size

The effect of particle size on the assembly process was studied. We tested the polystyrene particles with the diameters of 2.9 μm, 1 μm and 0.5 μm and the rest parameters were held unchanged. The particles assembly with 1 μm particles was observed much slower than which of 2.9 μm particles, as seen in Figure 6.14. On one hand, since DEP and chain forces are proportional to r^3 and r^2 respectively, the decrease of particle size results in a sharply reduction of driven force and thus slow

down the particles assembly. On the other hand, the value of $\mathrm{Re}\left|f_{CM}(\omega)\right|$ for 1 μm particles at 1 MHz is very small (as seen in Figure 6.12) and thus further weakens the driven force. For 0.5 μm particles, the DEP and chain force get over a hundred times and about 36 times weaker, respectively. As a result, even the electric voltage was applied over 2 minutes, particles relocation is still not observed yet in the experiment, due to the slight driven force acting on the particles. In addition, once the particle size reduces to submicron range, the effect of Brownian motion on the particles becomes significant, and thus the particles assembly process is retarded. The Brownian force for small suspended particles is modeled as (Li and Ahmadi 1992; Ramos et al. 1998; Kim and Zydney 2004),

$$F_B = \varsigma\sqrt{\frac{12\pi a\eta k_b T}{\Delta t}} \tag{6.3}$$

where ς is a Gaussian random number with zero mean and unit variance and Δt is the magnitude of the time step. The time-averaged randomizing force F_B due to Brownian motion is zero. The DEP force and Brownian force acting on the particles can be estimated by using equation (6.1) and (6.3). For example, for 2.9 μm particles suspended in the carrier medium over an observation time of 0.5 s, the DEP force and Brownian force acting on the particle near the electrode edge are approximately $\sim 2.4\times10^{-12}$ N and $\sim 2.2\times10^{-14}$ N, respectively. Therefore, the effect of Brownian force on the particles assembly process can be safely ignored. While, for 0.5 μm particles, the DEP force and Brownian force acting on the particle near the electrode edge over

an observation time of 0.5 s are ~1.1×10^{-14} N and ~0.8×10^{-14} N, respectively. Obviously, the particles assembly process is significantly affected by the presence of Brownian motion.

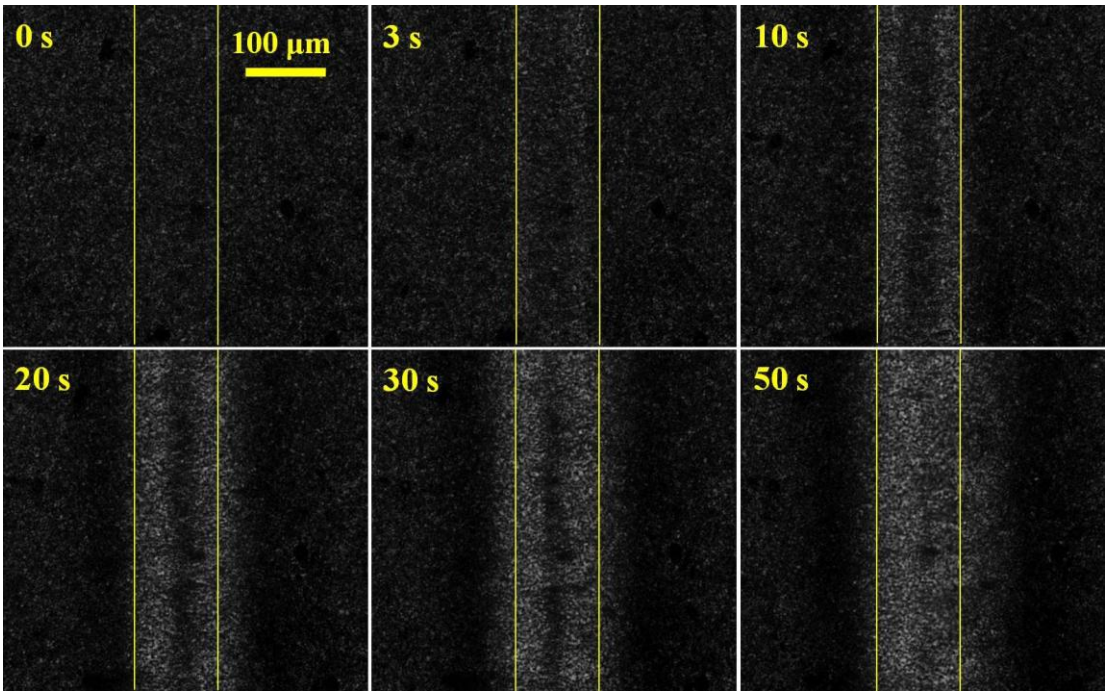

Figure 6.14 The physical process of 1.0 μm microsphere assembly under non-uniform electric field. An AC electric field of 10 Vpp and 1 MHz is applied across the co-planar electrodes with a 100 μm inter-electrode separation. The light lines in the figure indicate the edges of electrodes.

6.4 Summary

The physical process of particle assembly in non-uniform electric field is experimentally investigated in this chapter. With co-planar electrodes patterned on an ITO substrate, the particles in the middle gap between electrodes can move to side

electrodes under an applied AC electric field. The process of particle assembly in non-uniform electric field includes two stages. At the first stage, the strong DEP force at the electrodes edges repel particles away from the high electric field regions, forming two defect bands along the electrodes inner edges. At the same time, particles in the middle electrodes gap assemble as a close-packed strip due to the dipole induced chain interaction under the AC electric field. At the second stage, the particles in the middle strip are gradually lifted and move toward each side as continuous chains with the effect of DEP and chain attraction. Finally, with a longer period after the AC electric field is applied, the particles in the middle electrode gap are completely transported to the electrode surfaces.

The particles assembly under non-uniform electric field is found to be enhanced with higher particle concentration, stronger electric voltage as well as narrower inter-electrode separation. The particle assembly also is affected by the frequency of the AC electric field and the particle size as well. Decreasing the frequency can retard the particle assembly due to drop of the value of $\mathrm{Re}\left[f_{CM}(\omega)\right]$ which weakens the driven forces acting on particles. However, further reducing the frequency, the DEP force acting on particles can become positive, resulting in particle assemble in the middle electrode gap. In addition, the particle assembly also is retarded with a decrease of particle sizes. Smaller particles get weaker DEP and chain forces but stronger Brownian effect, thus the response slows down. Limited by the ITO electrodes, the work presented in this chapter involved the use of DI water solution only. More investigations should be conducted in the future to explore the particle assembly at

high-concentration electrolyte and non-aqueous media by using gold/platinum sputtered electrodes.

Chapter 7: A novel electronic paper display based on the combined effects of dielectrophoresis and dipole force

7.1 Introduction

The past decades has witnessed the fast development of the electronic paper technologies. With the rise of electrophoretic display (EPD) media, the world is opening up for new uses of electronic displays. In the late of 1990s, the first demonstration of microcapsulated EPD in Massachusetts Institute of Technology and its subsequently works lead to dramatic improvements in EPD performance and the commercial EPDs now ubiquitous in e-Readers.

Although the EPD technology has been commercialized for over 10 years, many improvements still remain to be implemented (Henzen and Van De Kamer 2006). The first challenge is the relatively low transmittance in e-paper. The transmittance characterizes the ability of light passes through and reflects on the electronic screen and is believed one of the most conspicuous properties of electronic paper display. The transmittance values of electronic papers lie between 20% for various LCD-based systems and about 40% for electrophoretic display. The fast switching response is the second challenge for the development of electronic paper display. Commercial electrophoretic displays now show a switching time of ~300 ms and can satisfy the

requirement of reading. But it is still much slower for video display. The third challenge is the demonstration of full color electronic paper display. The current e-reader and e-book products rely on EPD technology can only show a black-and-white display, which extremely limits their further development. Even if attempts with color filter or RGB sub pixels were made, the commercialization of full color electronic paper is still up in the air because the screen looks washed-out with a color filter and both contrast and brightness are sacrificed with the RGB mode. In addition, a high resolution is an important criterion for electronic paper display as well. A 170-μm linewidth for gray-scale displays is acceptable for most of the current e-papers. However, if the standard RGB stripe configuration is used, the linewidth should have to be reduced to less than 60 μm.

Moreover, as introduced in chapter 5, the current EPD products rely on titanium oxide or toner particles suspended in oil mixture. In order to maximize the surface charge on the particles, very complicated chemical processes are always inevitable. As a result, attempts of manufacturing cost reduction and performance improvement on the current EPD products are limited by their structures and fabrications.

In this chapter, another type of novel electronic paper display is proposed and experimentally demonstrated. The operational principle of the proposed electronic paper display relies on the fundamental physical phenomenon investigated in chapter 6. By patterning straight co-planar electrodes on the backplane of the electronic display panel, information screening is realized by relocating pigment particles from

the inter-electrode gap to the aside electrode surface. According to the experimental observations shown in chapter 6, the response of the particles assembly within the microchip is extremely accelerated by scaling down the electrodes dimensions. Therefore, the most distinguishing feature of the current electronic paper display is that with a smaller electrodes dimension design, both the resolution and switching response are dramatically enhanced simultaneously. In addition, as particles in the middle gap between the co-planar electrodes can be totally cleared after the electric field is applied, a remarkable transmittance is realized by using the current technique. Due to the fact that particles are rearranged horizontally in parallel to the electrodes surface, a full color electronic paper display is also likely to be realized by stacking multi electronic display cells with different dyed color particles.

7.2 Experiment

7.2.1 Microchip fabrication

The microchip used in this study is similar to the prototype used in chapter 5 and was fabricated with the identical method. Briefly, the transparent electrodes were patterned on 0.7 mm thick Indium Tin Oxide (ITO) glasses with an electric resistance of 10 ohm/sq. A piece of plain silica glass (without any electrodes) with a thickness of 1 mm was covered on the ITO glass as the front plane and they are sandwiched with a 60 μm thick dry adhesive layer. Two 1 mm holes were drilled on the corner of the top silica glass in order to feed the particle solution (Figure 7.1).

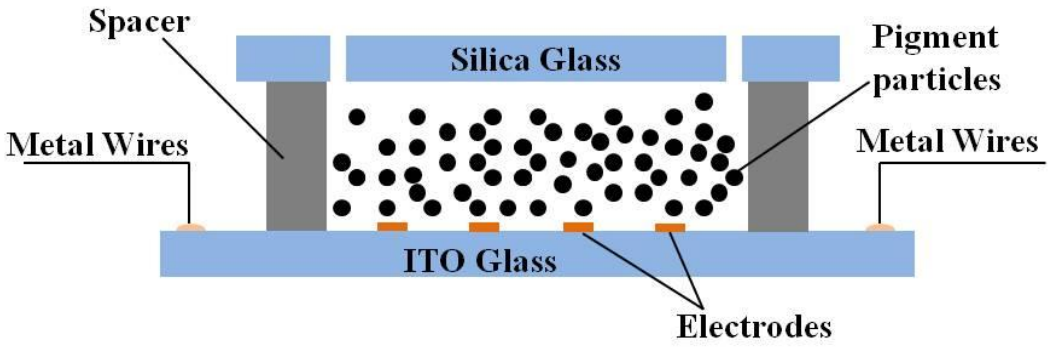

(a)

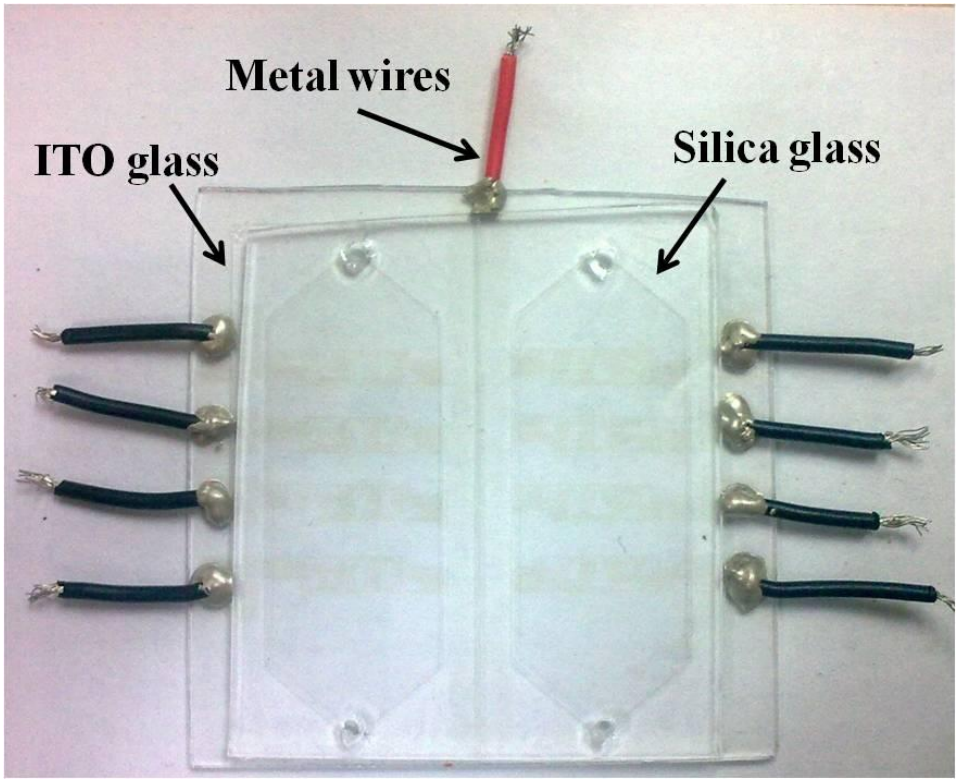

(b)

Figure 7.1 (a) the schematic illustration (cross-sectional view, not in scale) and (b) photograph (top view) of a prototype of the electronic paper display.

7.2.2 Materials and methods

Polystyrene microspheres (white color) with 2.9 μm in diameter were used in this study. The original particle solution was dehydrated and resuspended in DI water at a weight/weight concentration of 3%, corresponding to 2.6×10^{8} particles/ml approximately. The AC electric signal was provided by a function generator (Agilent 33250A, USA). The microscale particles displacements were captured by an optical microscope (Zeiss, Germany) equipped with a CCD camera (Sensovation, Germany) at a rate of 15 frames per second (fps). The information screened on the electronic display panel was recorded by a digital camera with a rate of 25 frames per second (fps).

7.3 Results and discussion

7.3.1 Information display on the electronic paper panel

A prototype of the electronic paper display based on the combined effect of DEP and dipole attractive force was tested in the experiment. Particles solution with 2.9 μm polystyrene microspheres suspended in DI water was filled into the cell and the device was tested with a 10 Vpp, 1 MHz AC electric voltage. The inter-electrode separation is 20 μm, which is known the smallest dimension fabricated by using the photolithography with a plastic film mask (Madou 2002). The experimental results are shown in Figure 7.2.

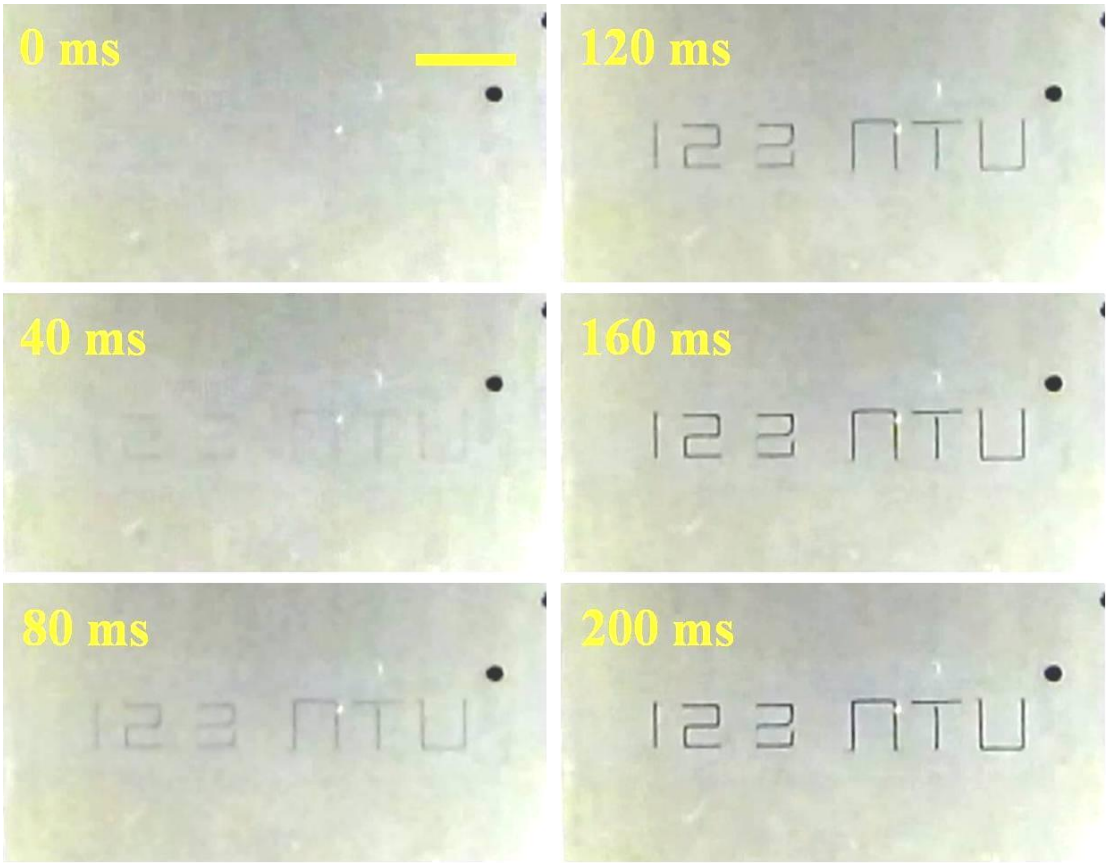

Figure 7.2 Sequential images taken for a prototype of the electronic paper display under combined effects of the DEP and dipole attractive force. An AC electric signal of 10 Vpp, 1MHz is used in the experiment. The inter-electrode separation is 20 μm. Scale bar represents 2 mm.

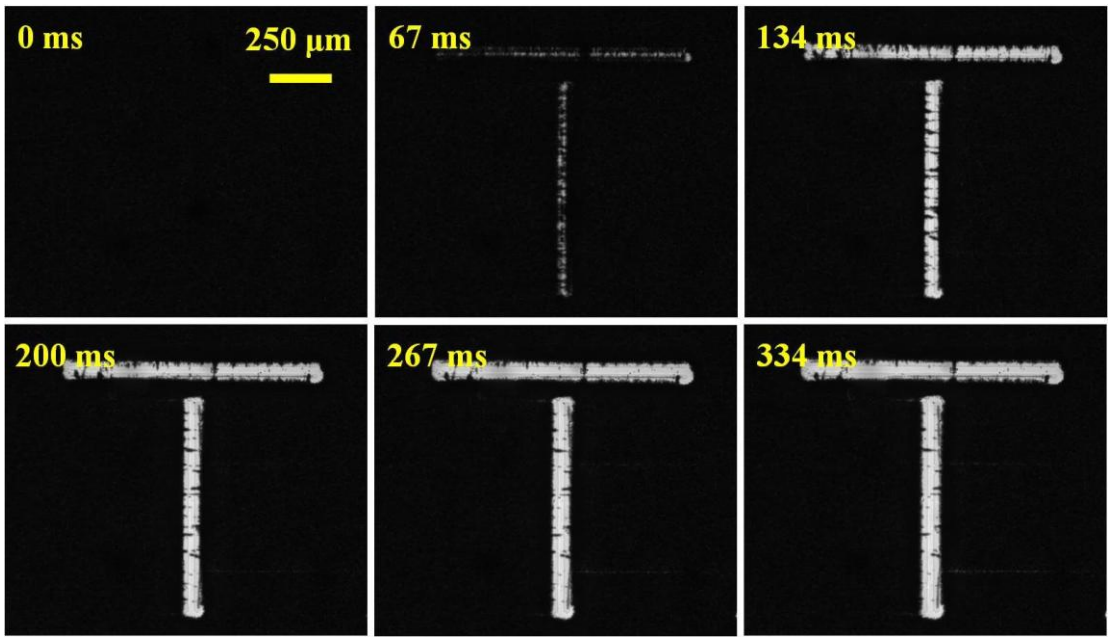

(a)

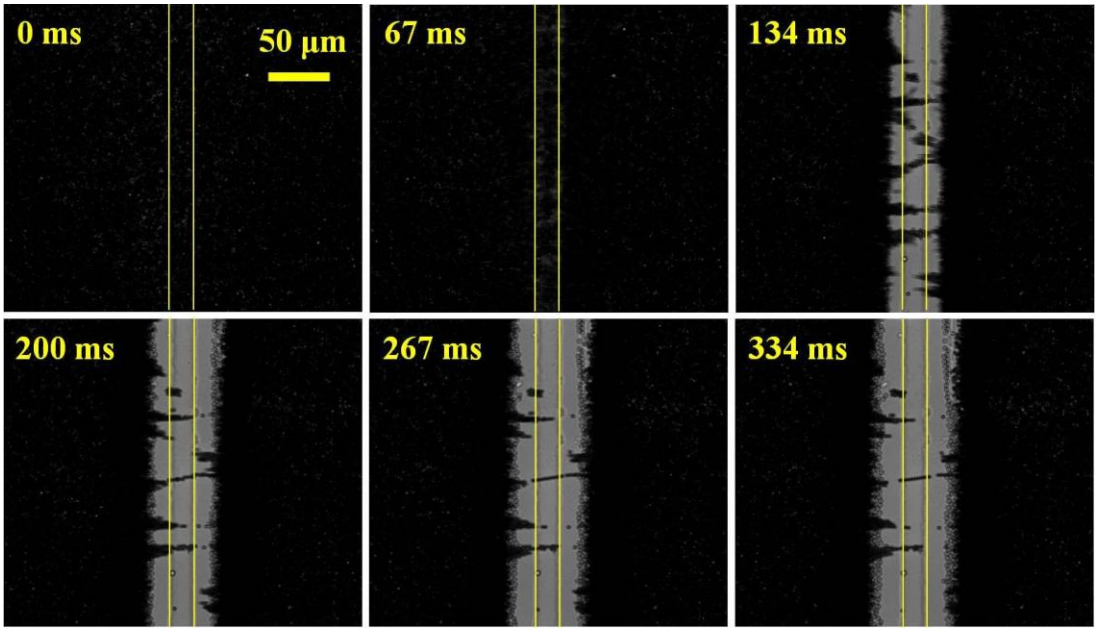

(b)

Figure 7.3 Microscopy images illustrating the process of particle patterns within the electronic display cell. An AC electric signal of 10 Vpp, 1MHz is used in the experiment. (a) Snap shots of the letter "T" with a 5× magnification and (b) snap

shots of the vertical strip of the letter "T" with a 20× magnification. The light lines in Figure 7.3 (b) indicate the 20 μm inter-electrode gap.

It is observed that after the electric voltage was turned on for 120 ms, a word "NTU" and digits "123" are screening on the electronic display panel. As the electric voltage is kept loading, the word becomes increasingly clear and a considerable contrast is created after the voltage is applied for 200 ms. The dimension of each letter and digit is less than 1 mm, indicating a remarkable resolution. The line width of each letter and digit is measured less than 60 μm, which is much favorable for the high resolution electronic paper display. Figure 7.3 shows the microscopy images of pigment particles rearrangement within the electronic display cell under an AC electric signal of 10 Vpp and 1MHz. Because the electric voltage on the co-planar electrodes with a 20 μm gap can create a considerable non-uniform electric field, a very fast particles displacement is thus achieved. By analyzing the transmittance of the electronic paper display versus time elapse based on binary images processing, it is found that the switching response of this electronic paper display is 230 ms (Figure 7.4).

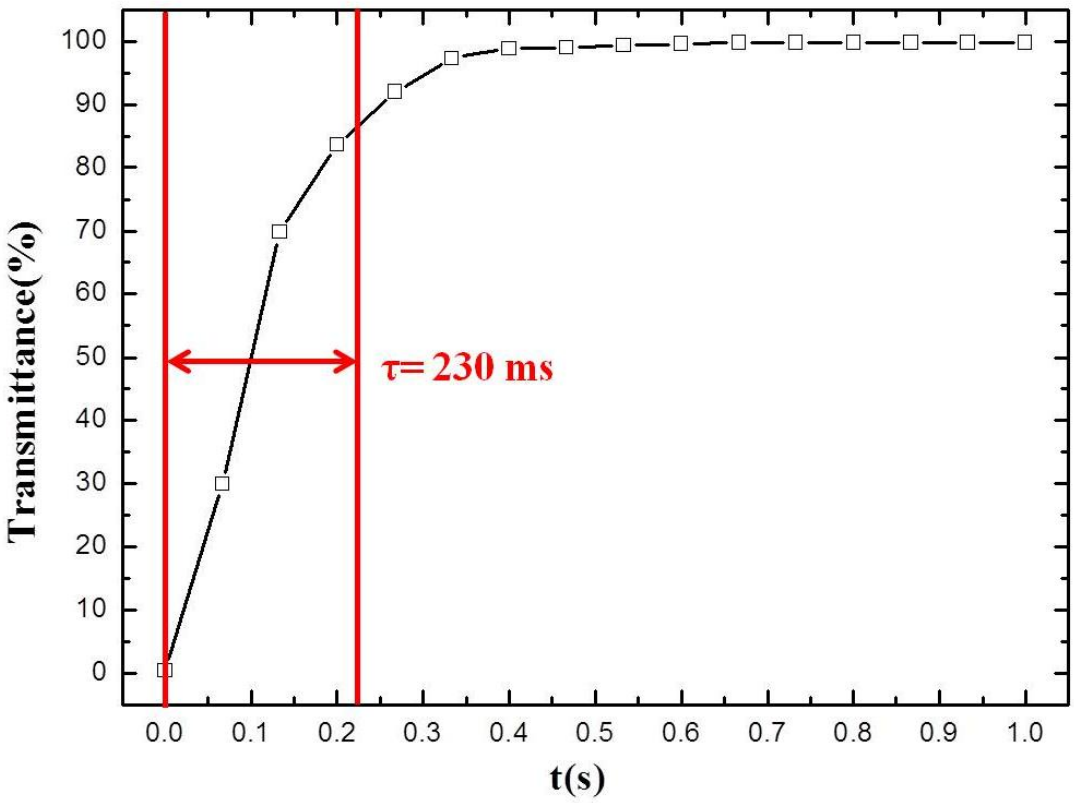

Figure 7.4 The transmittance of the electronic paper display varies with time.

7.3.2 Effect of inter-electrode separation

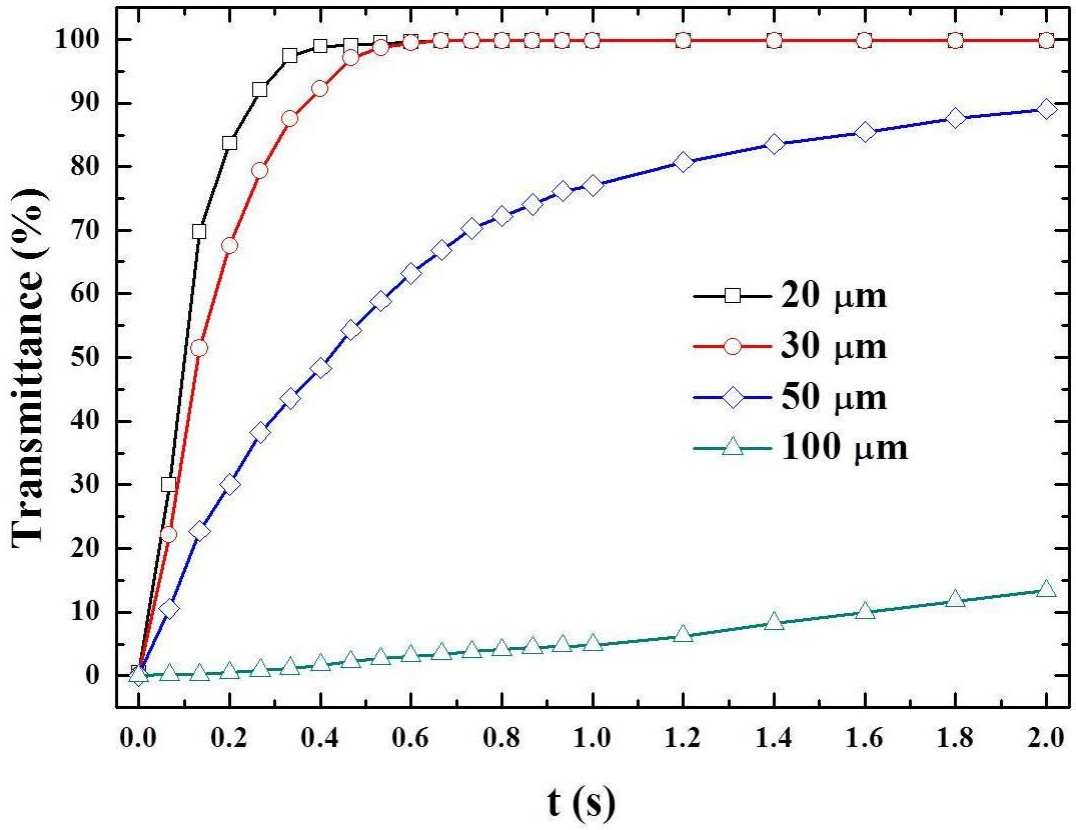

Figure 7.5 Effect of inter-electrode separation on the transmittance of the electronic paper display. An AC electric signal of 10 Vpp, 1MHz is used in the experiment.

Figure 7.5 shows the effect of inter-electrode separation on the transmittance of the electronic paper display. With the enlargement of the inter-electrode gap, both the intensity and the gradient of the electric field generated by the co-planar electrodes are weakened. Because the DEP force and dipole attractive force are proportional to ∇E^2 and E^2, respectively, the increment of inter-electrode gap leads to a significantly decline of driven forces acting on pigment particles. As a result, the

particles rearrangement within the microchip is significantly retarded with the enlargement of the inter-electrode gap. Figure 7.6 demonstrates the photographs of information screening on the electronic display panel with different inter-electrode gaps after the electric voltages are applied for 200 ms. It is seen that, once the inter-electrode gap is enlarged, the update response of the electronic paper display degrades sharply.

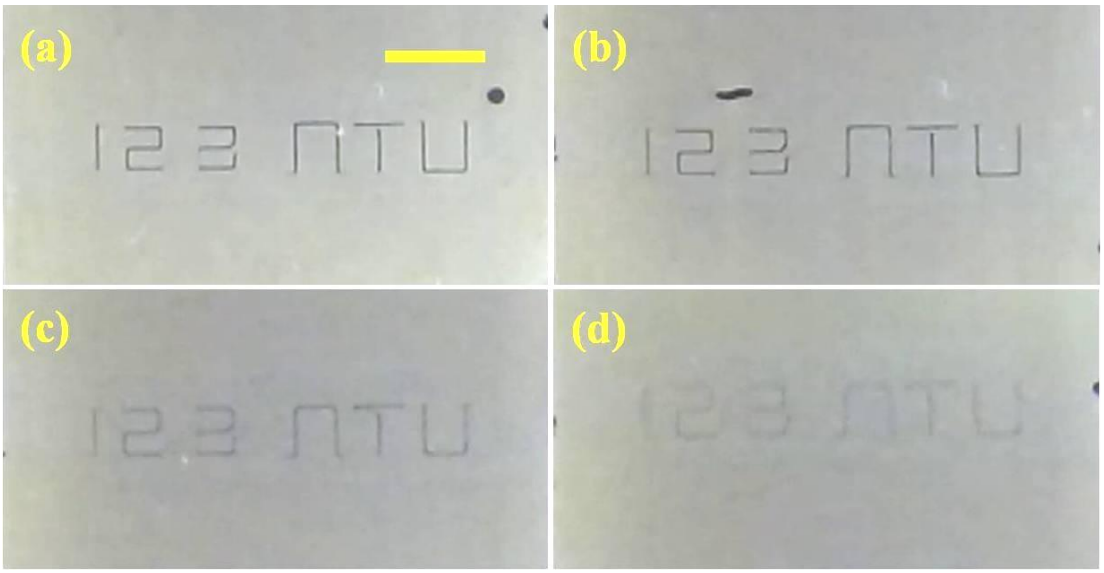

Figure 7.6 Photographs of information screening on a prototype under the combined effect of DEP and dipole attractive force after the electric field is turned on for 200 ms with inter-electrode separation of (a) 20 μm, (b) 30 μm, (c) 50 μm and (d) 100 μm. An AC electric signal of 10 Vpp, 1MHz is used in the experiment. Scale bar represents 2 mm.

7.3.3 Effect of applied electric voltage

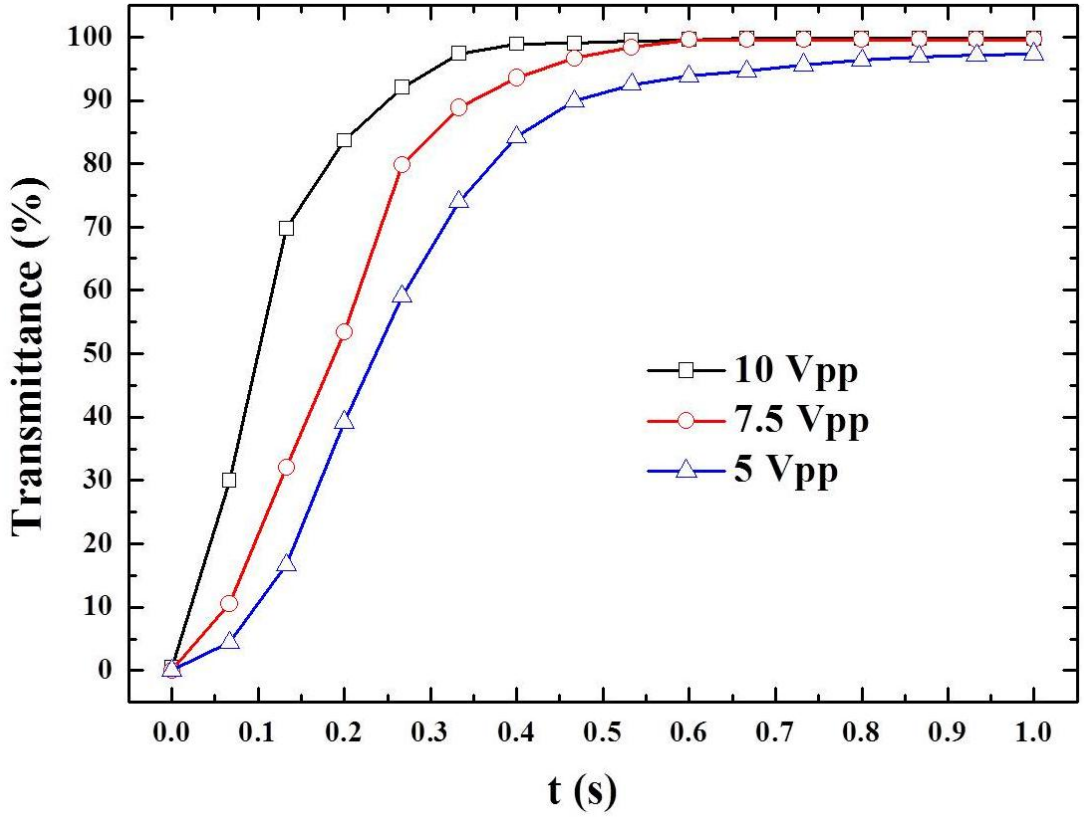

Figure 7.7 Effect of applied electric voltage on the transmittance of the electronic paper display. The frequency of the AC electric signal is fixed at 1MHz in the experiment. The inter-electrode inter-electrode separation is 20 μm.

The effect of applied electric voltage on the transmittance of the electronic paper display is shown in Figure 7.7. According to the experimental results in chapter 6, the microscale particles rearrangement is retarded with the decline of applied electric voltage. Once the voltage drops, the driven force acting on particles is reduced, yielding a slow update response of the electronic paper display.

7.3.4 Effect of frequency of the electric field

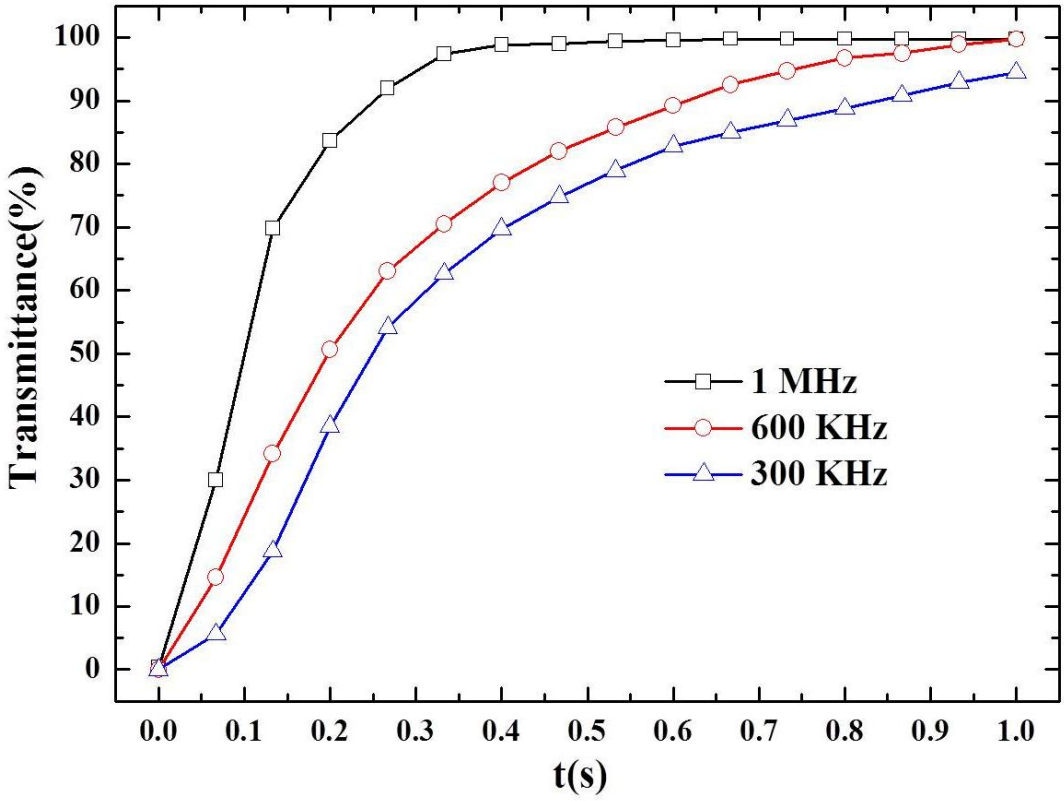

Figure 7.8 Effect of frequency of the applied electric field on the transmittance of the electronic paper display. The amplitude of the AC electric signal is fixed at 10 Vpp in the experiment. The inter-electrode separation is 20 μm.

Figure 7.8 shows effect of frequency of the applied electric field on the transmittance of the electronic paper display. Similar to the effect of the applied electric voltages, the decline of the frequency of applied electric field can result in the drop of $\mathrm{Re}\left|f_{CM}(\omega)\right|$, and thus lead to the reduction of driven force acting on the particles. In order to avoid presence of positive DEP force during the experiment, only the frequencies above 300 KHz were tested. The experimental results suggest that the

response of the electronic paper display becomes slowly with the drop of the frequency, due the decline of DEP force and dipole force acting on the particles.

7.4 Summary

A novel electronic paper display technique by using the combined effect of DEP force and dipole attractive force is developed and demonstrated in this chapter. A prototype of the proposed electronic paper display is fabricated. Experimental results suggest that information screening on the electronic display panel is achieved within 230 ms after the voltage is turn on. It is found that the switching response of the proposed electronic paper display is retarded by either reducing the frequency or voltage of the applied electric field. Moreover, because the enlargement of the inter-electrode gap can significantly weaken both the intensity and the gradient of the applied electric field simultaneously, the performance of the proposed electronic paper display is extremely degraded with the increase of the inter-electrode gap.

The greatest strengths of this novel electronic paper display are known from two aspects. Firstly, according to the experimental results, both the switching response and the resolution of the electronic paper can be greatly enhanced simultaneously by reducing the dimension of the electrodes. Secondly, as particles within the inter-electrode gap can be relocated to the electrodes completely after the electric field is applied, the proposed electronic paper can achieve a remarkable transmittance. This is

very important to the investigation of color display as the full color electronic paper can be realized by stacking multi-cells with each cell feeding by different dyed pigment particles.

One drawback of the current electronic display is that the device has to be actuated at a high frequency (i.e. 1 MHz used in this chapter). Hence, the portability of the device remains challengingly. Actually, 1 MHz frequency is employed only because a stronger negative DEP force can be yielded above this frequency for 2.9 μm polystyrene particles (as explained by Figure 6.12). Once pigment particles with different materials and sizes are extensively investigated, the working frequency of such electronic paper display technology is expected to be reduced and thus this drawback could be resolved.

Chapter 8: Conclusions and future works

8.1 Contributions of this thesis

In this thesis, electrokinetic transport and manipulation of microparticles in confined microfluidic domains are investigated. The investigation is carried out in two parts, namely, electrokinetic transport phenomena in confined microfluidic devices and particle manipulation in closed microfluidic structures. The first part concentrates on the complicated particle-fluid-wall interactions in open ended microfluidic channels and the second part focuses on the electrokinetic manipulation of particles in closed microfluidic structures without externally fluid flow. The major contributions made by this thesis research can be summarized as follows:

1. Wall effects on electrokinetic transport of microspheres in a rectangular microchannel.

The near wall enhancement of the electrophoretic mobility of microsphere transport in a rectangular microchannel is experimentally validated for the first time. Although the wall effects on electrokinetic transport of particles have been extensively studied in the past decades, the experimental verification is still challenging because both the control and measurement of the tiny particle-wall gap are very difficult. In order to solve this problem, the focus was placed on the *x*-*z* vertical plane instead of the *x*-*y* horizontal plane, and hence the narrow gap could be accurately adjusted by means of the force balance between the DEP force against the gravitational force. Both

experimental results and numerical simulations suggest that the electrophoretic mobility of particles is obviously enhanced with reducing the particle-wall separation. This is because as the narrow gap shrinks to a certain value, the effect of electric stress due to the squeezed local electric field can overcome the viscous retardation from the solid boundary, and thus the particle motion is accelerated.

In order to directly observe the particle displacement within the channel vertical direction, an experimental setup was employed with a side-mounted CCD camera by laterally turning an optical microscope in 90^{o}. In addition, a protocol for assembling the microchip with smooth PDMS side surfaces is proposed. With these efforts, the particle transport processes within the microchannel can be clearly observed from side view through the PDMS channel wall.

2. Continuous concentration of particles in a confined microfluidic chamber.

A method for continuous concentration of microspheres in a confined microfluidic chamber is proposed and also studied experimentally and numerically. Microsphere enrichment is achieved by applying a very low DC electric voltage across a pair of two electrodes and feeding the particles solution with a syringe pump. It is shown that higher electric voltage, larger feeding flow rate, electrolyte solution with lower concentration, or/and biger particle size are favorable for such particles enrichment.

Moreover, a new fabrication method for creating three dimensional electrodes in PDMS microfluidic devices is proposed and demonstrated. 3D side-wall electrodes

within the confined microfluidic chamber were realized by embedding copper strips into the PDMS microchannel. Experimental study showed that the electrodes work well during the course of the experiment.

3. A novel electronic paper display based on the in-plane dielectrophoresis.

A novel electronic paper display technology based on the in-plane dielectrophoresis was developed. A prototype of the proposed electronic paper display was fabricated. Pigment polystyrene particles dispersed in DI water within the electronic display cell can be patterned by using in-plane DEP force under an applied AC electric field across co-planar electrodes with varied inter-electrode separations. Experimental results showed that the information display on the panel is achieved within 850 ms after the voltage is turned on. It is found that the switching response of the electronic paper can be enhanced by reducing the minimum inter-electrode gap, optimizing the electrode configurations, and increasing the amplitude and frequency of applied electric voltage. As the proposed electronic paper display does not have any specific requirement on both the pigment particles and carrier fluid, it is expected the proposed novel electronic paper display technology will have low manufacturing costs.

4. On-chip particle assembly by using co-planar electrodes induced non-uniform electric field.

The detailed physical process of particle assembly in non-uniform electric field is experimentally investigated. The non-uniform electric field is created by applying AC

electric voltage across a pair of co-planar electrodes patterned on the ITO substrate. After the electric signal is imposed, the particles in the middle gap between electrodes can move toward side electrodes. The process of particle assembly in such non-uniform electric field includes two stages. At the first stage, the strong DEP forces at the electrodes edges repel particles from the high electric field regions, forming two bands along the inner electrodes edges. At the same time, particles in the middle electrode gap accumulate as a closely-packed strip due to the dipole induced chain interaction under the AC electric field. At the second stage, the particles in the middle strip are gradually lifted and are formed as chains to move toward each side under the effects of DEP and chain attraction. Finally, the particles in the middle electrodes gap are completely transported to the electrode surfaces. The particle assembly in non-uniform electric field is found to be enhanced with higher particle concentration, stronger electric voltages and narrower inter-electrode separations. Also, the particle assembly is affected by the frequency of the AC electric field and the particle size as well. Reduce the frequency and particle size can significantly hinder the particle assembly process.

5. A novel electronic paper display based on the combined effects of dielectrophoresis and dipole force.

A novel electronic paper display technology by using a combined effect of DEP force and dipole attractive force is developed and demonstrated. The proposed electronic paper display employs the operation principle developed in chapter 6. A prototype of the proposed electronic paper display was fabricated. Experimental results showed

that information shown on the electronic display panel is achieved within 230 ms after the voltage is turned on. It is found that the switching response of the proposed electronic paper display is retarded by reducing the frequency and voltage of the applied electric field. Moreover, because increasing the inter-electrode gap can weaken both the intensity and the gradient of the applied electric field simultaneously, the performance of the proposed electronic paper display deteriorates significantly with increasing the inter-electrode gap.

As the particles within the inter-electrode gap can be relocated to the electrodes completely after the electric field is applied, the proposed electronic paper can achieve remarkably high transmittance. On the other hand, both the switching response and the resolution of the electronic paper can be greatly enhanced simultaneously by reducing the dimension of the electrodes.

8.2 Recommendations for future studies

Based on the results presented in this thesis, some recommendations are made for the future investigations as listed below.

1. Wall effect on dielectrophoresis of microspheres in a microchannel

Due to the presence of the particle near the channel boundary, the flow field and the electric potential distribution are disturbed when microparticles are electrokinetically transported in a microchannel. In this situation, both the electrophoresis and

dielectrophoresis will be affected by the solid boundaries due the particle-fluid-wall interactions. Although the investigation of wall effects on the electrophoresis of near wall particle transport has been reported, the study of solid boundary effects on the dielectrophoresis of particles is also interesting. For example, based on existing studies on electrokinetic transport of particles in microfluidic devices, it is found that the numerical simulation can only reasonably predict the trend of particle trajectory but needs a correction factor in the DEP force so that simulation results could match with experimental observations. Therefore, in order to understanding on how the finite particle size and the wall boundary can affect conventional DEP force, systematical studies of particle-wall interactions on dielectrophoresis are necessary.

2. Optimization of the novel electronic paper display technologies.

In this thesis, two types of novel electronic paper display technologies are proposed and developed. Experimental results showed that the performance of the novel electronic papers are affected by many factors, such as the dimension and configurations of electrodes, applied electric field, particle size, particle concentration, electric and dielectric properties of the particles and fluid etc. Future study will aim to optimize the performance of these two novel electronic paper display technologies to achieve better electronic papers with faster switching update and higher resolution.

3. Programmable control of information display on the proposed novel electronic paper technologies.

Novel electronic paper display technologies are proposed and developed in this thesis. However, these studies are proof-of-concepts only. To commercialize these novel electronic paper display technologies, improvements on many aspects are needed. Programmable control of information screening on the electronic display panel is one of the most important goals in the next step. With a pixel matrix addressing scheme, each pixel of the electronic paper display can be stimulated individually by using a pilot circuit connected with a controlling platform.

4. Investigation of full color electronic paper displays.

Currently, full color display is still challenging for particle based electronic paper technologies. Although Philips Research has developed a full color electronic paper relying on the phenomenon of in-plane electrophoresis, the update refreshing of their products is too slow for normal reading uses. The second type electronic paper display proposed in Chapter 7 of this thesis provides a novel technology with fast switching response and high resolution and transmittance. The future study aims to realize full color display on the electronic paper with two methods (i) employing a multi-layers structure of the electronic paper display by stacking individual electronic display cells with each cell fed with particular kind of dyed particles, and (ii) employing a single layer electronic display cell with three different dyed particles such that the color is shown by controlling the CM factor of each kind of particles with specific frequency of the electric signal.

Appendix A: Soft lithography method for microchannel fabrication

Soft lithography refers to a Micro-electromechanical Systems (MEMS) technique developed for fabricating or replicating structures using elastomeric stamps, molds, and conformable photo masks. The terminology "Soft lithography" is defined because elastomeric materials, most notably poly-dimethylsiloxane (PDMS), are always used to construct features measured on the micrometer or even nanometer scale.

Figure A.1 shows the flow chart of the fabrication procedure of the microfluidic devices where the photolithography is used. A negative photoresist SU 8 50 is used in this study. A piece of silicon wafer is firstly cleaned prior to spin-coating a 100 μm thick SU 8 layer on the wafer. The silicon wafer with negative photoresist layer undergoes a pre-bake on a hotplate at 65 ^{0}C for 10 mins. Then the wafer is placed under the photo mask, and exposed to UV light. The exposed part of the SU8 is hardened due to the cross-links between molecules. Followed by a softbake at 95 ^{0}C for 30 mins and the development process, a SU8 microchannel mold with a height of 100 μm is thus defined.

Followed with a postbake at 120 ℃ for 45 mins, pure Liquid PDMS is poured on the silicon mold and then baked in the Oven at 80 ℃ for 1h. After that, the cured PDMS layer together with microchannel stamp is peeled off from the Silicon wafer. Finally,

the peeled PDMS layer and a glass slide are bonded together to form a microchannel structure after plasma treatment.

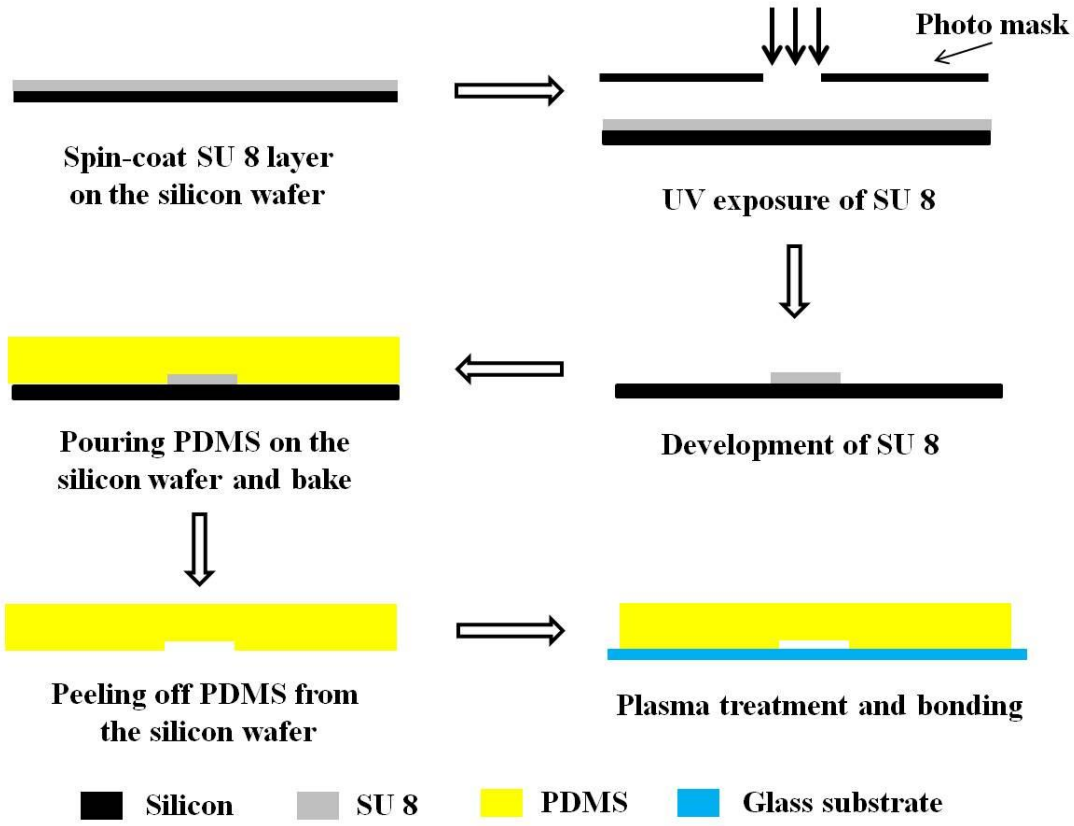

Figure A.1 Schematic of the fabrication procedures for the microchannel used in the experiment.

Appendix B: Electrodes patterning procedure on ITO glasses

Indium tin oxide (ITO) is a solid solution made of 90% In_2O_3 and 10% SnO_2 by weight. It is transparent and colorless in thin layers. Because of its two distinguish features, i.e. electrical conductivity and optical transparency, ITO is one of the most widely used transparent conductive materials.

The ITO glass is a kind of glasses with conductive films coated on its surface. It is commercial available in the market. However, to obtain the desired electrodes patterns in the experiment, a few actions are needed to process the ITO glasses.

As shown in Figure A.2, a piece of ITO glass is firstly cleaned prior to spin-coating a 2 μm thick positive photoresist AZ 7220 layer on its surface. The ITO glass with AZ 7220 layer undergoes a pre-bake on a hotplate at 100 ^{0}C for 90 s. Then the ITO glass is placed under the photo mask, and exposed to UV light for 8 s. Followed by a softbake at 110 ^{0}C for 60 s and the development process, the desired electrodes parts on the ITO glass surface are thus covered by positive photoresist. Subsequently, after hardbake at 120 ^{0}C for 45 mins, the ITO glass is immersed into etching solution for 4 mins at the room temperature. The etching solution consists 37.5 % HCl, 70% HNO_3 and DI water with a volume ratio of 4:1:2. Finally, after remove the positive photoresist on the ITO surface, the desired electrodes patterns are thus obtained.

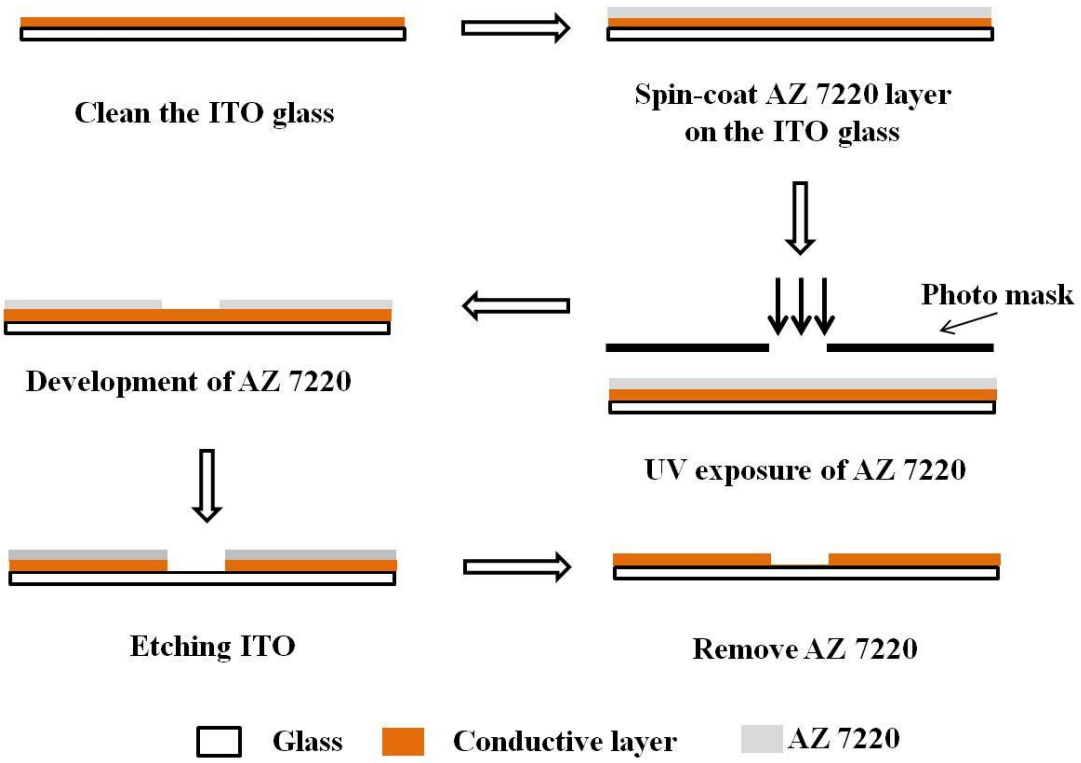

Figure A.2 Schematic of the fabrication procedures of electrodes patterning on the ITO glass.

References

Ahn Y H, Yu G C, Kim Y C, Lee S S, Kim J (2008). Electro-optic response characteristics of a dual particle electrophoretic display system. Molecular Crystals and Liquid Crystals 492: 322-327.

Anderson J L (1989). Colloid transport by interfacial forces. Annu. Rev. Fluid Mech. 21: 61-99.

Aoki R, Yamada M, Yasuda M, Seki M (2009). In-channel focusing of flowing microparticles utilizing hydrodynamic filtration. Microfluidics and Nanofluidics 6: 571-576.

Asbury C L, Diercks A H, Van Den Engh G (2002). Trapping of DNA by dielectrophoresis. Electrophoresis 23: 2658-2666.

Baker M A, Shrivastava A, Chatha K S (2007). Smart driver for power reduction in next generation bistable electrophoretic display technology. CODES+ISSS 2007: International Conference on Hardware/Software Codesign and System Synthesis.

Besra L, Liu M (2007). A review on fundamentals and applications of electrophoretic deposition (EPD). Progress in Materials Science 52: 1-61.

Bhatt K H (2006). On-chip manipulation and controlled assembly of colloidal particles using alternating electric fields. United States -- North Carolina, North Carolina State University**:** 131 p.

Bousse L, Cohen C, Nikiforov T, Chow A, Kopf-Sill A R, Dubrow R, Parce J W (2000). Electrokinetically controlled microfluidic analysis systems. Annual Review of Biophysics and Biomolecular Structure. 29**:** 155-181.

Brisson V, Tilton R D (2001). Self-assembly and two-dimensional patterning of cell arrays by electrophoretic deposition. Biotechnology and Bioengineering 77: 290-295.

Chang Y C, Keh H J (2008). Diffusiophoresis and electrophoresis of a charged sphere perpendicular to two plane walls. Journal of Colloid and Interface Science 322: 634-653.

Chein R, Dutta P (2009). Effect of charged membrane on the particle motion through a nanopore. Colloids and Surfaces A: Physicochemical and Engineering Aspects 341: 1-12.

Chen D, Du H (2010). A microfluidic device for rapid concentration of particles in continuous flow by DC dielectrophoresis. Microfluidics and Nanofluidics 9: 281-291.

Chen D F, Du H, Li W H (2006). A 3D paired microelectrode array for accumulation and separation of microparticles. Journal of Micromechanics and Microengineering 16: 1162-1169.

Chen S C, Chiu C P, Hsu C H, Fan S K (2009). Reflective electronic paper display by particle polarization with tunable stability. 2009 International Display Manufacturing Conference, 3D Systems and Applications, and Asia Display, IDMC/3DSA/Asia Display 2009.

Chen X Q, Saito T, Yamada H, Matsushige K (2001). Aligning single-wall carbon nanotubes with an alternating-current electric field. Applied Physics Letters 78: 3714-3716.

Chiou P Y, Ohta A T, Wu M C (2005). Massively parallel manipulation of single cells and microparticles using optical images. Nature 436: 370-372.

Chiu C P, Hsu C H, Chiang M T, Mo C N, Fan S K (2008). Reflective electronic paper by particle polarization on a 5×5 pixel array. IDW '08 - Proceedings of the 15th International Display Workshops.

Chiu C P, Huang P W, Fan S K, Wei J H, Hsu W (2007). Reflective electronic paper display utilizing electric polarized particle chains. Digest of Technical Papers - SID International Symposium.

Choi S, Park J K (2005). Microfluidic system for dielectrophoretic separation based on a trapezoidal electrode array. Lab on a Chip - Miniaturisation for Chemistry and Biology 5: 1161-1167.

Chou C F, Tegenfeldt J O, Bakajin O, Chan S S, Cox E C, Darnton N, Duke T, Austin R H (2002). Electrodeless dielectrophoresis of single- and double-stranded DNA. Biophysical Journal 83: 2170-2179.

Chunag C H, Chen Y C, Hsu Y M, Huang H S, Hsiao F B, Wang C H (2009). A DEP chip with arc-shape microelectrode arrays for the separation of different-size particles. 4th IEEE International Conference on Nano/Micro Engineered and Molecular Systems, NEMS 2009.

Comiskey B, Albert J D, Yoshizawa H, Jacobson J (1998). An electrophoretic ink for all-printed reflective electronic displays. Nature 394: 253-255.

Dalir H, Yanagida Y, Hatsuzawa T (2009). Probing DNA mechanical characteristics by dielectrophoresis. Sensors and Actuators, B: Chemical 136: 472-478.

Dalisa A L (1977). Electrophoretic display technology. IEEE Transactions on Electron Devices ED-24: 827-834.

Dassanayake U, Fraden S, Van Blaaderen A (2000). Structure of electrorheological fluids. Journal of Chemical Physics 112: 3851-3858.

Deen W M (1998). Analysis of Transport Phenomena. New York, Oxford University Press.

Dhopeshwarkar R, Sun L, Crooks R M (2005). Electrokinetic concentration enrichment within a microfluidic device using a hydrogel microplug. Lab on a Chip - Miniaturisation for Chemistry and Biology 5: 1148-1154.

Dorfman K (2008). Electrophoresis. Encyclopedia of Microfluidics and Nanofluidics. Li D. New York, Springer Science+Business Media, LLC**:** 580-587.

Drzaic P (2009). Displays: Microfluidic electronic paper. Nature Photonics 3: 248-249.

Durr M, Kentsch J, Müller T, Schnelle T, Stelzle M (2003). Microdevices for manipulation and accumulation of micro- and nanoparticles by dielectrophoresis. ELECTROPHORESIS 24: 722-731.

Ebel J P, Anderson J L, Prieve D C (1988). Diffusiophoresis of latex particles in electrolyte gradients. Langmuir 4: 396-406.

Ennis J, Anderson J L (1997). Boundary Effects on Electrophoretic Motion of Spherical Particles for Thick Double Layers and Low Zeta Potential. Journal of Colloid and Interface Science 185: 497-514.

Ennis J, Zhang H, Stevens G, Perera J, Scales P, Carnie S (1996). Mobility of protein through a porous membrane. Journal of Membrane Science 119: 47-58.

Erickson D (2008). Electroosmotic Flow (DC). Encyclopedia of Microfluidics and Nanofluidics. Li D. New York, Springer Science+Business Media, LLC**:** 560-566.

Feenstra B J, Hayes R A, Camps I G J, Hage L M, Johnson M T, Roques-Carmes T, Schlangen L J M, Franklin A R, Valdes A F, Ford R A (2004). A video-speed reflective display based on electrowetting: Principle and properties. Journal of the Society for Information Display 12: 293-299.

Fiedler S, Shirley S G, Schnelle T, Fuhr G (1998). Dielectrophoretic Sorting of Particles and Cells in a Microsystem. Analytical Chemistry 70: 1909-1915.

Fuhr G, Arnold W M, Hagedorn R, Muller T, Benecke W, Wagner B, Zimmermann U (1992). Levitation, holding, and rotation of cells within traps made by high-frequency fields. Biochimica et Biophysica Acta - Biomembranes 1108: 215-223.

Fuhr G, Muller T, Schnelle T, Hagedorn R, Voigt A, Fiedler S, Arnold W M, Zimmermann U, Wagner B, Heuberger A (1994). Radio-frequency microtools for particle and live cell manipulation. Naturwissenschaften 81: 528-535.

Gascoyne P, Mahidol C, Ruchirawat M, Satayavivad J, Watcharasit P, Becker F F (2002). Microsample preparation by dielectrophoresis: Isolation of malaria. Lab on a Chip - Miniaturisation for Chemistry and Biology 2: 70-75.

Ge Z (2011). Microfluidic Temperature Gradient Focusing by Electrokinetically Induced Joule Heating Singapore -- Singapore, Nanyang Technological University**:** 177.

Graham-Rowe D (2007). Electronic paper rewrites the rulebook for displays. Nature Photonics 1: 248-251.

Gray D S, Tan J L, Voldman J, Chen C S (2004). Dielectrophoretic registration of living cells to a microelectrode array. Biosensors and Bioelectronics 19: 771-780.

Green N G, Morgan H (1999). Dielectrophoresis of submicrometer latex spheres. 1. Experimental results. Journal of Physical Chemistry B 103: 41-50.

Greenberg A E, Clesceri L S, Eaton A D (2005). Standard Methods for the Examination of Water and Wastewater. 21st edn, American Public Health Association, American Water Works Association, and Water Environment Federation.

Gulley G L, Tao R (1997). Structures of an electrorheological fluid. Physical Review E - Statistical Physics, Plasmas, Fluids, and Related Interdisciplinary Topics 56: 4328-4336.

Gupta S, Alargova R G, Kilpatrick P K, Velev O D (2009). On-chip dielectrophoretic coassembly of live cells and particles into responsive biomaterials. Langmuir 26: 3441-3452.

Hames B D, Higgins S J (1995). Gene Probes: A Practical Approach. Oxford, Oxford University Press.

Hattori R, Asakawa M, Masuda Y, Nihei N, Yokoo A, Yamada S, Tanuma I (2007). Passive-matrix flexible electronic paper using quick-response liquid powder display (QR-LPD) technology and custom driver circuits. Digest of Technical Papers - IEEE International Solid-State Circuits Conference.

Hattori R, Masuda Y, Nihei N, Sakurai R, Yamada S (2006). Power consumption of a Quick-Response Liquid Powder Display (QR-LPD). Proceedings of International Meeting on Information Display.

Hayes R A, Feenstra B J (2003). Video-speed electronic paper based on electrowetting. Nature 425: 383-385.

Heida T, Rutten W L C, Marani E (2002). Understanding dielectrophoretic trapping of neuronal cells: Modelling electric field, electrode-liquid interface and fluid flow. Journal of Physics D: Applied Physics 35: 1592-1602.

Heikenfeld J, Drzaic P, Yeo J S, Koch T (2011). Review paper: A critical review of the present and future prospects for electronic paper. Journal of the Society for Information Display 19: 129-156.

Heikenfeld J, Zhou K, Kreit E, Raj B, Yang S, Sun B, Milarcik A, Clapp L, Schwartz R (2009). Electrofluidic displays using Young-Laplace transposition of brilliant pigment dispersions. Nature Photonics 3: 292-296.

Henzen A, Van De Kamer J (2006). The present and future of electronic paper. Journal of the Society for Information Display 14: 437-442.

Hopper M A, Novotny V (1979). ELECTROPHORETIC DISPLAY, ITS PROPERTIES, MODEL, AND ADDRESSING. IEEE Transactions on Electron Devices ED-26: 1148-1152.

House D L, Luo H (2011). Effect of direct current dielectrophoresis on the trajectory of a non-conducting colloidal sphere in a bent pore. Electrophoresis 32: 3277-3285.

Hsu C H, Chiu C P, Chiang M T, Mo C N, Fan S K (2008). Reflective electronic paper by polarization and electrophoresis of toner in oil. IDW '08 - Proceedings of the 15th International Display Workshops.

Hsu J P, Chen C Y, Lee D J, Tseng S, Su A (2008). Electrophoresis of a charge-regulated sphere at an arbitrary position in a charged spherical cavity. Journal of Colloid and Interface Science 325: 516-525.

Hsu J P, Kao C Y (2002). Electrophoresis of a finite cylinder along the axis of a cylindrical pore. Journal of Physical Chemistry B 106: 10605-10609.

Huang Y, Joo S, Duhon M, Heller M, Wallace B, Xu X (2002). Dielectrophoretic cell separation and gene expression profiling on microelectronic chip arrays. Analytical Chemistry 74: 3362-3371.

Hunter R J (1981). Zeta Potential in Colloid Science. New York, Academic Press.

Jones T B (1995). Electromechanics of Particles. New York, Cambridge University Press.

Kang Y, Li D (2009). Electrokinetic motion of particles and cells in microchannels. Microfluidics and Nanofluidics 6: 431-460.

Kawabata T, Washizu M (2001). Dielectrophoretic detection of molecular bindings. IEEE Transactions on Industry Applications 37: 1625-1633.

Keh H J, Anderson J L (1985). Boundary effects on electrophoretic motion of colloidal spheres. Journal of Fluid Mechanics Digital Archive 153: 417-439.

Keh H J, Chen S B (1988). Electrophoresis of a colloidal sphere parallel to a dielectric plane. Journal of Fluid Mechanics Digital Archive 194: 377-390.

Kim C A, Joung M J, Ahn S D, Kim G H, Kang S Y, You I K, Oh J, Myoung H J, Baek K H, Suh K S (2005). Microcapsules as an electronic ink to fabricate color electrophoretic displays. Synthetic Metals 151: 181-185.

Kim M M, Zydney A L (2004). Effect of electrostatic, hydrodynamic, and Brownian forces on particle trajectories and sieving in normal flow filtration. Journal of Colloid and Interface Science 269: 425-431.

Kim S, Asmatulu R, Marcus H L, Papadimitrakopoulos Fotios F (2011). Dielectrophoretic assembly of grain-boundary-free 2D colloidal single crystals. Journal of Colloid and Interface Science 354: 448-454.

Kim S M, Burns M A, Hasselbrink E F (2006). Electrokinetic protein preconcentration using a simple glass/ poly(dimethylsiloxane) microfluidic chip. Analytical Chemistry 78: 4779-4785.

Kirk L K (2009). Electronic paper's next chapter. Commun. ACM 52: 15-17.

Klingenberg D J, Zukoski C F, Hill J C (1993). Kinetics of structure formation in electrorheological suspensions. Journal of Applied Physics 73: 4644-4648.

Koshimizu M (2008). The past, present, and future of electronic paper. Information Display 24: 22-25.

Krupke R, Hennrich F, Lhneysen H V, Kappes M M (2003). Separation of metallic from semiconducting single-walled carbon nanotubes. Science 301: 344-347.

Krupke R, Hennrich F, Weber H B, Kappes M M, Lhneysen H V (2003). Simultaneous deposition of metallic bundles of single-walled carbon nanotubes using ac-dielectrophoresis. Nano Letters 3: 1019-1023.

Lapizco-Encinas B H, Simmons B A, Cummings E B, Fintschenko Y (2004). Insulator-based dielectrophoresis for the selective concentration and separation of live bacteria in water. ELECTROPHORESIS 25: 1695-1704.

Lee D S, Kim D W, Kim H S, Lee S W, Jhang S H, Park Y W, Campbell E E B (2005). Extraction of semiconducting CNTs by repeated dielectrophoretic filtering. Applied Physics A: Materials Science and Processing 80: 5-8.

Lee K, Ahn B, Oh K W (2010). Hydrodynamic focusing based particle filtration using an Island structure with built-in valves. ASME International Mechanical Engineering Congress and Exposition, Proceedings.

Lenssen K-M H, Baesjou P J, Budzelaar F P M, van Delden M H W M, Roosendaal S J, Stofmeel L W G, Verschueren A R M, van Glabbeek J J, Osenga J T M, Schuurbiers R M (2009). Novel concept for full-color electronic paper. Journal of the Society for Information Display 17: 383- 388.

Lenssen K M H, Baesjou P J, Budzelaar F P M, Van Delden M H W M, Roosendaal S J, Stofmeel L W G, Verschueren A R M, Van Glabbeek J J, Osenga J T M, Schuurbiers R M (2008). Invited paper: Novel design for full-color electronic paper. Digest of Technical Papers - SID International Symposium.

Lewpiriyawong N, Kandaswamy K, Yang C, Ivanov V, Stocker R (2011). Microfluidic characterization and continuous separation of cells and particles

using conducting poly(dimethyl siloxane) electrode induced alternating current-dielectrophoresis. Analytical Chemistry 83: 9579-9585.

Lewpiriyawong N, Yang C, Lam Cheong Y (2008). Dielectrophoretic manipulation of particles in a modified microfluidic H filter with multi-insulating blocks. Biomicrofluidics 2.

Lewpiriyawong N, Yang C, Lam Y C (2010). Continuous sorting and separation of microparticles by size using AC dielectrophoresis in a PDMS microfluidic device with 3-D conducting PDMS composite electrodes. Electrophoresis 31: 2622-2631.

Lewpiriyawong N, Yang C, Lam Y C (2012). Electrokinetically driven concentration of particles and cells by dielectrophoresis with DC-offset AC electric field. Microfluidics and Nanofluidics 12: 723-733.

Li A, Ahmadi G (1992). Dispersion and deposition of spherical particles from point sources in a turbulent channel flow. Aerosol Science and Technology 16: 209-226.

Li D (2004). Electrokinetics in Microfluidics. London, Academic Press.

Li H, Friend J R, Yeo L Y (2007). Surface acoustic wave concentration of particle and bioparticle suspensions. Biomedical Microdevices 9: 647-656.

Liang L, Ai Y, Zhu J, Qian S, Xuan X (2010 a). Wall-induced lateral migration in particle electrophoresis through a rectangular microchannel. Journal of Colloid and Interface Science 347: 142-146.

Liang L, Qian S, Xuan X (2010 b). Three-dimensional electrokinetic particle focusing in a rectangular microchannel. Journal of Colloid and Interface Science 350: 377-379.

Liang R C, Hou J, Zang H M, Chung J, Tseng S (2003). Microcup displays: Electronic paper by roll-to-roll manufacturing processes. Journal of the Society for Information Display 11: 621-628.

Liu H (2005). Modeling particle-fluid interactions in microfluidic systems under the action of an electric field. United States -- Pennsylvania, University of Pennsylvania**:** 197.

Liu H, Bau H H, Hu H (2004 a). On the translation of a cylinder in a long tube. Physics of Fluids 16: 998-1007.

Liu H, Bau H H (2004 b). The dielectrophoresis of cylindrical and spherical particles submerged in shells and in semi-infinite media. Physics of Fluids 16: 1217-1228.

Liu H, Bau H H, Hu H H (2004 c). Electrophoresis of concentrically and eccentrically positioned cylindrical particles in a long tube. Langmuir 20: 2628-2639.

Liu H, Qian S, Bau H H (2007). The effect of translocating cylindrical particles on the ionic current through a nanopore. Biophysical Journal 92: 1164-1177.

Lumsdon S O, Kaler E W, Velev O D (2004). Two-Dimensional Crystallization of Microspheres by a Coplanar AC Electric Field. Langmuir 20: 2108-2116.

Madou M J (2002). Fundamentals of Microfabrication: The Science of Miniaturization. Boca Raton, CRC Press.

Manaresi N, Romani A, Medoro G, Altomare L, Leonardi A, Tartagni M, Guerrieri R (2003). A CMOS Chip for Individual Cell Manipulation and Detection. IEEE Journal of Solid-State Circuits 38: 2297-2305.

Masliyah J H, Subir B (2006). Electrokinetic and colloid transport phenomena, Wiley-Interscience.

Maynes D, Webb A R (2002). Velocity profile characterization in sub-millimeter diameter tubes using molecular tagging velocimetry. Experiments in Fluids 32: 3-15.

McDonald J C, Duffy D C, Anderson J R, Chiu D T, Wu H, Schueller O J A, Whitesides G M (2000). Fabrication of microfluidic systems in poly(dimethylsiloxane). Electrophoresis 21: 27-40.

Minerick A R, Ostafin A E, Chang H C (2002). Electrokinetic transport of red blood cells in microcapillaries. Electrophoresis 23: 2165-2173.

Minerick A R, Zhou R, Takhistov P, Chang H C (2003). Manipulation and characterization of red blood cells with alternating current fields in microdevices. Electrophoresis 24: 3703-3717.

Morgen H, Green N (2008). Dielectrophoresis. Encyclopedia of Microfluidics and Nanofluidics. Li D. New York, Springer Science+Business Media, LLC**:** 560-566.

Nilsson A, Petersson F, Jonsson H, Laurell T (2004). Acoustic control of suspended particles in micro fluidic chips. Lab on a Chip 4: 131-135.

Ota I, Ohnishi J, Yoshiyama M (1973). ELECTROPHORETIC IMAGE DISPLAY (EPID) PANEL. Proceedings of the IEEE 61: 832-836.

Paulson L D (2003). New Electronic Paper Can Display Moving Images. Computer 36: 26.

Pethig R (2010). Dielectrophoresis: Status of the theory, technology, and applications. Biomicrofluidics 4: 1-35.

Pethig R, Huang Y, Wang X-B, Burt J P H (1992). Positive and negative dielectrophoretic collection of colloidal particles using interdigitated castellated microelectrodes. Journal of Physics D: Applied Physics 25: 881-888.

Prasad S, Ozkan M (2004). Electric field assisted patterning and characterization of live neuronal networks for the study of brain functions. Materials Research Society Symposium Proceedings.

Probstein R F, Sengun M Z, Tseng T C (1994). Bimodal model of concentrated suspension viscosity for distributed particle sizes. Journal of Rheology 38: 811-829.

Ramos A, Morgan H, Green N G, Castellanos A (1998). Ac electrokinetics: A review of forces in microelectrode structures. Journal of Physics D: Applied Physics 31: 2338-2353.

Ren L (2004). Transport phenomena in microfluidic devices. Canada, University of Toronto (Canada)**:** 251.

Reyes D R, Iossifidis D, Auroux P-A, Manz A (2002). Micro Total Analysis Systems. 1. Introduction, Theory, and Technology. Analytical Chemistry 74: 2623-2636.

Sakurai R, Hattori R, Asakawa M, Nakashima T, Tanuma I, Yokoo A, Nihei N, Masuda Y (2008). A Flexible electronic-paper display with an ultra-thin and

flexible LSI driver using quick-response liquid-powder technology. Journal of the Society for Information Display 16: 155-160.

Sarkar P, Nicholson P S (1996). Electrophoretic deposition (EPD): Mechanisms, kinetics, and application to ceramics. Journal of the American Ceramic Society 79: 1987-2002.

Schoch R B, Han J, Renaud P (2008). Transport phenomena in nanofluidics. Reviews of Modern Physics 80: 839-883.

Schwartz J A, Vykoukal J V, Gascoyne P R C (2004). Droplet-based chemistry on a programmable micro-chip. Lab on a Chip - Miniaturisation for Chemistry and Biology 4: 11-17.

Shafiee H, Caldwell J L, Davalos R V (2010). A Microfluidic System for Biological Particle Enrichment Using Contactless Dielectrophoresis. JALA - Journal of the Association for Laboratory Automation 15: 224-232.

Shilton R, Tan M K, Yeo L Y, Friend J R (2008). Particle concentration and mixing in microdrops driven by focused surface acoustic waves. Journal of Applied Physics 104.

Shugai A A, Carnie S L (1999). Electrophoretic Motion of a Spherical Particle with a Thick Double Layer in Bounded Flows. Journal of Colloid and Interface Science 213: 298-315.

Simon L, Orlin V (2008). Electrically Functional Nanostructures. Dekker Encyclopedia of Nanoscience and Nanotechnology, Second Edition - Six Volume Set (Print Version), CRC Press**:** 1171-1188.

Squires T M, Bazant M Z (2004). Induced-charge electro-osmosis. Journal of Fluid Mechanics: 217-252.

Stone H A, Stroock A D, Ajdari A (2004). Engineering flows in small devices. Annual Review of Fluid Mechanics 36: 381-411.

Suzuki S, Yamanashi T, Tazawa S I, Kurosawa O, Washizu M (1998). Quantitative analysis of DNA orientation in stationary AC electric fields using fluorescence anisotropy. IEEE Transactions on Industry Applications 34: 75-83.

Takagi K, Kaga N, Tanuma I (2007). Novel type of bistable reflective display (QR-LPD) and material design of electronic liquid powder. International Conference on Digital Printing Technologies.

Trau M, Sankaran S, Seville D A, Aksay I A (1995). Electric-field-induced pattern formation in colloidal dispersions. Nature 374: 437-439.

Trau M, Saville D A, Aksay I A (1997). Assembly of colloidal crystals at electrode interfaces. Langmuir 13: 6375-6381.

Trau M, Seville D A, Aksay I A (1996). Field-induced layering of colloidal crystals. Science 272: 706-709.

Unni H N, Keh H J, Yang C (2007). Analysis of electrokinetic transport of a spherical particle in a microchannel. eletrophoresis 28: 658-664.

Velev O D (2004). Assembly of Electrically Functional Microstructures from Colloidal Particles. Colloids and Colloid Assemblies, Wiley-VCH Verlag GmbH & Co. KGaA**:** 437-464.

Velev O D, Bhatt K H (2006). On-chip micromanipulation and assembly of colloidal particles by electric fields. Soft Matter 2: 738-750.

Verschueren A R M, Stofmeel L W G, Baesjou P J, Van Delden M H W M, Lenssen K M H, Mueller M, Oversluizen G, Van Glabbeek J J, Osenga J T M, Schuurbiers R M (2010). Optical performance of in-plane electrophoretic color e-paper. Journal of the Society for Information Display 18: 1-7.

Visor G C, Schulman S G (1981). Fluorescence immunoassay. Journal of Pharmaceutical Sciences 70: 469-475.

Wang W, Yang C, Cui X Q, Bao Q L, Li C M (2010). Droplet microfluidic preparation of au nanoparticles-coated chitosan microbeads for flow-through surface-enhanced Raman scattering detection. Microfluidics and Nanofluidics 9: 1175-1183.

Wang W, Yang C, Li C M (2009). On-demand microfluidic droplet trapping and fusion for on-chip static droplet assays. Lab on a Chip - Miniaturisation for Chemistry and Biology 9: 1504-1506.

Wang W, Yang C, Liu Y, Li C M (2010). On-demand droplet release for droplet-based microfluidic system. Lab on a Chip - Miniaturisation for Chemistry and Biology 10: 559-562.

Washizu M (1998). Electrostatic actuation of liquid droplets for microreactor applications. IEEE Transactions on Industry Applications 34: 732-737.

Washizu M, Kurosawa O (1990). Electrostatic manipulation of DNA in microfabricated structures. IEEE Transactions on Industry Applications 26: 1165-1172.

Washizu M, Kurosawa O, Arai I, Suzuki S, Shimamoto N (1995). Applications of electrostatic stretch-and-positioning of DNA. IEEE Transactions on Industry Applications 31: 447-456.

Washizu M, Suzuki S, Kurosawa O, Nishizaka T, Shinohara T (1994). Molecular dielectrophoresis of biopolymers. IEEE Transactions on Industry Applications 30: 835-843.

Wen W, Weisbuch C, Phuong D M, Lu G, Ge W, Chan C T, Sheng P (2005). Neutral nanoparticle-based display. Nanotechnology 16: 598-601.

Whitesides G M (2006). The origins and the future of microfluidics. Nature 442: 368-373.

Whitesides G M, Ostuni E, Takayama S, Jiang X, Ingber D E (2001). Soft lithography in biology and biochemistry. Annual Review of Biomedical Engineering. 3**:** 335-373.

Xie J Y, Feng Y Q, Li X G, Wang J, Meng S X (2005). Progress in microcup electrophoretic display. Gongneng Cailiao/Journal of Functional Materials 36: 1320-1323.

Xie R, Liu X Y (2008). Electrically directed on-chip reversible patterning of two-dimensional tunable colloidal structures. Advanced Functional Materials 18: 802-809.

Xie R, Liu X Y (2009). Controllable epitaxial crystallization and reversible oriented patterning of two-dimensional colloidal crystals. Journal of the American Chemical Society 131: 4976-4982.

Xuan X, Raghibizadeh S, Li D (2006). Wall effects on electrophoretic motion of spherical polystyrene particles in a rectangular poly(dimethylsiloxane) microchannel. Journal of Colloid and Interface Science 296: 743-748.

Xuan X, Ye C, Li D (2005 a). Near-wall electrophoretic motion of spherical particles in cylindrical capillaries. Journal of Colloid and Interface Science 289: 286-290.

Xuan X, Xu B, Li D (2005 b). Accelerated Particle Electrophoretic Motion and Separation in Converging-Diverging Microchannels. Analytical Chemistry 77: 4323-4328.

Yamada M,Seki M (2005). Hydrodynamic filtration for on-chip particle concentration and classification utilizing microfluidics. Lab on a Chip 5: 1233-1239.

Yariv E, Brenner H (2003). Near-contact electrophoretic motion of a sphere parallel to a planar wall. Journal of Fluid Mechanics 484: 85-111.

Ye C, Li D (2002). Electrophoretic Motion of a Sphere in a Microchannel under the Gravitational Field. Journal of Colloid and Interface Science 251: 331-338.

Ye C, Sinton D, Erickson D,Li D (2002). Electrophoretic motion of a circular cylindrical particle in a circular cylindrical microchannel. Langmuir 18: 9095-9101.

Ye C, Xuan X, Li D (2005). Eccentric electrophoretic motion of a sphere in circular cylindrical microchannels. Microfluidics and Nanofluidics 1: 234-241.

Yeo L Y, Chang H C (2005). Static and spontaneous electrowetting. Modern Physics Letters B 19: 549-569.

Yeo L Y, Chang H C (2006). Electrowetting films on parallel line electrodes. Physical Review E - Statistical, Nonlinear, and Soft Matter Physics 73.

Young E W K, Li D (2005). Dielectrophoretic Force on a Sphere near a Planar Boundary. Langmuir 21: 12037-12046.

Zang H, Wang F, Kang Y M, Chen Y, Lin W (2007). Microcup E-paper for embedded and flexible designs. IDMC 2007 - International Display Manufacturing Conference and FPD Expo - Proceedings.

Zhang A, Liu W, Jiang Z, Fei J (2009). Rapid concentration of particle and bioparticle suspension based on surface acoustic wave. Applied Acoustics 70: 1137-1142.

Zhang K Q, Liu X Y (2004). In situ observation of colloidal monolayer nucleation driven by an alternating electric field. Nature 429: 739-743.

Zhang K Q, Liu X Y (2006). Two scenarios for colloidal phase transitions. Physical Review Letters 96.

Zhao C (2012). InducedCharge Nonlinear Electrokinetic Phenomena and Applications in Micro/Nano fluidics. Singapore -- Singapore, Nanyang Technological University**:** 228.

Zhao H (2008). Modeling electrokinetics with applications to micro and nano fluidic systems. United States -- Pennsylvania, University of Pennsylvania**:** 276.

Zhao H, Bau H H (2007). On the effect of induced electro-osmosis on a cylindrical particle next to a surface. Langmuir 23: 4053-4063.

Zydney A L (1995). Boundary Effects on the Electrophoretic Motion of a Charged Particle in a Spherical Cavity. Journal of Colloid and Interface Science 169: 476-485.